

OrbShake Bioreactors for Mammalian Cell Cultures: Engineering and Scale-up

THÈSE N° 5135 (2011)

PRÉSENTÉE LE 26 AOÛT 2011

À LA FACULTÉ SCIENCES DE LA VIE

LABORATOIRE DE BIOTECHNOLOGIE CELLULAIRE

PROGRAMME DOCTORAL EN BIOTECHNOLOGIE ET GÉNIE BIOLOGIQUE

ÉCOLE POLYTECHNIQUE FÉDÉRALE DE LAUSANNE

POUR L'OBTENTION DU GRADE DE DOCTEUR ÈS SCIENCES

PAR

Stéphanie TISSOT

acceptée sur proposition du jury:

Prof. H. Vogel, président du jury
Prof. F. M. Wurm, directeur de thèse
Dr M. Farhat, rapporteur
Dr A. Kadouri, rapporteur
Dr D. Mueller, rapporteur



ÉCOLE POLYTECHNIQUE
FÉDÉRALE DE LAUSANNE

Suisse
2011

Acknowledgments

This study started in the beginning of 2008 at the Laboratory of Cellular Biotechnology (LBTC), Institute of Bioengineering, Ecole Polytechnique Fédérale de Lausanne. Working on this exciting project led to a lot of fruitful collaborations that I really appreciated and would like to acknowledge here.

First of all, I would like to warmly thank Professor Florian Wurm for his guidance and very friendly and patient attitude towards my straight opinions. Many thanks for giving me the opportunity and necessary support, advice and encouragements to present our work at international conferences. Working in your group and under your supervision was a valuable experience and I can not thank you enough for that.

I acknowledge Dr. Avinoam Kadouri, Dr. Dethardt Müller and Dr. Mohamed Farhat who generously gave their time and expertise for reviewing this thesis. Many thanks also to Prof. Horst Vogel for accepting on short notice to preside this thesis jury. I warmly thank all the members of the jury for their valuable comments and advice for the improvement of this thesis.

I wish to thank Dr. Lucia Baldi, Dr. Patrik Michel and Dr. David Hacker for their help, their useful advice and the revision of my manuscripts and thesis.

A big thank you to Fabienne Rudin for her support and help for administrative and organizational issues. Thank you for your smile and good humour.

I would like to acknowledge all the people who worked with me on the project of bioreactors at the LBTC: Clara Douet, Sarah Grezet, Andrea Okroy, Gilles Broccard and Dominique Monteil.

I express my thanks to the collaborators of the Sinergia project from the Laboratory of Hydraulic Machines: Dr. Mohamed Farhat, Martino Reclari, Matthieu Dreyer and from the Modeling and Scientific Computing Chair: Professor Alfio Quarteroni, Dr. Marco Discacciati, Samuel Quinodoz, Dr. Nicola Parolini and Suzanna Carcano for their contributions to this work.

I am thankful to our partners from ExcellGene SA: Dr. Maria de Jesus and Cédric Bürki and from Kühner AG: Markus Kühner and Dr. Tibor Anderlei for their precious support and advice from an industrial point of view.

I wish to acknowledge Professor Jochen Büchs and Wolf Klöckner from the Chair of Biochemical Engineering at the RWTH Aachen University for their collaboration on the volumetric power input measurement.

Un grand merci à André Fattet et à Supardi Sujito ainsi qu'à leur équipe des ateliers mécaniques et électroniques de l'EPFL pour leurs bonnes idées et leurs solutions ingénieuses. Je ne sais pas comment j'aurais fait sans votre aide les gars, merci infiniment.

Un grand merci à tous mes collègues du LBTC et de l'EPFL passés ou présents pour les bons moments passés ensemble: Anne-Laure Dessimoz, Dr. Sophie Nallet, Dr. Agata Oberbek, Dr. Isabelle Magold, Ione Gutscher, Guillaume Lüthi, Joao Pereira, Sarah Thurnheer, Virginie Bachmann, Dr. Mattia Matasci, Dr. Xiaowei Zhang. A special thanks to my two office mates, Divor Kiseljak and Yashas Rajendra, who supported me by keeping themselves more or less quiet during the writing of my thesis.

The financial support from the KTI-Program of the Swiss Economic Ministry and the Swiss National Science Foundation is gratefully acknowledged.

Résumé

La plupart des médicaments biopharmaceutiques sont produits par des cellules animales de nos jours. La demande mondiale pour un certain groupe de médicaments biopharmaceutiques, les anticorps monoclonaux, a particulièrement augmenté cette dernière décennie. Les anticorps monoclonaux sont utilisés notamment pour lutter contre le cancer et les maladies auto-immunes. La plupart des anticorps monoclonaux sont produits en utilisant des cellules mammaliennes qui assurent des modifications post-traductionnelles permettant d'obtenir un produit fonctionnel du point de vue biologique. Néanmoins, les bioprocédés impliquant des cellules mammaliennes sont généralement coûteux et de larges quantités d'anticorps sont requises. Ceci conduit à un besoin accru de bioprocédés flexibles et rentables à la fois pour la recherche et le développement de nouveaux produits biopharmaceutiques et pour la production des thérapeutiques déjà agréés. Les bioréacteurs à agitation orbitale (OSRs) sont basés sur la technologie des produits à usage unique (jetables) et sont dès lors très flexibles. Ce travail a pour but d'améliorer notre compréhension du mode de fonctionnement de ces bioréacteurs en étudiant leurs principes d'ingénierie tels que le mélange, le transfert de gaz ou l'hydrodynamique, tout ceci dans le cadre de la culture des cellules mammaliennes. L'étude du mélange a démontré que les OSRs assurent l'homogénéité des cultures jusqu'à une échelle de 1500 L avec des temps de mélange en dessous de 30 s. En conservant les rapports géométriques (diamètre d'agitation, diamètre du bioréacteur et hauteur de liquide) ainsi que le nombre de Froude constants, le mélange et la forme de la surface libre d'un OSR de 1500 L ont pu être reproduits dans un OSR de 30 L. Une valeur minimale pour le coefficient de transfert d'oxygène ($k_L a$) est requise afin de pouvoir effectuer une culture de cellules mammaliennes sans contrôleurs pour compenser le pH ou la concentration en oxygène dis-

sout (DO). Cette valeur minimale dépend de la lignée cellulaire et se trouve typiquement dans la fourchette entre 7 et 10 h⁻¹. Les cultures ayant les mêmes valeurs de $k_L a$ ont les mêmes caractéristiques de croissance, concentrations de protéines recombinantes, conditions de culture (pH et DO) et profils de métabolites. Un bioprocédé opéré dans un OSR de 200 L sans utiliser de contrôleur a donné les mêmes courbes de croissance, concentrations en protéine recombinante et conditions de culture (pH et DO) que le même bioprocédé dans des OSRs d'1 et 5 L. Les valeurs maximales de tension de cisaillement calculées au moyen d'un modèle de dynamique computationnelle des fluides (CFD) dans un OSR d'1 L agité à 110 rpm sont 10 à 100 fois plus petites que celle rapportées comme nocives pour les cellules mammaliennes. Les simulations CFD démontrent que la valeur maximale de tension de cisaillement se situe en tête de la vague de la surface libre. Les premières observations de dommage cellulaire dans un OSR d'1 L ont été faites à partir de 170 rpm ce qui correspond à une valeur maximale de tension de cisaillement de 0.2 Pa. Des bioprocédés opérés sans contrôleurs dans des OSRs ont été comparés avec des bioprocédés complètement contrôlés dans des bioréacteurs à cuve agitée (STRs). Les bioprocédés dans les OSRs étaient aussi efficaces que ceux dans les STRs. De plus, la variabilité de bioprocédés opérés sans contrôleur dans des OSRs de 5 L était inférieure ou égale à 10% pour la densité cellulaire, la concentration en protéine recombinante et les profils de pH et d'oxygène dissout. Ces résultats démontrent de manière générale que des bioprocédés peuvent être opérés sans contrôleur à des échelles allant de 50 mL à 200 L dans des OSRs.

Mots clés: Bioréacteur, Agitation orbitale, Culture de cellules mammaliennes, Bioréacteurs à usage unique, Transfert de gaz, Mélange, Hydrodynamique, Mécanique des fluides numériques, Mise à l'échelle.

Zusammenfassung

Die meisten heute erhältlichen Biopharmaka werden in Tierzellen erzeugt. Die weltweite Nachfrage nach monoklonalen Antikörpern (mAbs), einer spezifischen Untergruppe von Biopharmaka also, hat während des vergangenen Jahrzehnts erheblich zugenommen. MAbs werden vor allem in Krebs- und Autoimmunkrankheitstherapien eingesetzt. Für die Produktion voll funktionsfähiger Proteine sind deren entsprechende humanbiologische posttranslationale Modifikationen grundlegend. Dies wird durch die rekombinante Proteinproduktion der mAbs in Säugerzellen erzielt. MAbs werden in grossen Massen benötigt und säugerzellbasierte Proteinproduktion ist normalerweise teuer. Dementsprechend stehen Kosteneffizienz und vielseitige Anwendungsmöglichkeiten bei den gegenwärtig in der Medikamentenproduktion verwendeten Bioprozessen und auch bei der bioprozessbasierten Medikamentenforschung und Entwicklung an forderster Stelle. Geschüttelte Bioreaktoren (OSRs) basieren auf der Wegwerftechnologie (Einwegbioreaktoren) und sind deshalb sehr vielseitig. Diese Arbeit zielt darauf ab, unser Verständnis dieser Bioreaktoren zu verbessern, indem sie ihre Technikprinzipien wie das Mischen, die Gasübertragung und die Hydrodynamik im Bereich der Säugetierzellkultur studiert. Die Mischstudie zeigte, dass OSRs Homogenität der Säugerzellkultur bis 1500 L bei Mischzeiten unter 30 s garantieren. Der Mischvorgang und die Freioberflächenform eines 1500-L OSR wurden in einem 30-L OSR bei konstanten geometrischen Verhältnissen (Durchmesser des Bioreaktors, Schürhmesser und Flüssigkeitshöhe) und konstanter Froude-Zahl simuliert (auch nachgeahmt). Es wurde ein minimaler volumetrischer Stoffübergangskoeffizient für Sauerstoff (k_La) benötigt, um die Säugerzellkultur ohne Steuergerät, das den pH-Wert oder die aufgelöste Sauerstoffkonzentration kompensiert, laufen zu lassen. Dieser minimale k_La war zelllinienabhängig und etwa $7\text{-}10\text{ h}^{-1}$. Zellkulturen

mit dem gleichen k_La zeigten die gleichen Wachstumseigenschaften, sowie die gleichen rekombinanten Proteinkonzentrationen, Kulturstände (pH und DO) und Stoffwechselproduktprofile. Ein sondenunabhängiger Bioprozess wurde in einem 200-L OSR bei gleichem k_La wie 1- und 5-L OSRs ablaufen gelassen. Es wurden ähnliches Zellwachstum, ähnliche rekombinante Proteinkonzentration, pH und DO Profile wie in den drei OSRs beobachtet. Die Computerströmungslehre (CFD)-berechnete Scherspannung in einem 1-L OSR bei 110 U/min war eine bis zwei Größenordnungen niedriger als die säugerzellschädigende. Die CFD-Simulationen zeigten, dass sich die maximale Scherspannung in OSRs an der Wellenspitze befand, während die meisten Flusszonen Scherspannungswerte bis zu 0.075 Pa hatten. Zellschädigung wurde in einem 1-L OSR bei Schüttelgeschwindigkeiten ≥ 170 U/min mit maximalen Scherspannungswerten entsprechend 0.2 Pa gemessen. Sondenunabhängige Bioprozesse in OSRs wurden mit völlig kontrollierten Bioprozessen in Rührkesselbioreaktoren (STRs) verglichen. OSRs und STRs zeigten gleiche Bioprozesseffizienz. Ferner wurde eine sehr geringe Variabilität ($\leq 10\%$ für Zellwachstum, rekombinante Proteinkonzentration, pH und DO Profile) in sondenunabhängigen Bioprozessen in 5-L OSRs beobachtet. Zusammengefasst zeigen die in dieser Dissertation beschriebenen Ergebnisse, dass sondenunabhängige Bioprozesse in OSRs von 50 mL bis 100 L skalierbar sind.

Stichwörter: Bioreaktor, Orbital schütteln, Säugetierzellen, einweg Bioreaktor, Gasübertragung, Mischen, Scale-up, Hydrodynamik, Computerströmungslehre

Abstract

Most of the biopharmaceuticals nowadays are produced by animal cells. The worldwide demand for a specific group of biopharmaceuticals, the monoclonal antibodies (mAbs), has significantly increased this last decade. The mAbs are used as therapeutics in particular against cancer and autoimmune disorders. Most of the mAbs are produced as recombinant proteins by mammalian cells which ensure human-like post-translational modifications to obtain a fully functional product. However, bioprocesses with mammalian cells are usually expensive and the mAbs are needed in large amounts. As a consequence, highly flexible and cost-effective bioprocesses are required for new drug research and development as well as for the production of approved biopharmaceuticals. Orbitally shaken bioreactors (OSRs) are based on the disposable technology (single-use bioreactors) and are therefore very flexible. This work aims to improve our understanding of these bioreactors by studying their engineering principles such as mixing, the gas transfer and the hydrodynamics in the frame of mammalian cell culture. The mixing study showed that OSRs ensure homogeneity of the mammalian cell culture at scales up to 1500 L with mixing times below 30 s. By keeping the geometric ratios (shaking diameter, inner diameter and liquid height) and the Froude number constant, mixing and the free-surface shape of a 1500-L OSR could be mimicked in a 30-L OSR. A minimal volumetric mass transfer coefficient of oxygen (k_La) was required to operate mammalian cell culture without needing controllers to compensate the pH or the dissolved oxygen concentration (DO). This minimal k_La was cell-line dependent and typically in the range of 7-10 h⁻¹. Cultures with the same k_La showed the same growth characteristics, recombinant protein concentrations, culture conditions (pH and DO), and metabolite profiles. A probe-independent bioprocess was run in a 200-L OSR at the same k_La as 1- and 5-L OSRs.

Similar cell growth, recombinant protein concentration, pH and DO profiles were observed in the three OSRs. The shear stress level calculated by computational fluid dynamics (CFD) in a 1-L OSR at 110 rpm was one to two orders of magnitude lower than the one reported to damage mammalian cells. The CFD simulations showed that the maximal shear stress in OSRs was located at the tip of the wave, while most of the zones in the liquid had shear stress values below or equal to 0.075 Pa. Cell damage in a 1-L OSR was recorded at agitation rates ≥ 170 rpm which corresponded to maximal shear stress values of 0.2 Pa. Probe-independent bioprocesses in OSRs were compared side-by-side with fully controlled bioprocesses in stirred-tank bioreactors (STRs). The bioprocesses in OSRs were as efficient as those in STRs. Furthermore, a very low variability ($\leq 10\%$ for cell growth, recombinant protein concentration, pH and DO profiles) was observed for probe-independent bioprocesses in 5-L OSRs. Together, the results presented in this thesis demonstrate that probe-independent bioprocesses are scalable in OSRs from 50 mL to 100 L.

Keywords: bioreactor, orbital shaking, mammalian cell culture, disposable bioreactor, gas transfer, mixing, scale-up, hydrodynamics, computational fluid dynamics

Contents

Acknowledgments	i
Résumé	iii
Zusammenfassung	v
Abstract	vii
List of Figures	xii
List of Tables	xv
Nomenclature	xvii
1 Introduction	1
2 Aims of the study	11
3 Mixing	13
3.1 Introduction	13
3.2 Material and Methods	16
Equipment	16
Measurement of mixing time	17
Free surface shape	17
Laser Doppler Velocimetry measurements	17
3.3 Results	18
In-house software for mixing study	18
Effects of operating parameters on the mixing time	21

	Mixing regime and free-surface shape	27
	Scale-up factor for mixing	28
	Velocity field measurements	30
3.4	Discussion	30
4	Gas transfer	35
4.1	Introduction	35
4.2	Material and Methods	38
	Gas transfer through sterile closures	38
	Volumetric mass transfer coefficient of oxygen	38
	Cell culture	39
	Cell analysis	40
	Protein quantification and analysis	41
4.3	Results	42
	Sterile closure limitations	42
	k_La limitations	50
	k_La as a scale-up factor for probe-independent bioprocesses	56
	Probe-independent bioprocesses in large-scale bioreactors	61
4.4	Discussion	62
5	Hydrodynamic stress	65
5.1	Introduction	65
5.2	Material and Methods	66
	Shear stress and hydrodynamic simulation	66
	Cell culture	66
	Volumetric power consumption measurement	67
	Detection of cell damages	69
5.3	Results	69
	Hydrodynamic stress under usual cultivation conditions	69
	The P_V as a scale-up factor for shear stress level	71
	Effects of cell culture age	71
	Kinetics of cell death induced by shear stress	76
	Shear stress thresholds in 1-L OSRs	77
5.4	Discussion	80
6	Variability of probe-independent bioprocesses	83
6.1	Introduction	83
6.2	Materials and Methods	84
	Cell cultivation systems	84
	Mixing time measurements and mixing maps	85
	Volumetric mass transfer coefficient of oxygen	85

	Volumetric power consumption measurement	86
	Mammalian cell culture	86
	Protein quantification and analysis	87
6.3	Results	88
	Mixing times and mixing maps	88
	Oxygen transfer	88
	Volumetric power consumption	91
	Comparison between bioprocesses in STR and OSR	91
	Variability of non-controlled bioprocesses in OSR	101
6.4	Discussion	107
7	Conclusion	111
	Bibliography	115

List of Figures

1.1	FDA-approved biopharmaceuticals.	2
1.2	Therapy area distribution of FDA-approved mAbs.	3
1.3	Animal cell lines producing FDA-approved biopharmaceuticals.	4
1.4	Upstream process for biopharmaceutical production.	5
1.5	Simplified diagram of a stirred-tank bioreactor.	6
1.6	Simplified diagram of an airlift bioreactor.	7
1.7	Simplified diagram of a wave bioreactor.	8
1.8	Simplified diagram of an orbitally shaken bioreactor.	9
3.1	Laser Doppler Velocimetry principles.	15
3.2	Frame extraction during image analysis.	19
3.3	Color channel evolution in time during image analysis.	19
3.4	Mixing map of a 30-L cylindrical container at 110 rpm.	20
3.5	Correlation plot of measured and calculated mixing times.	21
3.6	Operating parameters of OSRs.	22
3.7	Effect of liquid height on mixing time.	23
3.8	Free surface shapes in a 30-L container at 80 and 95 rpm.	23
3.9	Effect of liquid height on mixing heterogeneity.	24
3.10	Effect of shaking diameter on mixing time.	25
3.11	Free-surface shapes in a 30-L container with a shaking diameter of 5 cm and 2.5 cm.	26
3.12	Effect of inner diameter on mixing time.	26
3.13	Correlation between free-surface shapes and mixing regimes.	28
3.14	Mixing times in a 1500-L OSR.	29
3.15	LDV measurements of fluid velocities in a 30-L cylinder.	31
4.1	Details of a 3-L STR.	36

4.2	Free surface in a 30-L OSR.	37
4.3	Pictures of screw and vented caps.	39
4.4	OSRs of nominal volumes of 1 L, 5 L, and 200 L.	41
4.5	Gas transfer resistance of screw and vented caps.	42
4.6	Cell density comparison between screw and vented caps.	44
4.7	Viability comparison between screw and vented caps.	44
4.8	Biomass volume comparison between screw and vented caps. . .	45
4.9	pH comparison between screw and vented caps.	45
4.10	Detailed comparison of cell growth and recombinant protein pro- duction between screw and vented caps.	46
4.11	Detailed comparison of oxygen profiles between screw and vented caps.	47
4.12	Detailed comparison of pH between screw and vented caps. . . .	48
4.13	Detailed comparison of metabolite profiles between screw and vented caps.	49
4.14	k_La values in cylindrical OSRs of 250 mL, 500 mL and 1 L. . . .	50
4.15	Effects of the k_La on cell growth.	52
4.16	Effects of the k_La on biomass accumulation.	53
4.17	Effects of the k_La on pH.	54
4.18	Effects of the k_La on DO.	55
4.19	Scalability of cell density based on k_La	57
4.20	Scalability of biomass accumulation based on k_La	58
4.21	Scalability of pH based on k_La	59
4.22	Scalability of DO based on k_La	60
4.23	Scalability of a probe-independent bioprocess in a 200-L bioreactor. .	61
5.1	Experimental set-up for P_V measurements in large-scale OSRs. .	68
5.2	Hydrodynamic stress in OSRs under standard conditions.	70
5.3	The P_V as a scale-up factor for mammalian cell culture.	71
5.4	Flow cytometry analysis of CHO cultures after 24 h at 110 rpm or at 200 rpm.	72
5.5	Effects of cell age on stress resistance assessed by the cell count- ing method.	73
5.6	Flow cytometry analysis of particle sizes measured by PCV method. .	74
5.7	Effects of cell age on stress resistance assessed by the biomass volume measurement method.	75
5.8	Effects of cell age on stress resistance assessed by the LDH de- tection method.	75
5.9	Kinetics of cell death induced by shear stress.	76
5.10	Relative cell growth rate of CHO cells in 1-L OSRs at various agitation rates.	77

5.11	CFD simulations of shear stress in 1-L OSRS at 150, 160, 170 and 180 rpm.	78
5.12	Histograms of the shear stress simulated by CFD in 1-L OSRs at 150, 160, 170 and 180 rpm.	79
6.1	Cell cultivation systems used in the comparison between stirring and orbital shaking.	85
6.2	Comparison of mixing between OSR and STR.	89
6.3	Comparison of gas transfer between OSR and STR.	90
6.4	Comparison of P_V between OSR and STR.	92
6.5	Comparison of CHO-TNFR cell growth between OSR and STR.	93
6.6	Comparison of CHO-TNFR culture conditions between OSR and STR.	94
6.7	Comparison of CHO-TNFR metabolite profiles between OSR and STR.	95
6.8	Comparison of CHO-TNFR recombinant protein production between OSR and STR.	96
6.9	Comparison of CHO-IgG cell growth between OSR and STR.	97
6.10	Comparison of CHO-IgG culture conditions between OSR and STR.	98
6.11	Comparison of CHO-IgG metabolite profiles between OSR and STR.	99
6.12	Comparison of CHO-IgG recombinant protein production between OSR and STR.	100
6.13	Variability of CHO-TNFR cell growth in non-controlled bioprocesses.	101
6.14	Variability of TNFR:FC production in non-controlled bioprocesses.	102
6.15	Variability of CHO-TNFR culture conditions in non-controlled bioprocesses	103
6.16	Variability of CHO-TNFR metabolite profiles in non-controlled bioprocesses	103
6.17	Variability of CHO-IgG cell growth in non-controlled bioprocesses.	104
6.18	Variability of IgG production in non-controlled bioprocesses.	105
6.19	Variability of CHO-IgG culture conditions in non-controlled bioprocesses.	105
6.20	Variability of CHO-IgG metabolite profiles in non-controlled bioprocesses.	106

List of Tables

1.1	Large-scale bioprocesses using animal cell lines.	6
3.1	Cylindrical containers used in the mixing time study.	16
3.2	Cylindrical containers used in the software development and validation.	18
6.1	Maximal variabilities measured during probe-independent bioprocesses.	106

Nomenclature

μ	Cell growth rate [h^{-1}]
ν	Kinematic viscosity [$\text{m}^2 \text{s}^{-1}$]
ρ	Fluid density [kg m^{-3}]
θ	Dimensionless mixing number [-]
A	Heat transfer area [$\text{m}^2 \text{m}^{-3}$]
a	Specific interfacial area [m^{-1}]
c^*	Dissolved oxygen concentration at saturation [M]
c_G	Concentration of oxygen in the gas phase [M]
c_G^*	Oxygen concentration of the surroundings [M]
c_L	Dissolved concentration of oxygen in the liquid phase [M]
C_p	Heat capacity [$\text{J m}^{-3} \text{K}^{-1}$]
D	Inner diameter of the container [m]
d	Inner diameter of the bioreactor [m]
d_i	Impeller diameter [m]
d_s	Shaking diameter [m]
Fr	Froude number [-]
g	Gravitational constant [m s^{-2}]

h	Liquid height [m]
k_{Ga}	Oxygen mass transfer coefficient in the gas phase [h^{-1}]
k_L	Mass transfer coefficient [m h^{-1}]
k_{La}	Volumetric mass transfer coefficient of oxygen [h^{-1}]
l	Characteristic length [m]
n	Agitation rate [rpm]
Ne	Newton number [-]
P	Power consumption [W]
P_V	Volumetric power consumption [W m^{-3}]
Re	Reynolds number [-]
T	Temperature of the water [K]
t	Time [h]
t_m	Mixing time [s]
T_{out}	Temperature of the surroundings [K]
U	Over-all heat transfer coefficient [$\text{J m}^{-2} \text{K}^{-1}$]
V	Working volume [m^3]
v	Characteristic velocity [m s^{-1}]
X	Cell density [million cells mL^{-1}]
AIID	Autoimmune and Inflammatory Disorders
anti-RhD IgG	Anti-rhesus D immunoglobulin
BHK	Baby hamster kidney
CFD	Computational fluid dynamics
CHO	Chinese hamster ovary
DISMT	Dual Indicator System for Mixing Time
DNA	Deoxyribonucleic acid

DO	Dissolved oxygen concentration
ELISA	Enzyme-linked immunosorbent assay
EPO	Erythropoietin
FDA	Food and Drug Administration
HEK	Human embryo kidney
ID	Infectious diseases
LDH	Lactate dehydrogenase
LDV	Laser Doppler Velocimetry
mAbs	Monoclonal antibodies
MW	Molecular weight
OSR	Orbitally shaken bioreactor
OTR	Oxygen transfer rate [$\text{mol L}^{-1} \text{ h}^{-1}$]
PCV	Packed cell volume
SDS-PAGE	Sodium dodecyl sulfate polyacrylamide gel electrophoresis
STR	Stirred-tank bioreactor
TNFR:Fc	Tumor necrosis factor receptor 2 fused with the Fc portion of a human IgG
tPa	Tissue plasminogen activator

Introduction

The history of animal cell cultivation started more than a century ago. In 1907, Ross Harrison cultivated small pieces of nerve fiber tissue from frog embryos for 30 days in a hanging drop under aseptic conditions (Harrison et al., 1907). This experiment showed that animal cells could be maintained and even grown in vitro (Harrison et al., 1907). However, the progresses in animal cell cultivation were limited for the next four decades due to sterility issues (Kretzmer, 2002). The discovery and development of antibiotics in the late 1940's was another important event in cell cultivation as it eased the handling of cell culture media which were biological fluids at this time (Kretzmer, 2002). In 1955, Eagle who studied extensively the requirements of cells in vitro established a chemically defined medium for mammalian cell culture (Eagle, 1955). This medium required however, the addition of undefined serum for proper cell growth and maintenance (Eagle, 1955). The first industrial process using animal cell cultivation was the production of the polio virus vaccine developed by Salk in 1954 (Salk et al., 1954). The cells used to produce the inactivated polio vaccine were primary cells isolated from monkey kidneys and were cultivated in roller bottles (multi-unit process) as adherent cultures (Duchene et al., 1990). In parallel, the establishment of permanent (immortalized) cell lines in the late 1950's which could be sub-cultivated indefinitely and grown in suspension paved the way for large-scale cultivation of animal cells (Puck et al., 1958). In the mid 1970's, a new type of cell lines called hybridoma were obtained by fusing murine lymphocytes with immortal myeloma cells (Köhler and Milstein, 1975). The resulting cells could produce antibodies against a specific antigen. This discovery led to an increasing production of monoclonal antibodies for diagnostic purpose because of a lower variability in comparison with the antibodies directly isolated from mice. However, these antibodies gen-

erated severe adverse immune reactions in humans because of their murine origin and could not be used as therapeutics. In the early 1980's, molecular cloning and recombinant DNA technologies allowed to stably insert a foreign gene into bacteria, yeast or animal cells to produce a recombinant protein. While the first recombinant protein commercialized as a drug was recombinant human insulin in 1982 produced in *Escherichia Coli* (Everett and Kerr, 1994), the first recombinant protein produced by animal cells was tissue plasminogen activator (tPa) in 1986 (Kretzmer, 2002). The tPa was produced by Chinese hamster ovary (CHO) cells stably transfected with the human tPa gene. This achievement opened the way for the next generation of recombinant proteins produced using animal cell technology including erythropoietin, blood factors and monoclonal antibodies (mAbs) (Hacker et al., 2010). In the last decade, the production of mAbs has significantly increased and represents nowadays 30% of the total biopharmaceutical production produced with animal cell technology (Fig. 1.1).

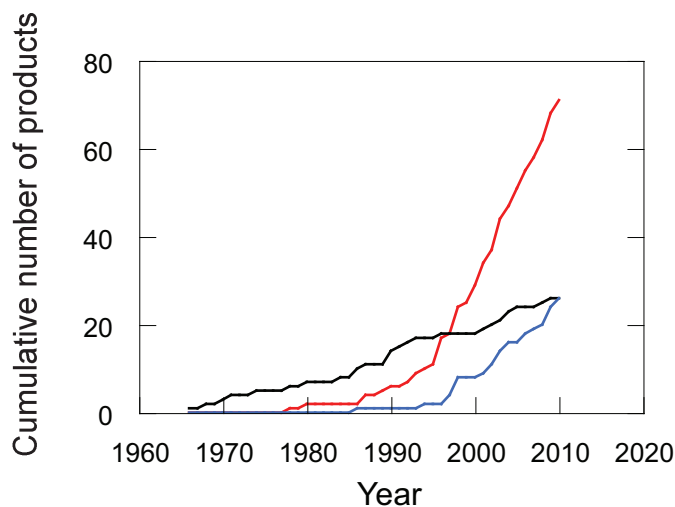


Fig. 1.1: Number of biopharmaceuticals approved by the FDA produced with animal cell technology (red) or derived from tissues or organs (black). Number of monoclonal antibodies produced with animal cell technology (blue). Adapted from ACTIP (2010).

The mAbs are able to target a wide range of antigens with a high specificity. As a consequence they are considered the best therapeutic candidates for several pathologies including cancers and immunological disorders

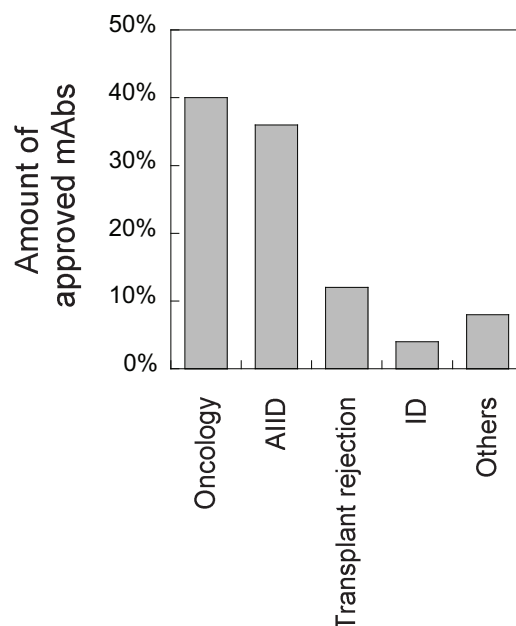


Fig. 1.2: Therapy area distribution of FDA-approved mAbs. AIID: Autoimmune and Inflammatory Disorders, ID: Infectious diseases. Adapted from ACTIP (2010).

(Fig. 1.2). The combined revenues of the mAbs in 2009 were over 35 billion dollars, according to the Datamonitor group (London, United Kingdom).

Interestingly, only a few cell lines produce the various biopharmaceuticals available on the market and the most common one is the CHO cell line (Fig. 1.3) (Hacker et al., 2010; Kelley, 2009). The mAbs approved by the FDA are mainly produced in mammalian cells because of their ability to have human-like post-translational modifications resulting in fully active products with a lower immunogenicity (Wurm, 2004).

Biopharmaceuticals produced by animal cells are expensive (ten thousand to one billion dollar/kg) and the demand usually small (1 kg/year for EPO in the USA in 1998). Consequently most of the recombinant proteins are traditionally produced in batch bioreactors at scales up to 10'000 L (Kretzmer, 2002). However, recombinant mAbs and vaccines are needed in higher amounts (100-1000 kg/year) (Kretzmer, 2002). This increasing demand is the driving force to the development of more cost-effective bioprocesses with higher yields to meet the worldwide demand at an affordable price (Kelley, 2009). While the batch mode is easy to scale up, its main

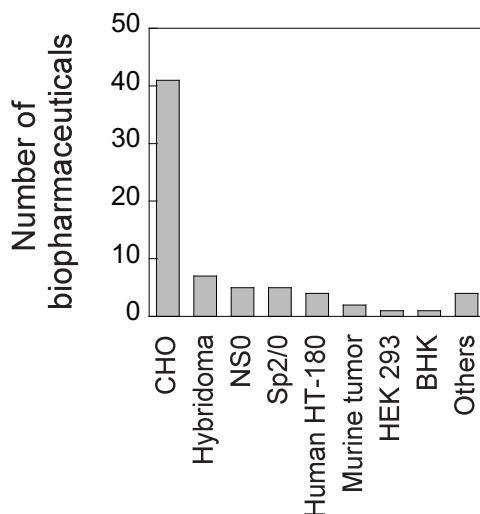


Fig. 1.3: Animal cell lines producing FDA-approved biopharmaceuticals. Adapted from ACTIP (2010)

inconveniences are the gradients of nutrients during the process and the accumulation of toxic metabolites (Rodrigues et al., 2010). The bioprocess yields can be improved by adding the required nutrients during the culture. This mode is known as the fed-batch mode and increases significantly the cell density and recombinant protein concentration in comparison with the batch mode (Rodrigues et al., 2010). Nevertheless, toxic metabolites are still not removed from the medium with the fed-batch mode. The continuous mode is not suitable for animal cells which have significantly lower growth rates than bacteria or yeasts. An alternative to the continuous mode is the cell retention which is known as the perfusion mode (Voisard et al., 2003). This mode allows detoxification of the bioreactors, but filter blocking and sterility maintenance over a long period of time are major drawbacks (Kretzmer, 2002). A volumetric productivity 10 times higher than for batch or fed-batch processes was reported for perfusion processes (Deo et al., 1996). This increase of yields leads to the use of smaller bioreactors for perfusion mode (Langer, 2009). However, the validation of perfusion bioprocesses is more time consuming and complex than the validation of batch cultures as the cultivation time can reach several months (185 days for the factor VIII produced by BHK cells by Bayer) (Kretzmer, 2002).

A large-scale bioprocess for recombinant protein production using animal cell technology is constituted of several steps (Fig. 1.4). After thawing a vial from the working cell bank, the inoculum is expanded into shaken flasks

or spinner flasks of an increasing size. The wave bioreactor equipped with a disposable bag is often used at the latest stage of operation of inoculum expansion before the seed bioreactors (Shukla and Thömmes, 2010). The cells are then transferred into the production bioreactor in which the oxygen and CO₂ concentrations, the pH and the temperature are controlled. At the end of the culture, the production medium is harvested to remove cells and cell debris prior the purification of the biopharmaceutical (downstream process).

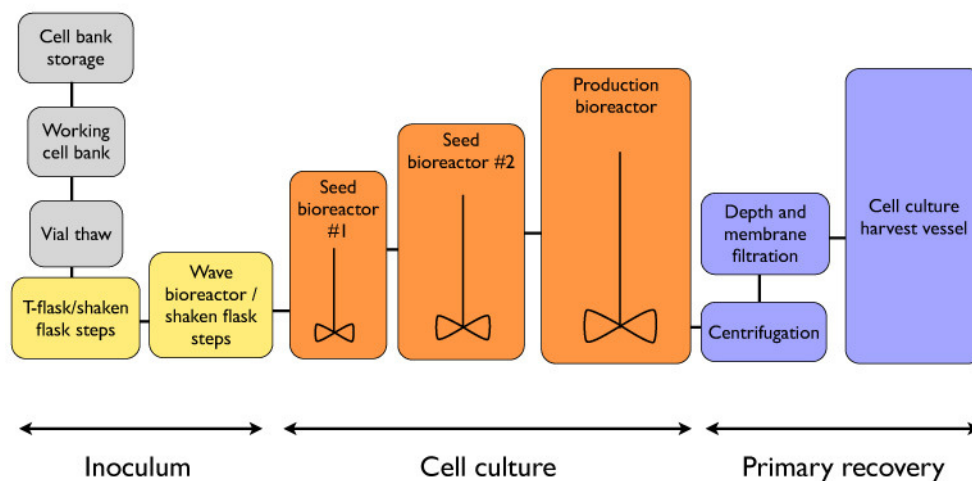


Fig. 1.4: Upstream process for biopharmaceutical production using animal cell lines. Adapted from Shukla and Thömmes (2010).

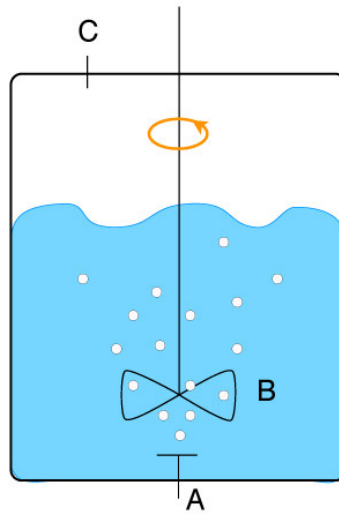
Most large-scale bioprocesses using animal cells are operated in stainless-steel stirred-tank bioreactors (STRs) (Table. 1.1) (Kretzmer, 2002). The STRs are equipped with impellers as agitation system and spargers to flush gases (air, oxygen, CO₂) in the culture medium (Fig. 1.5). These bioreactors have been used extensively in the past for microbial fermentation and are therefore better characterized with more familiar scale-up principles than other types of bioreactors (Rodrigues et al., 2010). This expertise also helps to obtain approval of production processes, as regulatory agencies are experienced with products obtained with these bioreactors. The STRs have been adapted to animal cell cultivation by modifying the impeller design and minimizing shear stress damage caused by gas sparging. However, gas transfer and homogeneity issues are often reported in large-scale STRs for

Table 1.1: Large-scale bioprocesses using animal cell lines. Adapted from Kretzmer (2002)

Scale (L)	Reactor	Cell line	Product
10'000	STR	BHK 21	Foot and mouth disease vaccine
10'000	STR	CHO	tPa
8'000	STR	Namalwa cells	Lymphoblastoid interferon
7'000	STR ^a	Bowes melanoma	tPa
2'000	Air-lift	Murine hybridoma	Monoclonal antibodies
1'000	STR ^a	Vero cells	Killed polio vaccine
1'000	STR	Murine hybridoma	Monoclonal antibodies
500	STR ^b	BHK	Factor VIII

^a Microcarrier cultures.^b Perfusion mode.

mammalian cell cultures as well as sterility issues due to the presence of invasive and moving components (Ozturk, 1996; Rodrigues et al., 2010).

**Fig. 1.5:** Simplified diagram of a stirred-tank bioreactor equipped with a sparger (A), an impeller (B) and a gas outlet (C).

Another type of bioreactor used for industrial bioprocesses is the air-lift bioreactor a particular type of bubble column. Gases are sparged at the bottom of the bioreactor to induce mixing and keep the cells in suspension with a circulating loop (Fig. 1.6). These bioreactors are less used than

STRs for mammalian cell cultivation as the know-how for scale-up and engineering principles is smaller. The fact that cells are highly sensitive to bubble rupture and mixing in air-lift bioreactors is ensured by bubble sparging may lead to limitations (Kretzmer, 2002). Furthermore, limited suitability for microcarrier cultivation has been reported for this type of bioreactor (Ozturk and Hu, 2006).

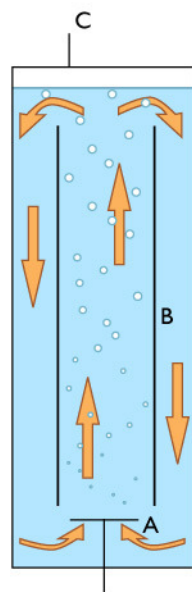


Fig. 1.6: Simplified diagram of an airlift bioreactor equipped with a gas sparging ring (A), baffles (B) and a gas outlet (C).

The wave bioreactor is one of the most common disposable bioreactor used as it was the first available on the market in 1999 (Eibl et al., 2010b; Singh, 1999). It consists of a plastig bag that sits on a rocking platform (Fig. 1.7). This bioreactor is limited in terms of size (1000 L) and is usually used for seed expansion and inoculation of the production bioreactors (Shukla and Thömmes, 2010).

The wave bioreactor opened a new way for disposable technology towards single-use bioreactors (Eibl et al., 2010a; Zhang et al., 2009b). Disposable bioreactors eliminate the risks of product cross contamination. As the sterilization and cleaning procedures are not needed anymore, the process validation is facilitated (Li et al., 2005). Furthermore, the initial investment for the material is lower for disposable than for stainless-steel

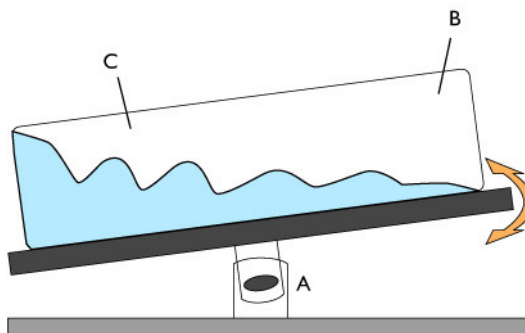


Fig. 1.7: Simplified diagram of a wave bioreactor equipped with a rocking platform (A), a gas inlet (B) and a gas outlet (C).

bioreactors (Pierce and Shabram, 2004). Nowadays, disposable STRs are also available on the market at scales up to 2000 L (Eibl et al., 2010a).

Orbitally shaken bioreactors (OSRs) are another type of disposable bioreactor based on the same agitation system as the shaken flasks (Fig. 1.8). No invasive components are used in the bag (no impeller or sparger). The agitation principle is the same as at small scale facilitating the scale-up of bioprocesses. A 200-L OSR is available on the market manufactured by Kühner AG (Birsfelden, Switzerland) and a larger prototype of 3500 L is currently under evaluation at ExcellGene SA (Monthey, Switzerland). OSRs are increasingly used for mammalian cell cultivation as an alternative to STRs, and optimization of the working conditions are becoming important issues (Muller et al., 2005; Stettler et al., 2007; Zhang et al., 2009b).

To further improve bioprocesses in orbitally shaken bioreactors, especially at large scale, a study of mixing, gas transfer and hydrodynamics in these bioreactors in the frame of mammalian cell cultivation was initiated. The first part of this thesis describes the mixing principles of OSRs at different scales. The second part reports experiments on gas transfer requirements for operating probe-independent bioprocesses in OSRs. We also tested the $k_L a$ as a scale-up factor at scales up to 200 L. In the third part of the thesis, we studied the hydrodynamics of OSRs and in the last chapter, we compared stirring and orbital shaking for mammalian cell culture at small scale.

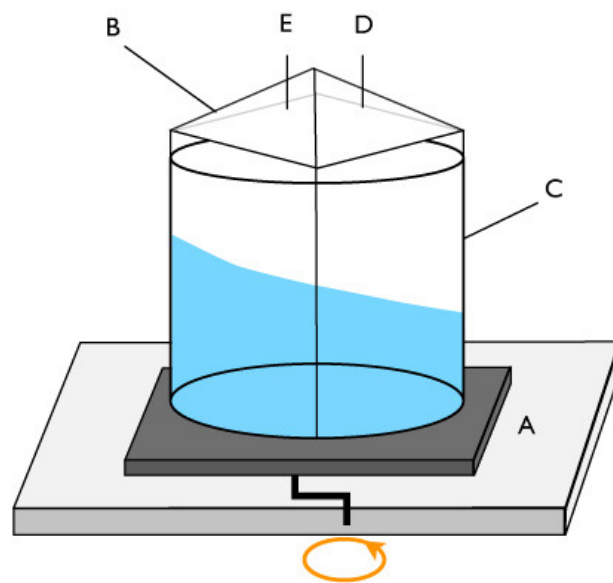


Fig. 1.8: Simplified diagram of an orbitally shaken bioreactor equipped with an orbital shaking platform (A), a single-use cell culture bag (B), an insulated stainless-steel cylindrical container with heating elements (C), a gas inlet (D) and a gas outlet (E).

Aims of the study

Orbitally shaken bioreactors (OSRs) have been reported to be scalable up to 2000 L for mammalian cell cultivation. However, their engineering principles are still poorly understood. To optimize the scale-up process, basic knowledge of transport phenomena such as mixing, gas transfer and hydrodynamic stress is required. Therefore the specific aims of this study were:

1. To describe mixing in orbitally shaken bioreactors and determine a scale-up factor.
2. To study the gas transfer and its implications for probe-independent bioprocesses, the final goal being to test the scalability of such bioprocesses in large-scale OSRs.
3. To investigate hydrodynamic and determine thresholds of shear stress for cell cultivation in OSRs.
4. To evaluate the variability of probe-independent bioprocesses in OSRs and compare their efficiency with fully controlled bioprocesses in stirred-tank bioreactors.

Mixing

3.1 Introduction

Mixing is a key engineering aspect in bioreactors as it ensures homogeneity of the culture (Micheletti et al., 2006). It can be defined as the use of mechanical energy to generate velocity fields for homogenization of concentrations. According to Beek and Miller (1959), mixing of liquids can be described in three steps:

- i Dispersal of a fluid into the other and uniformization of average composition by convection (macro-mixing). This occurs without decreasing local concentration gradients.
- ii Increase of contact between regions of different composition by turbulence.
- iii Decrease of local concentration gradients by molecular diffusion (micro-mixing).

In this chapter, we will focus on macro-mixing in orbitally shaken bioreactors (OSRs). We will identify the poorly mixed zones and assess the concentration gradients that cells may encounter. The mixing intensity of bioreactors is evaluated by measuring the mixing time, defined as the time needed to achieve a specified degree of homogeneity in the liquid (Zlokarnik, 2003). Methods for the measurement of the mixing time can be divided into local and global types. Local methods, based on physical measurements (pH and conductometry), are intrusive and provide information on mixing only where the probe is situated. In contrast, global methods (Schlieren and colorimetric) are not intrusive and provide global information on differentially

mixed zones in a reactor (Hiby, 1981; Kaoppel, 1979; Kasat and Pandit, 2004). However, the global methods are considered subjective and less precise than the local methods because they are usually performed visually. The Dual Indicator System for Mixing Time (DISMT) is a colorimetric method using an acid/base reaction in the presence of two pH indicators rather than one (Melton et al., 2002). With this method, the mixing time is defined as the time needed for the liquid to become completely yellow, corresponding to 95% of the infinite mixing time (Melton et al., 2002). This method improves the resolution during experiments since the liquid appears yellow only when it is mixed within a 5% deviation of the infinite mixing time (Melton et al., 2002). It also allows the identification of zones with different mixing times (Cabaret et al., 2007; Koynov et al., 2007), and it can be used at different scales, as long as the liquid in the container is visible.

Mixing studies in large-scale bioreactors are important, because the mixing time usually increases with the bioreactor scales (Lara et al., 2006; Xing et al., 2009). Contrary to chemical processes, the mixing time is generally not kept constant during the scale-up of bioreactors for animal cell cultures, as short mixing times (few seconds) are unnecessary for slow biological reactions (Junker, 2004; Xing et al., 2009). Furthermore if the mixing time is kept constant during the scale-up of stirred-tank bioreactors, the volumetric power consumption increases as the 2/3-th power of the bioreactor volume ($P_V \propto V^{2/3}$) leading to values detrimental for the cells (Ju and Chase, 1992). For these reasons, longer mixing times and the formation of concentration gradients are often observed in large-scale bioreactors for animal cell culture (Lara et al., 2006; Xing et al., 2009).

To extrapolate transport phenomena such as mixing from small- to large-scale bioreactors, dimensionless groups are commonly used (Mithani et al., 1990; Verma et al., 2007). Dimensional analysis shows that the dimensionless mixing number (θ) is in principle dependent on both the Reynolds (Re) and Froude (Fr) numbers. θ represents the number of rotations necessary to obtain homogeneity (Zlokarnik, 2003). Re represents the ratio of inertial to viscous forces and is described by Eq. 3.1:

$$Re = \frac{vl}{\nu} \quad (3.1)$$

where v and l denote the characteristic velocity [m s^{-1}] and length [m] and ν the kinematic viscosity [$\text{m}^2 \text{s}^{-1}$]. Fr represents the ratio of inertia and gravity forces and is defined as follows (Eq. 3.3):

$$Fr = \frac{v}{\sqrt{gl}} \quad (3.2)$$

where g is the gravitational constant [m s^{-2}]. However, in stirred-tank bioreactors equipped with baffles to avoid vortex formation and in laminar or transitional flow regimes, θ is assumed to be a function of Re only as the free surface is approximately flat (Yamaguchi, 2008). On the other hand, for agitated systems with a vortex or a non-flat free surface as in OSRs, Fr must also be taken into account since it describes the effect of the wave at the free surface (Rushton, 1952).

Mixing is related to the velocity fields, thus their measurement may help to characterize the agitation system. Laser Doppler Velocimetry (LDV) is a non intrusive method that measures fluid velocity in a section of the fluid. Two laser beams are focused at a defined location of the fluid called the control volume (Fig. 3.1). The two laser beams interfere with each other

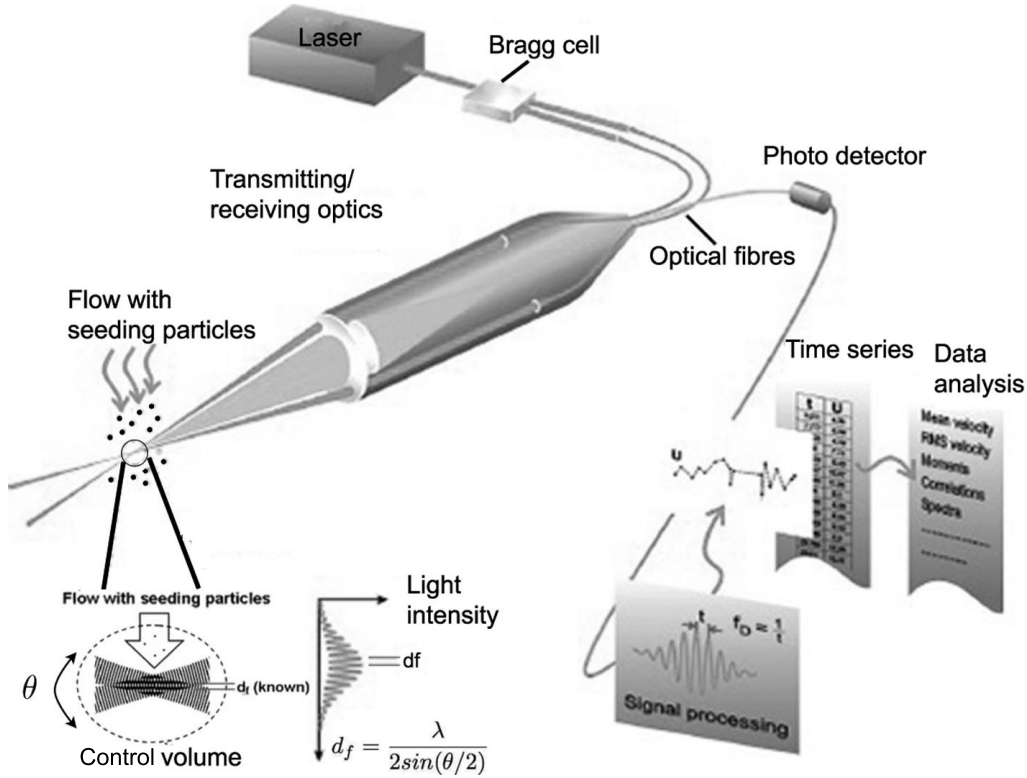


Fig. 3.1: Laser Doppler Velocimetry principles. Adapted from Dantec Dynamics A/S, Skovlunde, Denmark.

leading to low and high intensity zones in the control volume defined as fringes. Fluorescent particles of similar density as the liquid are added into it. When these particles cross the control volume, the scattered light

varies in intensity with a frequency (Doppler frequency) proportional to the velocity of the particle (Fig. 3.1). Knowing the distance between two fringes and the time between two intensity peaks, the velocity of the particle can be calculated. To detect a particle at rest or distinguish two particles moving at the same speed but in opposite directions, the system is equipped with a Bragg cell which moves the fringe pattern at a constant velocity by inducing a frequency shift (Fig. 3.1).

In this chapter, we describe mixing and its scalability in orbitally shaken cylindrical bioreactors used for mammalian cell culture. The effects of various operating parameters on the mixing time were investigated at volumetric scales up to 30 L. From these results, a scale-up factor was determined and validated in a 1500-L OSR. The velocity fields of a 30-L cylindrical container were investigated by LDV and compared to the mixing time measurements.

3.2 Material and Methods

Equipment

Studies on the factors influencing the mixing time in OSRs were carried out in different transparent cylindrical containers (Table 3.1). The containers were agitated on an ES-W shaker (Adolf Kühner AG, Birsfelden, Switzerland) with a shaking diameter of 5 cm unless otherwise stated.

Table 3.1: Characteristics of the cylindrical containers used in the mixing time study.

Nominal volume (L)	Inner diameter (cm)	Height (cm)	Material	Source
2	10	25	PP ^a	VitLab GmbH
2	13	15	Glass	Schott AG
3	16 ^b	15	PP ^a	VitLab GmbH
30	28.7	46	PMMA ^a	In-house
1500 ^c	125	122	LDPE ^a	Sartorius AG

^a PP: polypropylene, PMMA: polymethylmethacrylate, LDPE: low-density polyethylene.

^b Diameter measured at the bottom of the container. At the top, the diameter was 17 cm.

^c A single-use polyethylene bag of 1500 L was inflated and fitted into a stainless steel cylindrical container mounted on a prototype shaker (Adolf Kühner AG).

Measurement of mixing time

The mixing time was measured by DISMT using two pH indicators as described (Melton et al., 2002). Stock solutions of 0.92 mg/mL thymol blue (AppliChem GmbH, Darmstadt, Germany) and 1.01 mg/mL methyl red (Fisher Scientific, Pittsburgh, PA) were prepared in 70% ethanol. For each experiment, the dyes were each used at a final concentration of 4.3 mg/L in deionized water at room temperature. The solution was acidified by adding a defined volume of 5 M HCl: 10 μ L for the 2- to 3-L containers, 0.1 mL for the 30-L container, and 10 mL for the 1500-L container. White paper was placed behind and at the bottom of the containers to improve color visibility. The mixing time was determined upon rapid addition (less than 1 s) of a stoichiometric amount of 5 M NaOH from a fixed position at the vessel wall. All the mixing times reported here were measured visually, and each mixing experiment was performed in triplicate.

The DISMT method enables the visualization of the different mixing zones during the mixing process. This information may help to understand better the mixing principles of OSRs if it can be captured for further analysis. Mixing experiments were therefore recorded in real-time with a digital video camera (PowerShot A640, Canon) at 30 frames per second and an image analysis software was developed to visualize the mixing zones of such bioreactors.

Free surface shape

The free surface recording and analysis were performed by Matthieu Dreyer at the Laboratory of Hydraulic Machines (LMH), EPFL, Switzerland. The free surface shape was recorded with a fast camera during at least 3 rotations. Frames were extracted from the resulting films and analyzed with an in-house image processing software developed in Matlab (The MathWorks, Inc., Natick, USA). The free surface shape was reconstructed into a 2D view where the evolution of the wave during a complete rotation was represented from the left to the right. This representation was obtained by taking a zone of a few pixels located at the center of the container in all the frames and by joining them. To improve the contrast at the gas-liquid interface, some milk was added to the water at a concentration of about 1%.

Laser Doppler Velocimetry measurements

The velocity fields of a 30-L cylindrical container were investigated by Matthieu Dreyer and Martino Reclari at the LMH with Laser Doppler Ve-

locimetry (LDV). The 30-L container was filled with water to a height of 20 cm and tracking particles (hollow glass spheres) with a diameter of $10\text{ }\mu\text{m}$ and a density of 1.1 kg/L were added to water. A Laser Doppler Velocimeter (Dantec Dynamics A/S, Skovlunde, Denmark) was used to obtain the axial (upward), radial and tangential velocities along a radius of the container. The beam convergence was obtained with a 250-mm focal-length lens, giving a control volume of $1.3\times 0.07\times 0.07\text{ mm}^3$ in the liquid.

3.3 Results

In-house software for mixing study

Software development for mixing map generation

The software was developed for video image analysis and evaluated as previously described (Cabaret et al., 2007). According to the red, green and blue (RGB) color system, the values for each color channel can range from 0 to 255. The level of mixing was determined by the evolution of RGB color channels of the pixels representing the liquid. To develop and validate the in-house software, mixing experiments were performed and recorded in containers from 1 to 30 L (Table 3.2).

Table 3.2: Geometrical features of the cylindrical containers used in the software development and validation.

Nominal volume (L)	Inner diameter (cm)	Working volume (L)	Agitation rate (rpm)	Material	Source
1	10.1	0.1-0.4	90-130	Glass	Schott AG
2	13.6	0.1	110-150	Glass	Schott AG
5	18.1	1	126-168	Glass	Schott AG
30	28.7	12	80-120	PMMA	In-house

To illustrate the different steps of the in-house software development, a mixing experiment in the 30-L container with a liquid height of 16 cm, an agitation rate of 110 rpm, and a shaking diameter of 5 cm was used as an example. First, the frames corresponding to each complete rotation of the bioreactor were extracted from the videos in such a way that the vessel and the free surface were in the same position in all frames (Fig. 3.2). The evolution of the three color channels was plotted against time for several

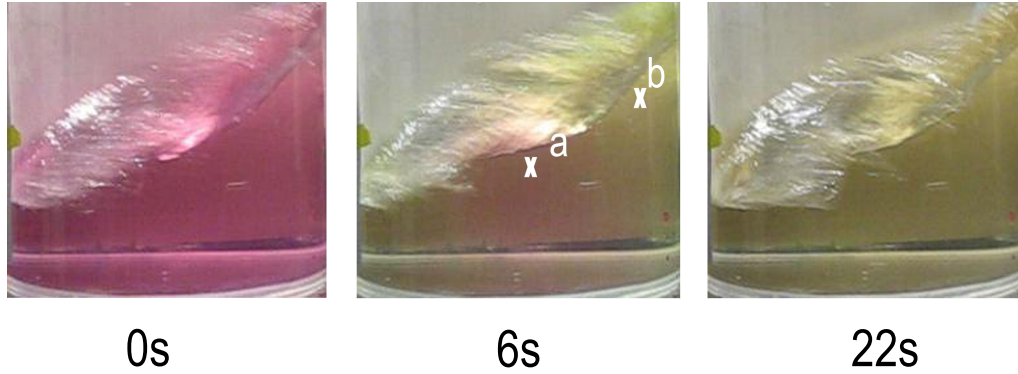


Fig. 3.2: Mixing experiment in a 30-L cylindrical container at 110 rpm with a liquid height of 16 cm and at a shaking diameter of 5 cm. Several frames corresponding to complete rotations extracted from the video of the mixing experiment at the times indicated.

pixels situated in different mixing zones (Fig. 3.3). The green channel varied the most during the experiments (Fig. 3.3). The brightness of the green channel increased during the mixing process until it reached a plateau corresponding to the mixed state of the pixel (Fig. 3.3). For a pixel situated in a poorly mixed zone like pixel 'a' in Fig. 3.2, the plateau was reached

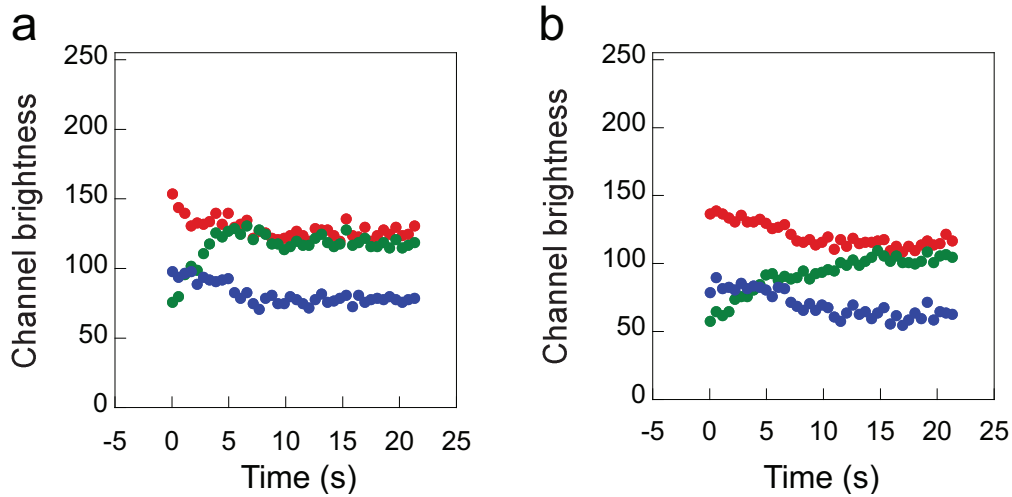


Fig. 3.3: Mixing experiment in a 30-L cylindrical container at 110 rpm with a liquid height of 16 cm and at a shaking diameter of 5 cm. Color channel evolution in time of the two pixels highlighted in Fig. 3.2. Red dots represent the red channel, green dots the green channel and blue dots the blue channel.

later (Fig. 3.3a) than for a pixel in the most rapidly mixed zone like pixel ‘b’ in Fig. 3.2 (Fig. 3.3b). Once the plateau was reached, the value of the green channel varied little (Fig. 3.3). A level of tolerance within which a pixel was considered mixed was then selected on a statistical basis. The mixing time of a pixel was defined as the time when the difference between the green channel value of the pixel differed by $\pm 3\%$ or less from the green channel value of the same pixel after complete mixing of the liquid.

The video image analysis of the mixing experiments by the in-house software was carried out in several steps. Once the frames corresponding to each complete rotation of the bioreactor were extracted from the videos, the software compared the first and last frames in each series to select the pixels to be analyzed. Only the pixels with a difference of at least 30 in green channel brightness were selected, and the pixels which were too close to the free surface were removed. Finally, the software analyzed the evolution in time of the green channel brightness and attributed the corresponding mixing time to each pixel. Colors were assigned to a range of times to obtain a mixing map, a color representation of the time needed for each pixel in the bioreactor to reach its final state (Fig. 3.4).

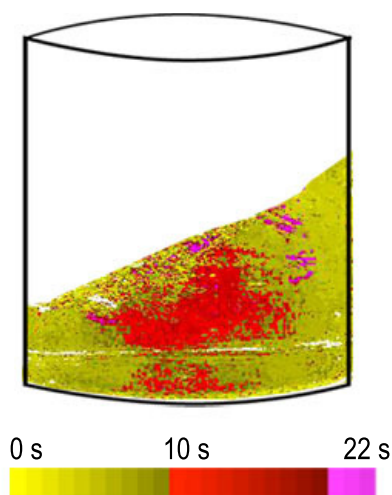


Fig. 3.4: Mixing map of a 30-L cylindrical container at 110 rpm with a liquid height of 16 cm and a shaking diameter of 5 cm. The bar below the mixing maps indicates the association between color and mixing time.

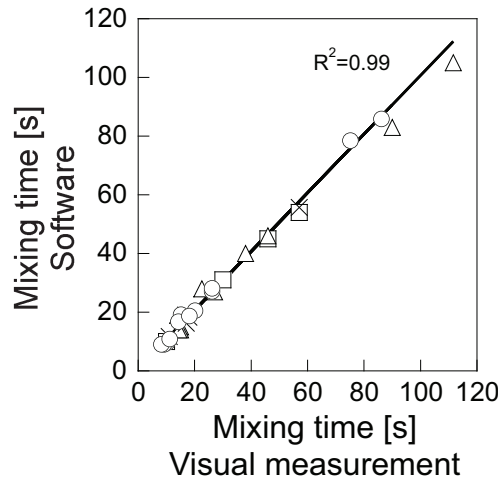
The software also measured the mixing time (i.e. the time needed to achieve homogeneity in the whole liquid), which was set as the time needed for the last pixel in the liquid to reach its final state. This value was

compared to the mixing time measured visually for the validation of the software.

Software validation

The software was validated by comparing the calculated mixing times with the mixing times obtained visually during the same experiment. Vessels from 1 to 30 L were tested at various agitation rates, working volumes, and at shaking diameters from 1.25 to 5 cm (Table 3.2).

The mixing times measured visually and those obtained using the software showed a correlation coefficient of 0.99 (Fig. 3.5). The correlation between the mixing times obtained visually or with the software was independent of the scale in vessels from 1 to 30 L (Fig. 3.5). The plastic or the glass material did not affect this correlation either. We therefore considered the software as valid for mixing time measurements and used it to further study mixing principles (Fig. 3.5).



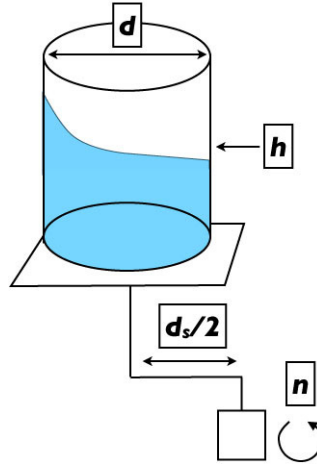


Fig. 3.6: Operating parameters of OSRs. Where n represents the agitation rate, h the liquid height, d_s the shaking diameter, and d the inner diameter.

d [m] (Fig. 3.6). These parameters were tested in a range of agitation rates specifically adapted for mammalian cell cultures. Since mammalian cells are cultivated in aqueous media with water-like viscosities, we assumed that the mixing experiments performed in water were a good approximation for mixing in cell culture media.

Effect of the liquid height

A 30-L cylindrical container was filled to liquid heights of 12, 20, and 28 cm, corresponding to 8, 13, and 18 L, respectively. The mixing time for each condition was measured at agitation rates from 80 to 130 rpm. For each liquid height, the mixing time decreased as the agitation rate increased from 80 to 95 rpm (Fig. 3.7). At higher agitation rates the mixing time tended to 10 s for all the liquid heights, and the slope of the curve tended towards 0 (Fig. 3.7). The liquid height affected the mixing time, but only at agitation rates lower than 95 rpm. At agitation rates of 95 rpm and higher, it did not have a noticeable effect on the mixing time (Fig. 3.7).

Interestingly, for all three liquid heights tested, similar free-surface shapes were observed at the same agitation rate. The height of the wave formed by the free surface was also similar at each liquid height. As the agitation rate increased, the free surface was more disturbed with an increasing amount of air bubbles entrained into the liquid. The sudden slope changes of the

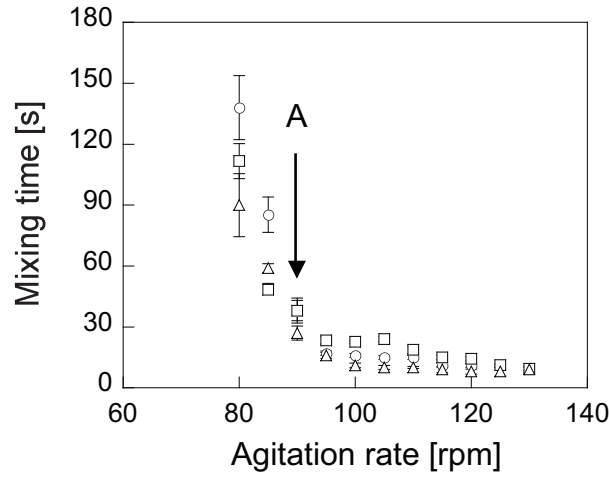


Fig. 3.7: Effect of liquid height on mixing time. The mixing time was measured by DISMT in a 30-L container with a liquid height of 28 cm (\circ), 20 cm (\square), or 12 cm (\triangle). The transition from a smooth to a rough free surface is marked (A).

mixing time curves at 95 rpm were associated with noise emission, which probably originated from entrained air bubbles (Fig. 3.8).

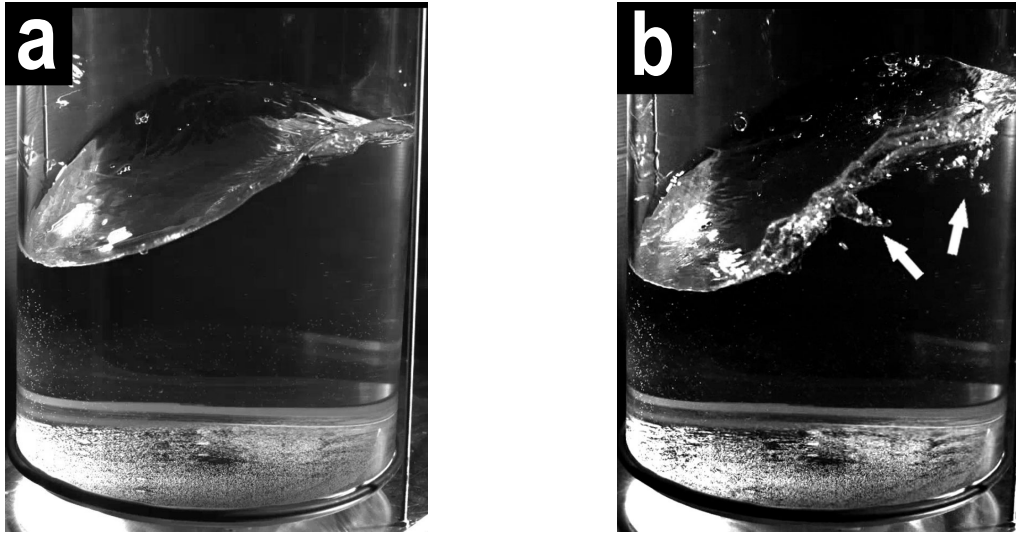


Fig. 3.8: Free surface shapes in a 30-L container at 80 (a) and 95 rpm (b). The pictures were extracted from fast-camera movies. The liquid height was 20 cm and the shaking diameter 5 cm.

With a liquid height of 28 cm and at agitation rates from 80 to 85 rpm, a zone appeared in the liquid close to the bottom of the container which seemed to mix mainly by diffusion. At these agitation rates, the height of the wave formed by the free surface was about 7 cm, which was less than half the liquid height at rest (28 cm). The height of the wave increased with the agitation rate and the diffusional zone close to the bottom of the container gradually diminished. As the height of the wave reached about 14 cm, half the liquid height at rest, the diffusional zone disappeared.

For the three liquid heights tested, a poorly mixed zone (darker zone) was observed in the center of the bulk liquid, while the most rapid mixing (lighter zone) was seen at the wall of the container, as judged from mixing maps (Fig. 3.9). At an agitation rate of 120 rpm, the mixing maps displayed the same mixing zones for all three liquid heights. Thus at this agitation rate, the mixing regime was independent of the liquid height (Fig. 3.9).

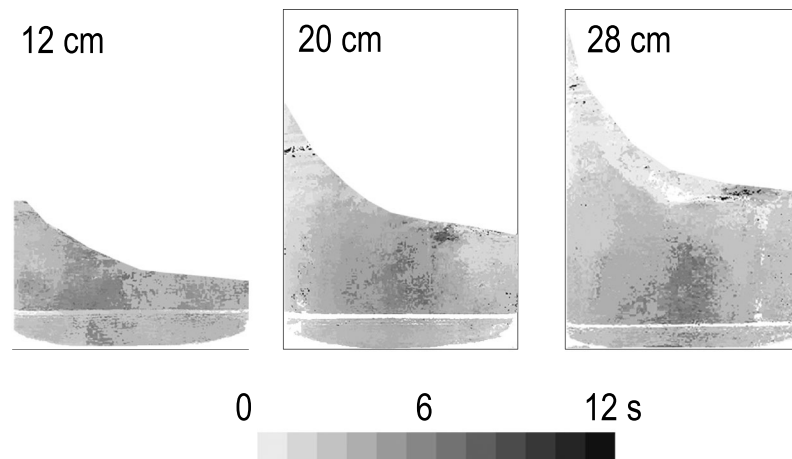


Fig. 3.9: Effect of liquid height on mixing heterogeneity. Mixing time measurements using DISMT were performed in a 30-L container with liquid heights of 12, 20, and 28 cm at an agitation rate of 120 rpm and were filmed in real time. Subsequent image analysis resulted in mixing maps associating a given mixing time to a given color. The bar below the mixing maps indicates the association between color and mixing time.

Effect of the shaking diameter

A 30-L cylindrical container was filled to a height of 20 cm. As the shaking diameters of the ES-W shaker (Adolf Kühner AG) have fixed values (2.5 and 5 cm), the mixing time was measured at these two shaking diameters and at agitation rates from 90 to 140 rpm. At agitation rates lower than

115 rpm, the mixing times at a shaking diameter of 5 cm were less than those at a shaking diameter of 2.5 cm (Fig. 3.10). In contrast, at agitation rates of 115 rpm and higher, no significant difference in mixing time was observed between the two shaking diameters (Fig. 3.10).

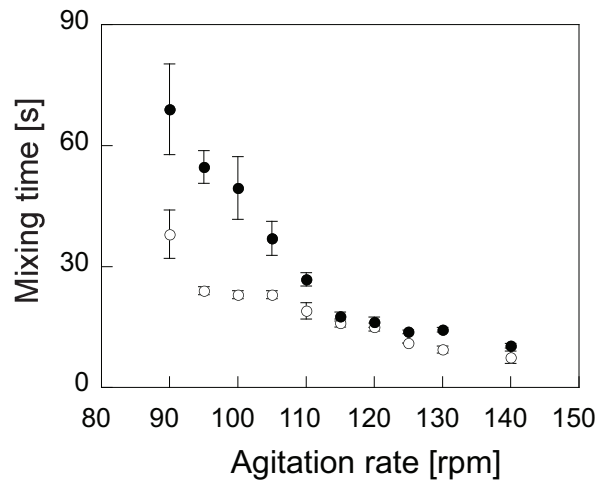


Fig. 3.10: Effect of shaking diameter on mixing time. The mixing time was measured by DISMT in a 30-L container with a shaking diameter of 5 cm (○) or 2.5 cm (●). The liquid height was 20 cm.

At shaking diameters of 5 and 2.5 cm, the transition from a smooth to a rough free surface occurred at 95 rpm and 115 rpm, respectively. Additionally, the free-surface shapes were different at the two shaking diameters (Fig. 3.11). With a shaking diameter of 5 cm a double-peaked wave was observed at agitation rates from 90 to 100 rpm (Fig. 3.11a). With a shaking diameter of 2.5 cm a single-peaked wave appeared at agitation rates from 90 to 110 rpm (Fig. 3.11b). A breaking wave, which was sharper and larger at the shorter shaking diameter, appeared at 90 and 100 rpm with shaking diameters of 5 and 2.5 cm, respectively (Fig. 3.11).

Effect of the inner diameter of the container

Three cylindrical containers with nominal volumes of 2 or 3 L and inner diameters of 10, 13, and 16 cm were filled to a working volume of 1 L, and the mixing time was measured at agitation rates from 100 to 140 rpm. The shortest mixing times were observed in the container with the largest diameter, while the container with the smallest diameter had the longest

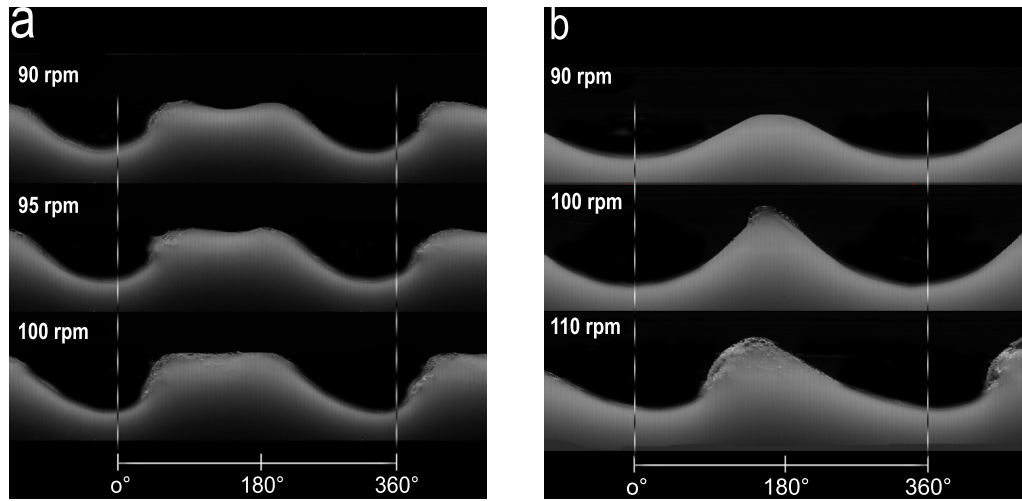


Fig. 3.11: Free-surface shapes in a 30-L container with a shaking diameter of 5 cm (a) and 2.5 cm (b). The liquid height was 20 cm. Courtesy of Matthieu Dreyer, LMH, EPFL.

mixing times over the range of agitation rates tested (Fig. 3.12). However, the differences between the mixing times of the three containers decreased as the agitation rate increased (Fig. 3.12).

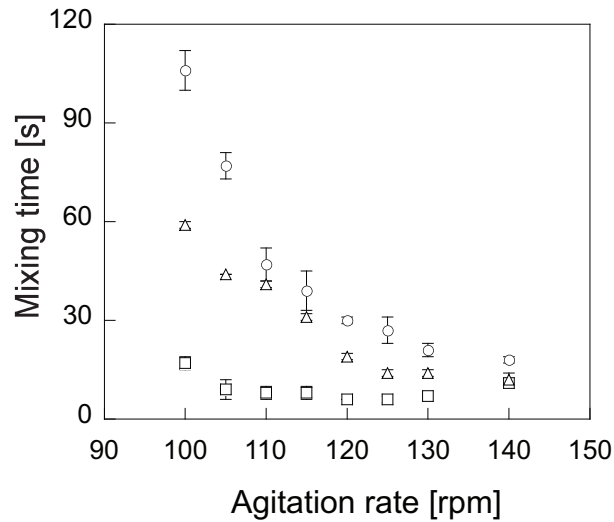


Fig. 3.12: Effect of inner diameter on mixing time. The mixing time was measured by DISMT in three containers with inner diameters of 10 cm (\circ), 13 cm (Δ) and 16 cm (\square). The working volume was 1 L.

Different free-surface shapes were observed in the three containers at the same agitation rate. The transition from a smooth to a rough free surface occurred at 115 and 130 rpm in the containers with inner diameters of 16 and 13 cm, respectively. This transition correlated with a change of the slope of the mixing time (Fig. 3.12). Such a transition was not observed in the container with an inner diameter of 10 cm at the agitation rates tested. At agitation rates up to 110 rpm we distinguished a diffusional zone close to the bottom of this container as described in Section 3.3. This zone disappeared at 120 rpm as the height of the wave formed by the free surface reached 6 cm, corresponding to half the liquid height at rest (12 cm). This confirmed the previous observation that the depth of mixing is about twice the height of the wave formed by the free surface.

Mixing regime and free-surface shape

The previous results suggested a strong correlation between the mixing capacity and the free-surface shape. To further investigate this point, we used a 30-L container filled to a height of 20 cm with water and agitated with a shaking diameter of 5 cm. We considered the Froude number (Fr), which represents the ratio of inertia and gravity forces and which is defined as follows (Eq. 3.3):

$$Fr = \frac{v}{\sqrt{gl}} \quad (3.3)$$

where v and l denote the characteristic velocity [m s^{-1}] and length [m], and g the gravitational constant [m s^{-2}]. For OSRs, the tangential velocity was defined as the characteristic velocity, and the inner diameter of the container (d) was considered the characteristic length as the centrifugal forces were assumed to be predominant (Eq. 3.4).

$$Fr = \frac{2\pi n(d + d_s)/2}{\sqrt{gd}} \quad (3.4)$$

In the 30-L container, the transitions of the mixing regime were observed at the same agitation rates as the transitions of the free-surface shape (Fig. 3.13). At $Fr \leq 0.7$, a flat free-surface shape was observed and the mixing regime was essentially diffusional with more slowly mixed zones situated close to the surface (Fig. 3.13a). The mixing time under these conditions was about 4.5 min. At $Fr = 0.8$, a double-peaked wave appeared and the mixing time was reduced to about 1 min (Fig. 3.13b). Under these conditions, the more slowly mixed zones were situated in the middle and at the bottom of the bulk liquid. At $Fr = 0.9$, turbulence and small vortices were

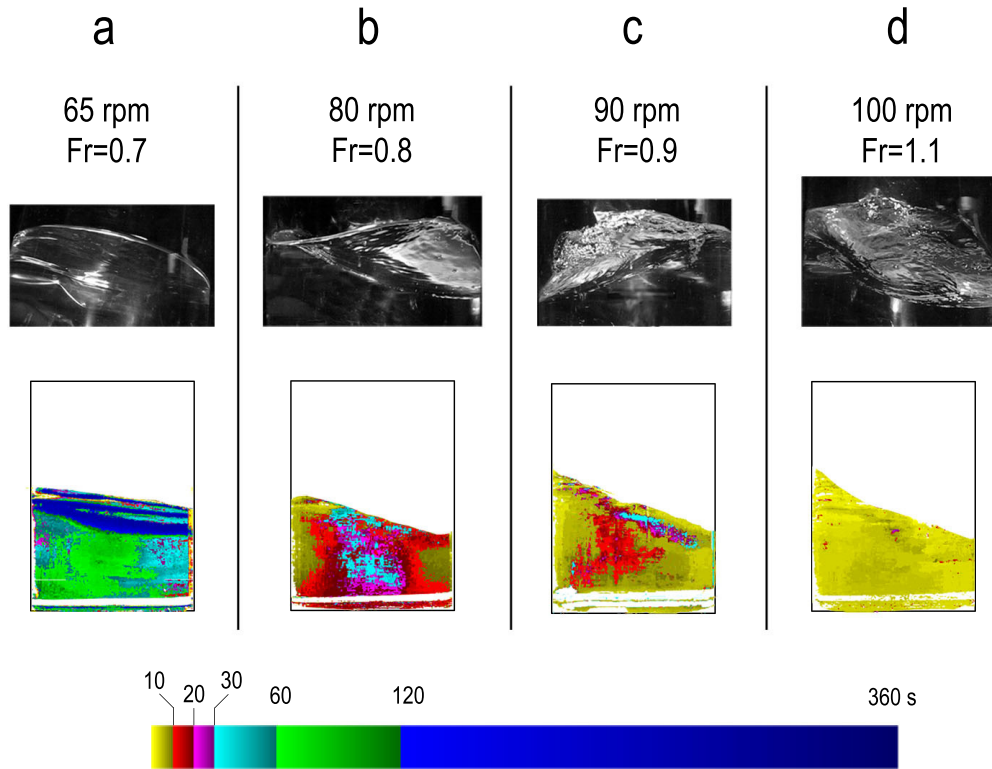


Fig. 3.13: (1st line) Images of the free-surface shape at different agitation rates in a 30-L cylindrical container with a liquid height of 20 cm. The shaking diameter was 5 cm. (2nd line) Mixing time measurements using DISMT were performed at the corresponding agitation rates and filmed in real time. Subsequent image analysis resulted in mixing maps associating a given mixing time to a given color as indicated by the bar below the mixing maps.

observed at the surface and the mixing time decreased to 30 s (Fig. 3.13c). The more slowly mixed zones were observed only in the center of the bulk liquid. At $Fr \geq 1.1$, a vortex was observed in the middle of the free surface and the mixing time reached its lowest value of about 10 s (Fig. 3.13d).

Scale-up factor for mixing

The results described above demonstrated that in orbitally shaken cylindrical bioreactors, the inner diameter of the container and the shaking diameter are the two geometric factors which significantly affect the mixing and the free-surface shape. Therefore, we hypothesized that by maintaining a constant d/d_s ratio, we could mimic the mixing regimes and the free-surface shapes of large-scale OSRs at a smaller scale.

To test the geometric ratio d/d_s as a scale-up factor for mixing, mixing times were measured in cylindrical containers of 1500 L and 30 L. Since the shaker supporting the 1500-L container has a defined shaking diameter of 10 cm, the shaking diameter of the 30-L container was changed to 2.5 cm to keep the d/d_s ratio about 12. To validate our hypothesis, mixing times were also measured in the 30-L cylinder with a shaking diameter of 5 cm which corresponded to a d/d_s ratio about 6. The working volume was 33% of the nominal volume in all the containers since this is the typical volume used for cell cultivation. The dimensionless mixing number θ was normalized by the ratio of the shaking diameter of the 30-L container to the shaking diameter of the 1500-L bioreactor (Eq. 3.5).

$$\theta = nt_m \left(\frac{d_s}{d_{s,1500L}} \right) \quad (3.5)$$

The mixing time in the 1500-L OSR decreased from 70 s to 15 s as the agitation increased from 40 to 50 rpm (Fig. 3.14a). At higher agitation

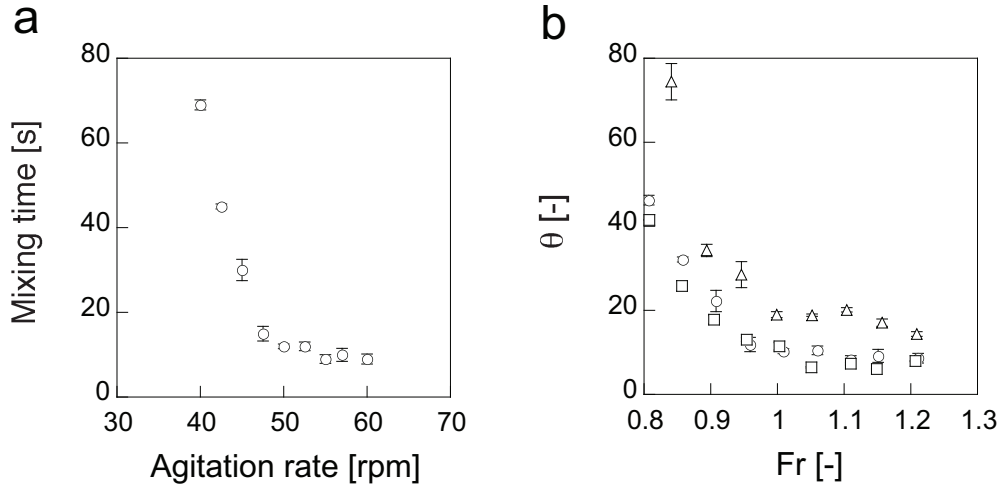


Fig. 3.14: (a) Mixing times in a 1500-L OSR with a working volume of 500 L and a shaking diameter of 10 cm. The mixing time was measured by DISMT. (b) Mixing numbers in a 1500-L at a shaking diameter of 10 cm (\circ) and in a 30-L container with shaking diameters of 2.5 cm (\square) and 5 cm (\triangle). The mixing numbers were calculated from Eq. 3.5.

rates, the mixing time tended to about 10 s. The same values of θ were observed at the same Fr for the 1500-L and the 30-L containers with the same d/d_s ratio, while higher θ values were measured for the 30-L container with the d/d_s ratio about 6 (Fig. 3.14b).

The free-surface shapes observed in the 1500-L and 30-L containers with the same d/d_s ratio were similar to each other, but different from that in the 30-L container with the d/d_s ratio of 6. With a d/d_s ratio of 12, a single-peaked wave was observed at Fr from 0.8 to 0.9 and a breaking wave appeared at $Fr=0.9$. By comparison, in the 30-L container with a d/d_s ratio of 6, a double-peaked wave was observed when Fr was between 0.8 and 0.9, and a breaking wave appeared at $Fr=0.9$. However, this breaking wave was less distinct than that in the containers with a higher d/d_s ratio. Interestingly, θ tended to a constant at $Fr \geq 1$ for the three containers, the point at which a transition from a smooth to a rough free surface occurred and a vortex appeared at the free surface. This vortex was also observed at higher Fr values in the three containers.

Velocity field measurements

The velocity fields of a 30-L container were measured by LDV at 60, 80, and 100 rpm with a liquid height of 20 cm and at a shaking diameter of 5 cm. At an agitation rate of 60 rpm, the velocity of the fluid was lower close to the bottom of the container ranging from 0.015 to 0.025 m/s (Fig. 3.15a). The velocity of the fluid increased as coming closer to the surface where the highest velocities were recorded (0.04-0.045 m/s) (Fig. 3.15a). At an agitation rate of 80 rpm, the highest fluid velocities (0.35-0.55 m/s) were correlated with the peak of the wave (Fig. 3.15b). The smallest velocities (0.06-0.1 m/s) were measured where the wave was the lowest and also at the center of the container (Fig. 3.15b). At an agitation rate of 100 rpm, the fluid velocity reached maximal values around 0.55 m/s (Fig. 3.15c). However, the fluid velocity at the center of the container did not increase significantly in comparison with the experiment at 80 rpm (Fig. 3.15c). The location of high and low fluid velocities according to the wave position was similar to that observed at 80 rpm (Fig. 3.15c). The velocity of the fluid close to the wall increased significantly with the agitation rate, but remained within similar ranges in the center of the liquid (Fig. 3.15).

3.4 Discussion

This study has shown that OSRs can be considered homogeneous for mammalian cell cultivation. Previous studies have reported that mixing times equal to or less than 100 s are necessary to avoid oxygen gradients in bioreactors (Lara et al., 2006). We conclude that the mixing in OSRs ensures

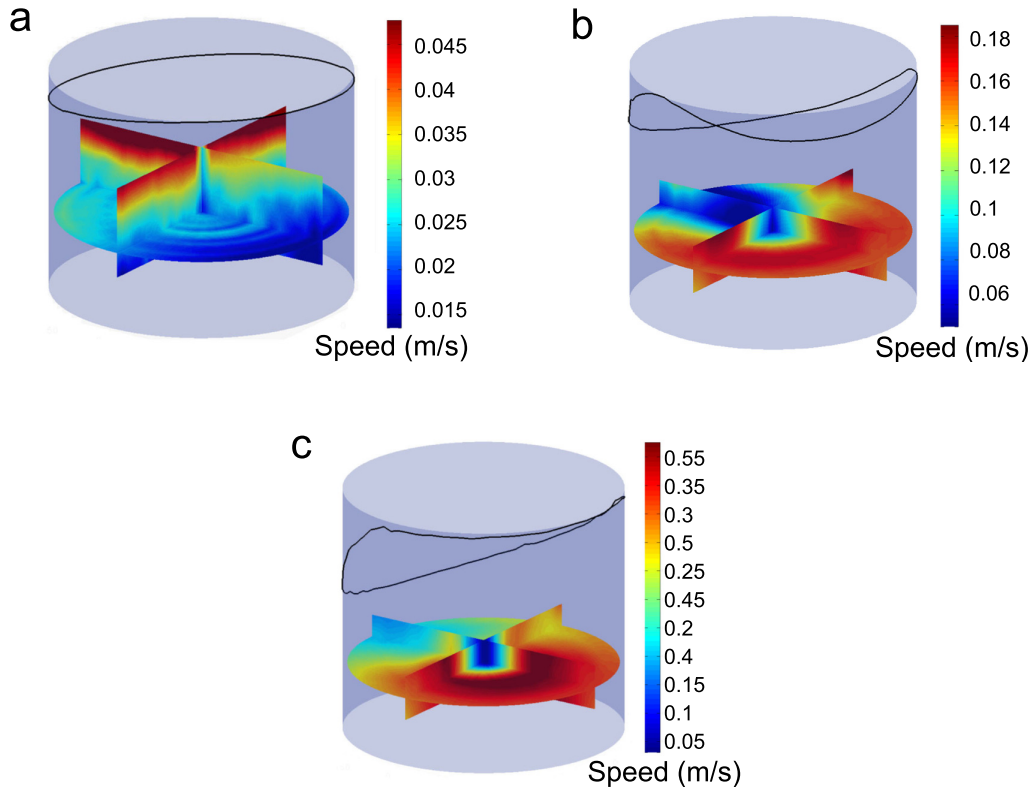


Fig. 3.15: LDV measurements of fluid velocities in a 30-L cylinder at (a) 60, (b) 80 and (c) 100 rpm. The velocities represented in this picture are the norm of the sum of the three measured velocities (radial, tangential and axial). The liquid height was 20 cm and the shaking diameter 5 cm. Courtesy of Matthieu Dreyer, Laboratory of Hydraulic Machines, EPFL.

homogeneity of mammalian cell cultures at scales up to 1500 L. In comparison, the mixing time in stirred-tank bioreactors for mammalian cell culture increases with the scale (Bonvillani et al., 2006) and can be more than 1 minute from 20-L bioreactors, inducing significant gradients in pH, nutrients, and dissolved oxygen concentration (Lara et al., 2006; Xing et al., 2009). Short mixing times are crucial for cell culture since base (i.e. NaOH) is added to help maintain a constant pH and may result in cell death at the site of addition if mixing is not efficient (Langheinrich and Nienow, 1999).

Furthermore, fed-batch processes are common for mammalian cell cultivation and imply an increase of the working volume over time. Such volume increase will increase the mixing time in stirred-tank bioreactors (Xing et al., 2009). However, this was not the case in OSRs as long as the height of the wave formed by the free surface was at least half the liquid

height at rest avoiding the formation of a diffusional zone at the bottom of the container. These results suggest that the mixing was induced by a pump motion of the free surface and that mixing was efficient to a depth equivalent to about twice the height of the wave.

By increasing the diameter of the container, shorter mixing times were reached at lower agitation rates. However, the free surface was rougher as the inner diameter increased, a characteristic which may induce foam formation during cell culture. However, similar mixing times as measured in the two larger containers were reached in the container with an inner diameter of 10 cm when the height of the wave formed by the free surface was at least half the liquid height at rest at higher agitation rates. In this container the free surface was smoother, which would mean less foam formation during cell cultivation.

This work suggest that mixing and the free-surface behavior in OSRs are scalable by keeping the d/d_s ratio and Fr constant. The ratio d/d_s describes the relationship between the two characteristic lengths involved in the centrifugal and inertial forces of OSRs. These results demonstrate that the free-surface shape as well as the mixing behavior in orbitally shaken containers are influenced by these two forces.

At all scales, the fastest mixed zones were situated close to the wall and a poorly mixed zone was observed in the center of the liquid. This poorly mixed zone was less affected by the agitation rate than the fastest mixed zones. LDV measurements confirmed these visual observations by showing low velocities in the center of the liquid which did not increase with agitation rate as much as the velocities of the fluid close to the wall.

In contrast to stirred-tank bioreactors where the mixing time increases with the scale (Xing et al., 2009), the mixing times measured in the 1500-L OSR were of the same order of magnitude as those in the 30-L container. In OSRs, the container moves with the shaker, inducing liquid motion through contact with the walls. This mixing system is the same regardless of the scale of operation. Thus, similar mixing principles can be expected at different scales. This may explain why the mixing time did not increase with the scale and why the mixing and the free surface of a large-scale container could be mimicked at small scale.

In this study, we focused on mixing in OSRs in the context of mammalian cell cultivation which is generally performed in media with water-like viscosities. A study involving liquids with higher viscosities than water would be necessary to approximate the mixing for microbial fermentations and plant cell cultures. Furthermore, Re evaluation is difficult in the OSRs as the velocity (inertial forces) varies in a wide range within the liquid making it difficult to define a reference value. Moreover, the unsteady boundary

layer and its interaction with the wave is adding more complexity to the evaluation of the turbulence and shear stress on the wall. Nevertheless, one may easily imagine that increasing Re (size of the bioreactor, agitation rate) may lead to the development of more turbulence within the liquid which will influence both mixing and gas transfer. Further investigations are needed to clarify Re effects in OSRs.

Gas transfer

4.1 Introduction

The gas transfer through the liquid and gas phases of bioreactors is essential as it ensures oxygen supply to the cells and CO₂ removal from the culture medium (Bonvillani et al., 2006; Garcia-Ochoa and Gomez, 2009). The oxygen transfer rate (*OTR*) through the liquid-gas interface is described by Eq. 4.1:

$$OTR = \frac{dc_L}{dt} = k_L a (c^* - c_L) \quad (4.1)$$

where c_L is the dissolved concentration of oxygen in the liquid phase [M], c^* is the dissolved oxygen concentration at saturation [M], t the time [h] and $k_L a$ the volumetric mass transfer coefficient of oxygen [h⁻¹]. The $k_L a$ is commonly used to evaluate the efficiency of the gas transfer in a bioreactor as it represents the rate at which oxygen molecules are transferred through the gas-liquid interface (Xing et al., 2009). The $k_L a$ is made of two terms: k_L the mass transfer coefficient [m/h] and a the specific interfacial area [m⁻¹]. While k_L is essentially influenced by physical-chemical properties of the liquid (diffusivity), a which represents the ratio of the interface area to the working volume depends on operating conditions such as the bioreactor geometry, the working volume or the agitation rate. Since animal cells have lower oxygen uptake rates than microbial organisms, the $k_L a$ values of bioreactors designed for animal cell cultivation are lower, typically in the range of 1-25 h⁻¹ as compared to 100-400 h⁻¹ for microbial cultures (Zhang et al., 2009b). The last term in Eq. 4.1 ($c^* - c_L$) is named the driving force. As c^* is proportional to the partial pressure of oxygen in the gas phase according to Henry's law, the *OTR* can be improved by increasing

the concentration of oxygen in the gas phase of the bioreactor (i.e. using pure oxygen).

In stirred-tank bioreactors (STRs), the gas transfer occurs through bubbles sparged usually at the bottom of the bioreactor (Fig. 4.1). However,

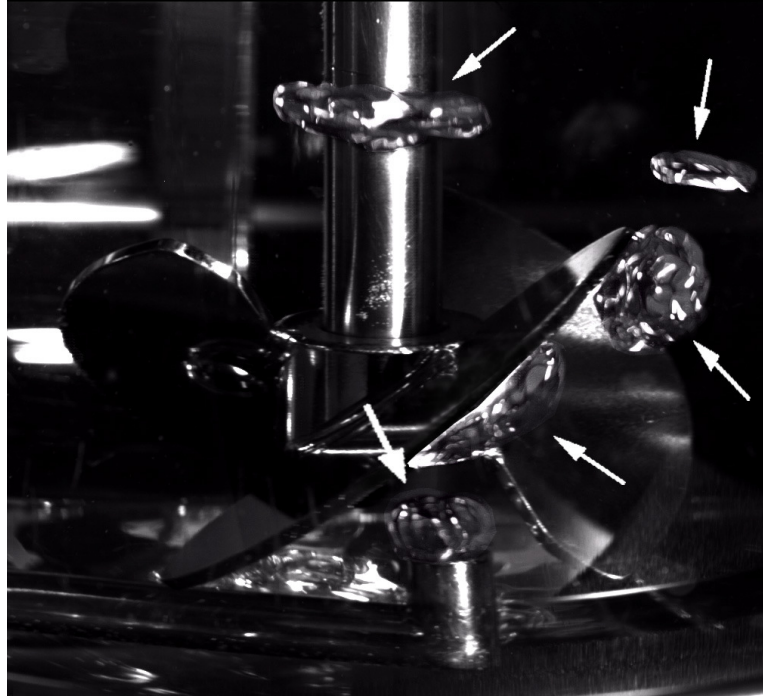


Fig. 4.1: Details of a 3-L STR: a pitched blade impeller and a sparger. Air was flushed at 0.3 L/min and the agitation rate set at 150 rpm. Bubbles are indicated by arrows.

shear stress induced by bubble breaking is harmful for the cells and prevents using too high agitation rates for mammalian cell cultures (Nienow, 2006). As a consequence bubbles may coalesce and restrain gas transfer efficiency, explaining why it is very difficult and often impossible to keep the k_La constant as the scale of operation increases, despite that the k_La is often reported as the scale-up parameter for cell cultures (Nienow, 2006). To compensate insufficient k_La values in STRs, pure oxygen is used to increase OTR and bases are added to counteract acidification of the medium due to CO_2 accumulation.

In orbitally shaken bioreactors (OSRs), the gas transfer occurs through the free surface (Fig. 4.2). In OSRs, k_La values in the range of 4-30 h^{-1}

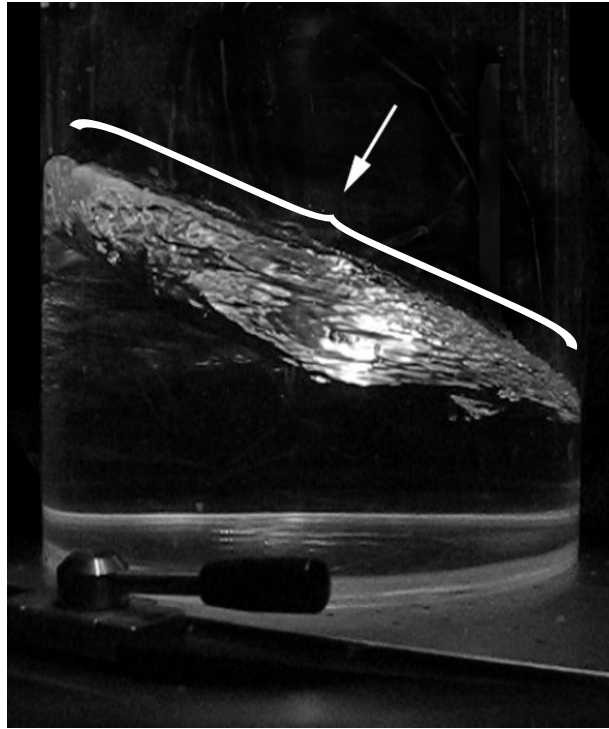


Fig. 4.2: Free surface in a 30-L OSR at 90 rpm with a shaking diameter of 5 cm and a liquid height of 12 cm.

have been reported for nominal volumes from 50 mL to 2000 L (Zhang et al., 2009a). Rapid bioprocess development is required in the biotechnology industry and OSRs are commonly used at this early stage. These bioreactors are usually operated without pH or dissolved oxygen concentration (DO) controllers contrary to STRs. As the culture conditions are different between the two types of bioreactors, the scale-up is not straightforward and the cell performance is often reduced in STRs (Xing et al., 2009). Since OSRs have been expanded from shaken flasks to disposable bioreactors of 200 and 2000 L for mammalian cell cultivation (Stettler, 2007; Stettler et al., 2007; Zhang et al., 2009b), they can now be considered as an alternative to STRs for large-scale bioprocesses involving mammalian cells. As the large-scale OSRs are based on the same agitation principles as the small ones, we can expect a more straightforward scale-up than with the STRs, providing that the same culture conditions can be maintained. At small scales, bottles are often used as OSRs and screw caps (Fig. 4.3a) are commonly used as sterile closures for mammalian cell cultures and opened to a quarter of a turn to allow the gas exchange (Muller et al., 2005). How-

ever, limitations of the gas phase renewal due to these closures may occur and as a consequence, the gas phase composition of the bioreactors may differ from the one of the incubators affecting the c^* and consequently the OTR (Eq. 4.1). Therefore, sterile closure resistance to mass transfer should be minimized to study the effects of the k_La .

In this chapter we describe the scalability of probe-independent bioprocesses in OSRs based on the k_La as the scale-up factor. First, to evaluate the effects of the limitations due to sterile closures, CHO cells were cultivated in 1-L OSRs equipped either with screw caps or vented caps (Fig. 4.3). Then, to test if the k_La is a good predictor for probe-independent bioprocesses, we cultivated the cells in OSRs with nominal volumes from 250 mL to 1 L at k_La values from 4 to 18 h⁻¹ by varying the working volumes from 20 to 60% of the nominal volumes. We also confirmed our hypothesis by operating a culture in a 200-L OSR without pH and DO controllers.

4.2 Material and Methods

Gas transfer through sterile closures

The oxygen mass transfer coefficient in the gas phase (k_Ga [h⁻¹]) represents the rate at which oxygen is transferred from the surroundings into the gas phase of the vessel (Nikakhtari and Hill, 2006). Thus, the k_Ga is related to the mass transfer resistance of the closures. Empty 1-L cylindrical bottles were filled with nitrogen until the concentration of oxygen in the gas phase (c_G) reached 0 M as measured by non-invasive O₂ sensors (PreSens, Regensburg, Germany). The bottles were then equipped with screw caps (Fig. 4.3a) or home-made vented caps (Polyether sulfones membrane with a diameter of 1.5 cm, Fig. 4.3b). The c_G was recorded over time as the bottles were agitated at 110 rpm. Each measurement was repeated twice. Assuming that the gas phase was well-mixed, the k_Ga was calculated from Eq. 4.2 where t represents the time [h] and c_G^* the oxygen concentration of the surroundings [M].

$$\frac{dc_G}{dt} = k_Ga(c_G^* - c_G) \quad (4.2)$$

Volumetric mass transfer coefficient of oxygen

The volumetric mass transfer coefficient of oxygen (k_La) [h⁻¹] was measured in 250-mL, 500-mL and 1-L cylindrical bottles with various working volumes at 37°C with a dynamic method using non-invasive O₂ sensors (PreSens,

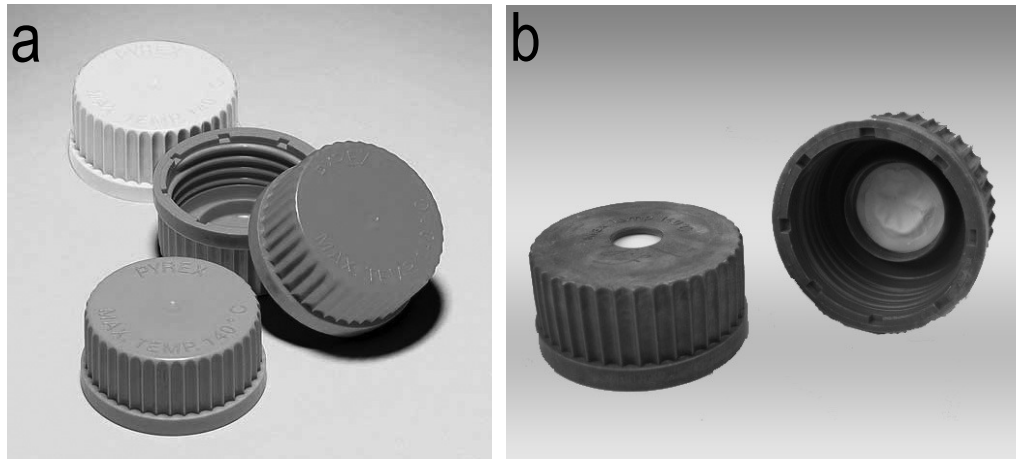


Fig. 4.3: Sterile closures used during mammalian cell cultures: screw caps (a) and home-made vented caps (Polyether sulfones membrane with a diameter of 1.5 cm) (b).

Regensburg, Germany) (Gupta and Rao, 2003). Nitrogen was sparged into the water until the DO was close to 0 M. Air was flushed into the gas phase to replace nitrogen and the bottles were agitated at 110 rpm. The increase of the DO was recorded and the k_{La} [h^{-1}] was calculated from Eq. 4.1.

Cell culture

Three CHO cell lines were cultivated: a CHO-DG44 cell line, a recombinant CHO cell line expressing the tumor necrosis factor receptor 2 fused with the Fc portion of a human IgG (TNFR:Fc) (CHO-TNFR) (Oberbek et al., 2011) and another expressing a human anti-RhesusD IgG monoclonal antibody (CHO-IgG) (Matasci et al., 2011). The CHO-TNFR and CHO-IgG cell lines derive from the CHO-DG44 cell line and also express the green fluorescent protein (GFP). All the cell lines were cultivated in suspension and expanded in ProCHO5 medium (Lonza, Verviers, Belgium) at 37°C with 5% CO₂ in cylindrical glass bottles (Pyrex laboratory glassware, SciLabware Ltd, Stone, United Kingdom) of various sizes and equipped with vented caps (Fig. 4.3b) at 110 rpm in an ISF4-W incubator (Kühner AG, Birsfelden, Switzerland).

Effects of sterile closures on cell growth

To evaluate the effects of the sterile closure limitations on cell growth and recombinant protein production, CHO-IgG cells were diluted to densities

between 0.3 and 0.5 million cells/mL in ProCHO5 and split into two sets of 1-L bottles with working volumes between 20 and 60% of the nominal volume. One set was equipped with screw caps and the other one with vented caps. The bottles were incubated at 110 rpm with air containing 5% CO₂ and at 37°C. This experiment was repeated twice.

Effects of the k_La on cell growth

To investigate the effects of the k_La on cell growth, the three CHO cell lines were diluted to densities between 0.3 and 0.6 million cells/mL in ProCHO5. The cells were split into 250-, 500-mL and 1-L bottles with working volumes between 20 and 60% of the nominal volumes. The bottles were equipped with vented caps and orbitally shaken at 110 rpm with air containing 5% CO₂ and at 37°C. This experiment was repeated twice.

The k_La as a scale-up factor

To test the k_La as a scale-up factor, CHO-IgG cells were inoculated at 0.3 million cells/mL in 100 L of ProCHO5 in a 200-L OSR (Kühner AG) agitated at 57 rpm (Fig. 4.23c). Air containing 5% CO₂ was flushed at 1 L/min during the whole experiment. After overnight cultivation, satellite cultures in 1- and 5-L bottles with vented caps were run in parallel (Fig. 4.23a,b) (De Jesus et al., 2004). The bottles were agitated at 110 rpm and the volume of the cultures was adjusted to obtain the same k_La as the one in the 200-L bioreactor (7 h⁻¹).

Cell analysis

For all cultures, the cell density and viability were determined manually by the Trypan blue exclusion method. The biomass was determined by the packed cell volume (PCV) method using VoluPAC tubes (Sartorius AG, Goettingen, Germany) (Stettler et al., 2006). The oxygen concentration of the gas and liquid phases were measured on-line with an optical sensor (PreSens, Regensburg, Germany). The glucose, lactate, glutamine and glutamate concentrations were determined off-line with a BioProfile Basic 4 Analyzer (Nova Biomedical, Waltham, MA). The pH was measured off-line with a 340 pH meter (Mettler-Toledo, Greifensee, Switzerland). The dissolved CO₂ concentration was assessed off-line with a BioProfile BiopHOx Analyzer (Nova Biomedical). The cell cycle was analyzed by flow cytometry



Fig. 4.4: OSRs of nominal volumes of 1 L (a), 5 L (b), and 200 L (c) used to test the k_La as a scale-up parameter.

using the Guava Cell Cycle Reagent according to manufacturer's protocol (Guava® EasyCyte™, Guava technologies, Millipore, Billerica, MA).

Protein quantification and analysis

Recombinant TNFR:Fc and anti-RhD IgG were quantified by sandwich ELISA. As coating, a goat anti-human Fc γ antibody (Jackson ImmunoResearch Laboratories, Inc., West Grove, PA, USA) and a goat anti-human κ light chain antibody (ADB Serotec, Düsseldorf, Germany) was used for TNFR:Fc (Matasci et al., 2011) and anti-RhD IgG, respectively. For both recombinant proteins, an alkaline phosphatase (AP)-conjugated goat anti-human gamma chain antibody (Invitrogen Corp., Basel, Switzerland) was used for detection (Meissner et al., 2001). As standards, affinity-purified recombinant human TNFR:Fc fusion protein (Enbrel®; Amgen, Zug, Switzerland) and ChromPure human IgG (Jackson ImmunoResearch Laboratories, Inc., West Grove, PA) were used for TNFR:FC and anti-RhD IgG quantification, respectively.

4.3 Results

Sterile closure limitations

To test the effects of the limitations due to sterile closures, we first measured the resistance of the screw caps and vented caps towards gas transfer. We then cultivated CHO-IgG cells in 1-L OSRs equipped either with screw caps or with vented caps to compare the performance of the cultures in terms of cell density and recombinant protein production.

Gas transfer resistance of sterile closures

The resistance of the screw and vented caps were assessed at 37°C and 110 rpm. The time needed to renew 95% of the gas phase was about 1 h and 18 h when the OSRs were equipped with vented or screw cap, respectively (Fig. 4.5). While k_Ga values of 30 h⁻¹ were calculated for vented caps,

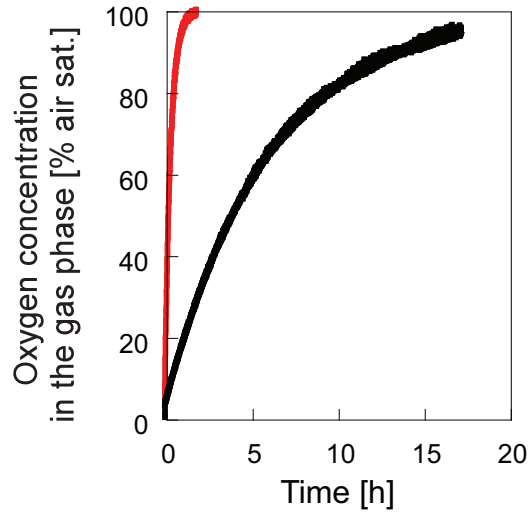


Fig. 4.5: Gas transfer resistance of sterile closures on 1-L OSRs at 37°C and 110 rpm. The OSRs were equipped either with a screw cap (black) or a vented (red) cap.

values of 0.15 h⁻¹ were observed for screw caps.

Comparison of cell culture performance between screw and vented caps

To test the effects of the limitations due to sterile closures on cell growth and recombinant protein production, we cultivated CHO-IgG cells in 1-L OSRs equipped either with screw caps or vented caps. The cell density of cultures in OSRs equipped with screw caps increased by at most 10 fold, although in the OSRs equipped with vented caps it increased by 15 fold (Fig. 4.6). In OSRs equipped with screw caps, the cultures of 500 and 600 mL showed an increase in the cell density twice lower than those in 200 and 300 mL at the end of the experiment (Fig. 4.6a). In OSRs equipped with vented caps, the increase in the cell density was 1.25 fold lower in cultures from 400 to 600 mL than in those of 200 and 300 mL (Fig. 4.6b).

The viability was higher than 90% in all the cultures (Fig. 4.7). No noticeable differences were observed between cultures in OSRs equipped with screw or vented caps (Fig. 4.7).

The biomass volume increased by 17 times in the 200 and 300-mL cultures equipped with screw caps and by 15 times in the 400- to 600-mL cultures (Fig. 4.8a). The biomass accumulation increased by 15 fold and was similar in all the cultures equipped with vented caps (Fig. 4.8b).

The pH decreased from 7.3 to 6.8 during the first 72 h of cultivation in the 200 and 300-mL cultures equipped with screw caps and remained within that range until the end of the experiment (Fig. 4.9a). The pH decreased from 7.2 to 6.5 in the cultures from 400 to 600 mL when equipped with screw caps (Fig. 4.9a). In the OSRs equipped with vented caps, the pH decreased from 7.1 to 6.7 during the first 24 h and remained within this range for the cultures from 200 to 400 mL, while it decreased to 6.6 and 6.5 in the 500- and 600-mL cultures, respectively (Fig. 4.9b).

Further analysis of the effects of sterile closures on culture environment and cell metabolism To study in further details the effects of the limitations due to sterile closures, CHO-IgG cells were cultivated in 1-L OSRs at 110 rpm and 37°C. The working volume was 400 mL and the OSRs were either equipped with a screw or a vented cap. The cells reached densities of 2.5 and 4 million cells/mL in the OSRs equipped with screw or vented caps, respectively (Fig. 4.10a). The viability was equal to or higher than 95% and no major differences were observed between the two types of closures (Fig. 4.10b). The PCV value was similar for the two cultures

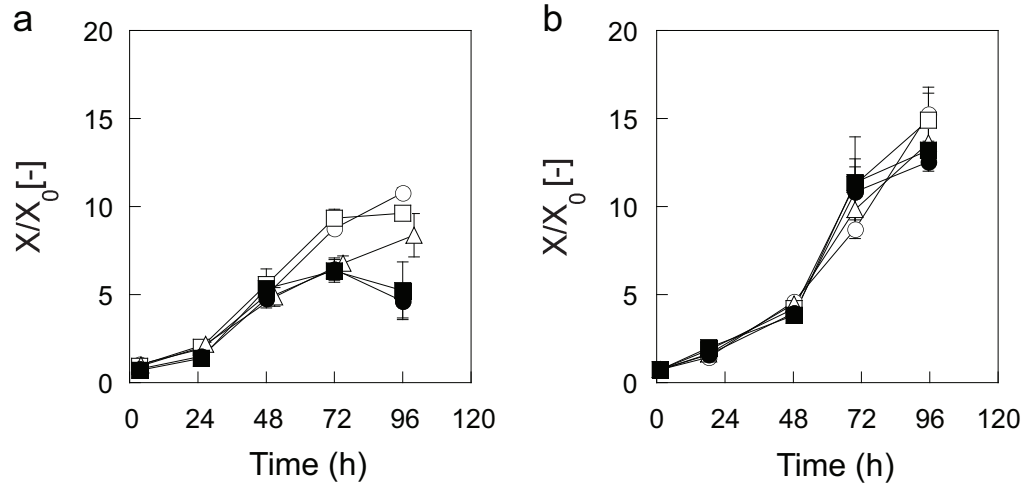


Fig. 4.6: CHO-IgG cell growth in 1-L OSRs with working volumes of 200 (○), 300 (□), 400 (△), 500 (●) and 600 mL (■). The cells were incubated at 37°C at 110 rpm in OSRs equipped with screw caps (a) or vented caps (b). The ratio of the cell density to its initial value was measured at the times indicated.

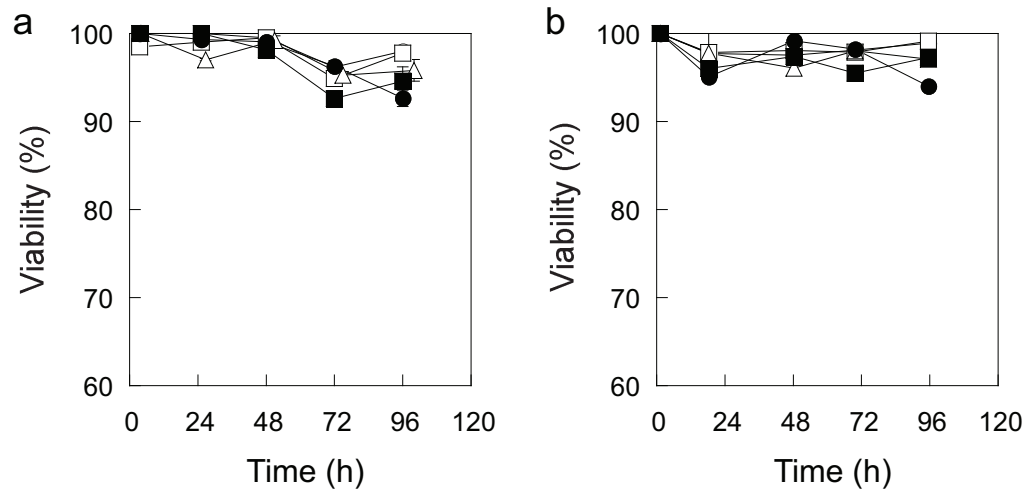


Fig. 4.7: CHO-IgG cell growth in 1-L OSRs with working volumes of 200 (○), 300 (□), 400 (△), 500 (●) and 600 mL (■). The cells were incubated at 37°C and 110 rpm in OSRs equipped with screw caps (a) or vented caps (b). The viability was measured at the times indicated.

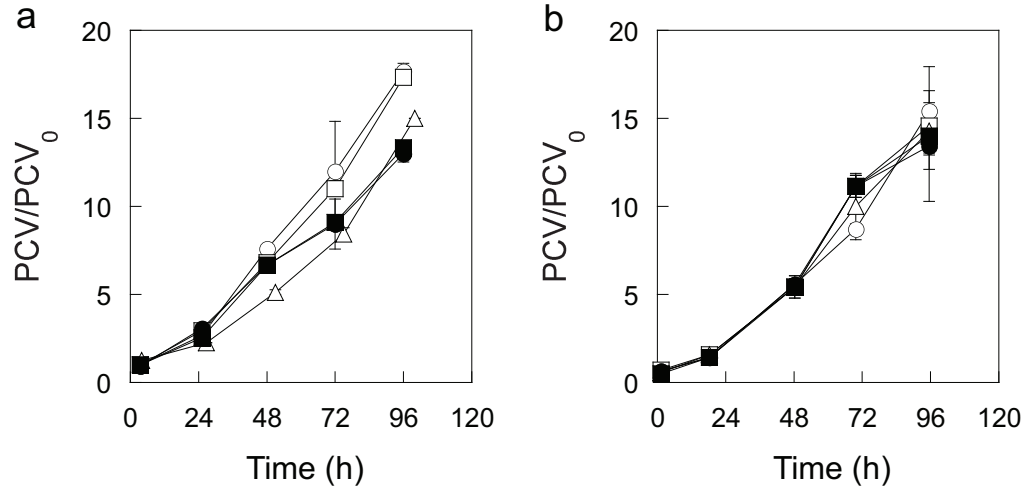


Fig. 4.8: CHO-IgG cell growth in 1-L OSRs with working volumes of 200 (○), 300 (□), 400 (△), 500 (●) and 600 mL (■). The cells were incubated at 37°C and 110 rpm in OSRs equipped with screw caps (a) or vented caps (b). The ratio of the biomass volume to its initial value was measured at the times indicated.

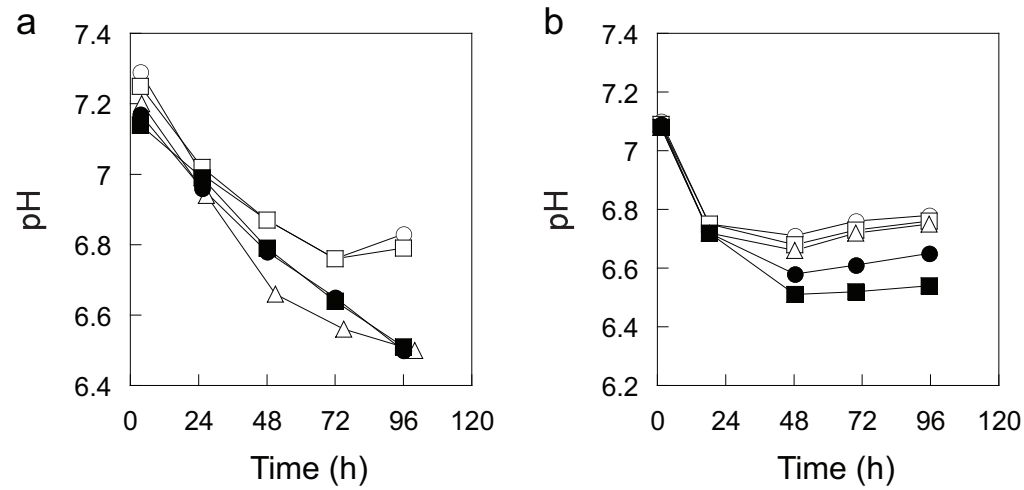


Fig. 4.9: CHO-IgG cell growth in 1-L OSRs with working volumes of 200 (○), 300 (□), 400 (△), 500 (●) and 600 mL (■). The cells were incubated at 37°C and 110 rpm in OSRs equipped with screw caps (a) or vented caps (b). The pH was measured at the times indicated.

and reached 1.2% at the end of the cultivation time (Fig. 4.10c). The concentrations of recombinant anti-RhD IgG were identical in the two cultures (Fig. 4.10d).

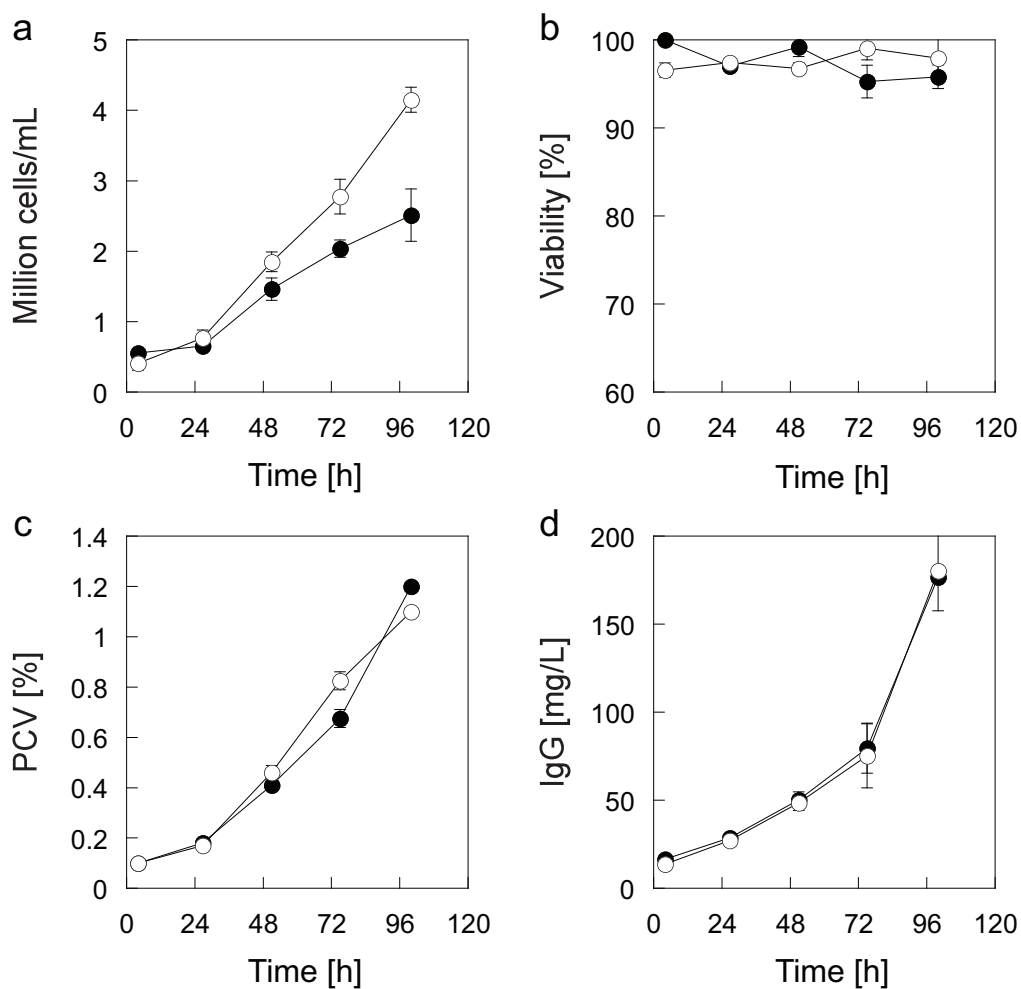


Fig. 4.10: CHO-IgG cell growth and recombinant protein production in 1-L OSRs equipped with screw caps (●) or vented caps (○) at 37°C and 110 rpm. The working volume was 400 mL and the viable cell density (a), viability (b), PCV (c), and recombinant anti-RhD IgG concentration (d) were measured at the times indicated.

In the OSRs equipped with screw caps, the concentration of oxygen decreased to 0% air sat in the liquid phase and 40% air sat in the gas phase after 96 h of cultivation (Fig. 4.11a). When the OSRs were equipped with

vented caps the concentration of oxygen after 96 h decreased to 30 and 95% air sat in the liquid and gas phase, respectively (Fig. 4.11b).

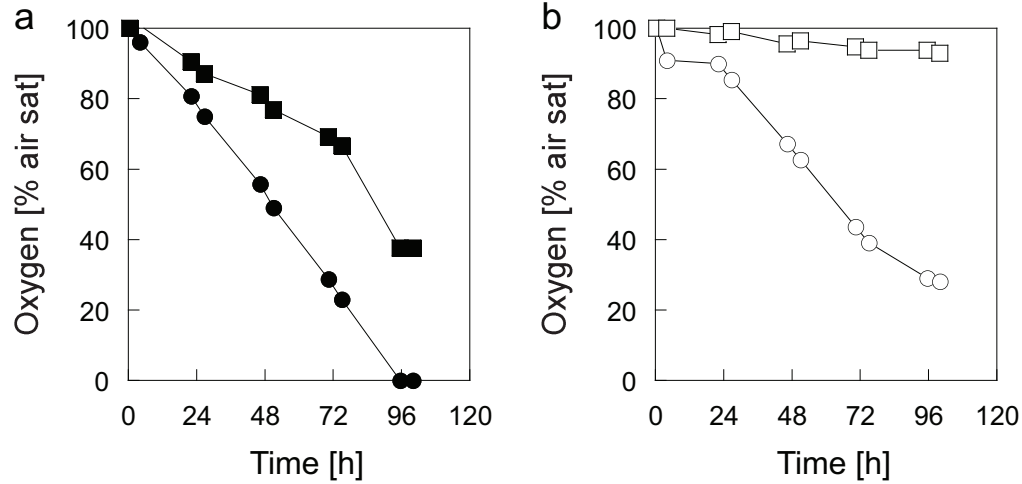


Fig. 4.11: Oxygen concentration during CHO-IgG cell growth in 1-L OSRs equipped with screw caps (a) or vented caps (b) at 37°C and 110 rpm. The working volume was 400 mL and the oxygen concentration in the liquid (●,○) and gas (■,□) phases were measured at the times indicated.

The pH decreased to 6.5 in OSRs equipped with screw caps and to 6.6 with vented caps (Fig. 4.12a). The dissolved CO₂ concentration remained around 5% in cultures with vented caps, although it increased to 12% in cultures with screw caps (Fig. 4.12b).

The glutamine was completely consumed after 72 h in the cultures equipped with screw caps and after 96 h in the cultures with vented caps (Fig. 4.13a). No significant differences were observed between the two types of closures in terms of glutamate, glucose and lactate concentrations (Fig. 4.13b,c,d). The glutamate concentration increased from 0.6 to 1 mM during the experiment (Fig. 4.13b). The glucose concentration decreased from 6.5 to 3.5 g/L (Fig. 4.13c), while the lactate concentration increased from 0.2 to 1.5 g/L (Fig. 4.13d).

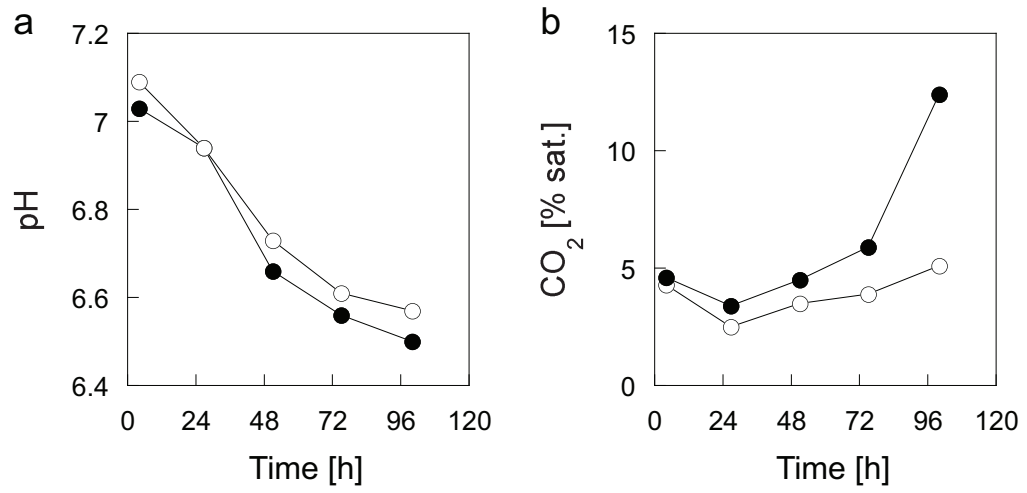


Fig. 4.12: Culture conditions during CHO-IgG cell growth in 1-L OSRs equipped with screw caps (●) or vented caps (○) at 37°C and 110 rpm. The working volume was 400 mL and the pH (a) and dissolved CO₂ concentration (b) were measured at the times indicated.

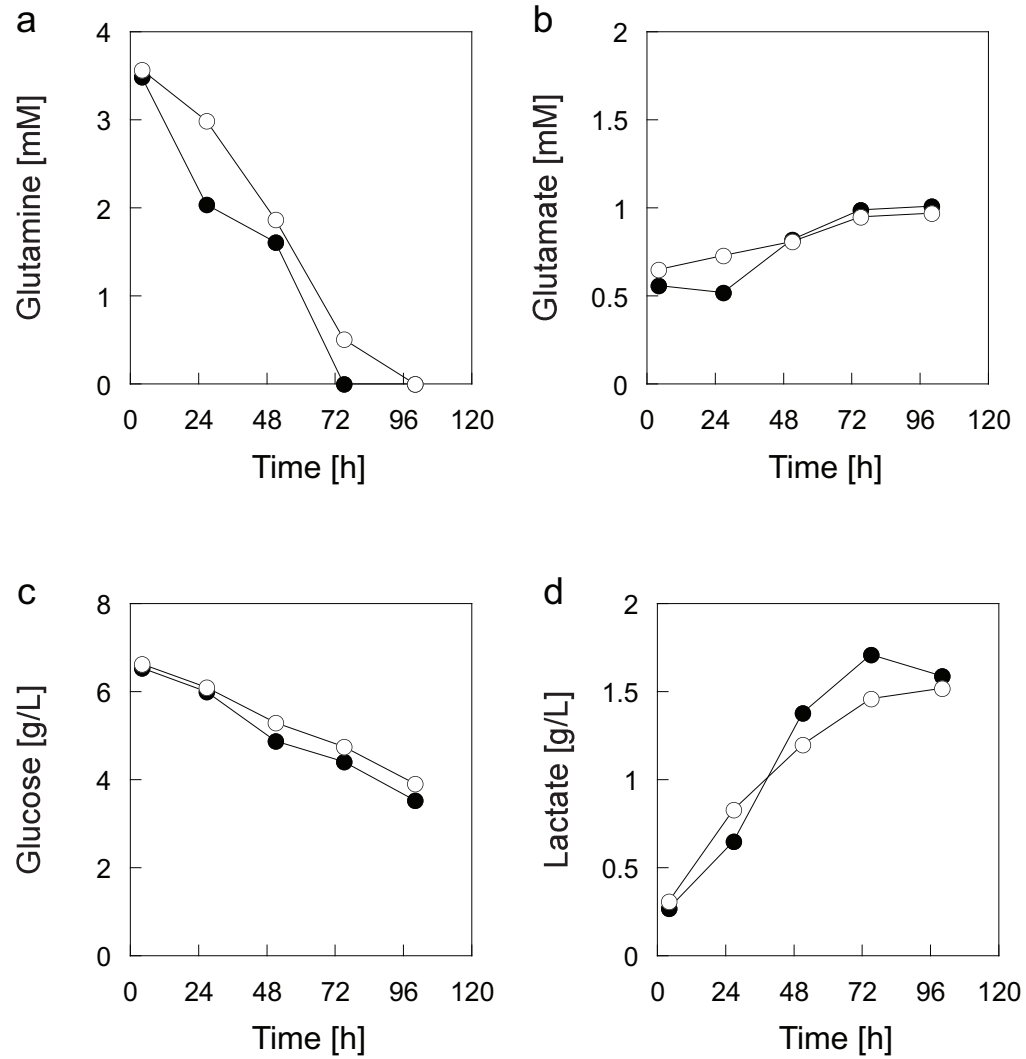


Fig. 4.13: Metabolite concentrations during CHO-IgG cell growth in 1-L OSRs equipped with screw caps (●) or vented caps (○) at 37°C and 110 rpm. The working volume was 400 mL and the glutamine (a), glutamate (b), glucose (c), and lactate (d) concentrations were measured at the times indicated.

k_La limitations

To test the effects of the k_La on the cell culture performance, the k_La values of working volumes between 20 and 60% of the nominal volumes were measured in OSRs of 250 mL, 500 mL and 1 L. Three CHO cell lines were then cultivated in these OSRs with the different working volumes to test the effects of the k_La on the cell growth and recombinant protein production and the scalability of probe-independent bioprocesses based on the k_La values.

Volumetric mass transfer coefficient of oxygen in cylindrical OSRs

The k_La values of working volumes between 20 and 60% of the nominal volumes were measured at 37°C in 250-mL, 500-mL and 1-L cylindrical OSRs at 110 rpm. The k_La decreased as the working volume increased in all the OSRs (Fig. 4.14). While it decreased from 18 to 5 h⁻¹ in the 250- and 500-mL OSRs, it diminished from 11 to 3.5 h⁻¹ in the 1-L OSR as the working volumes increased from 20 to 60% of the nominal volumes (Fig. 4.14).

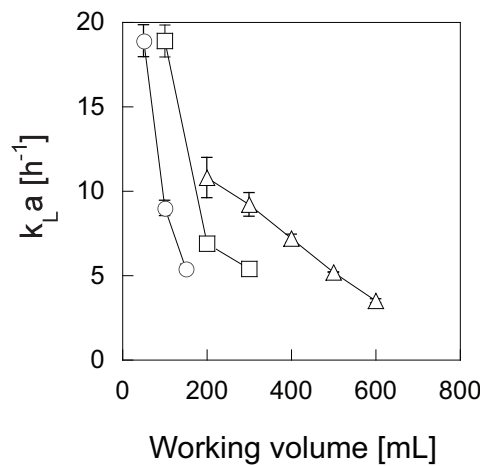


Fig. 4.14: k_La values in cylindrical OSRs of 250 mL (○), 500 mL (□) and 1 L (△) were measured at 37°C at 110 rpm.

Effects of the k_La on cell growth and recombinant protein production

CHO-DG44, CHO-IgG and CHO-TNFR cells were cultivated during 5 days in 1-L OSRs at various working volumes from 200 to 600 mL at 37°C and 110 rpm. As the working volume increased beyond a threshold of 300 mL ($k_La < 9 \text{ h}^{-1}$) for the CHO-DG44 cells and 400 mL ($k_La < 7 \text{ h}^{-1}$) for the CHO-IgG and CHO-TNFR cells, the maximal cell density decreased (Fig. 4.15). In cultures with working volumes lower than or equal to the thresholds, CHO-DG44, CHO-IgG and CHO-TNFR cell densities increased by 11, 10 and 8, respectively (Fig. 4.15). For working volumes larger than the threshold, cell densities decreased by 20% in CHO-DG44 and CHO-TNFR cultures and by 40% in CHO-IgG cultures (Fig. 4.15).

For all the cell lines, no significant difference in the biomass volume was observed between the different working volumes (Fig. 4.16). The biomass volume increased by 8, 12 and 5 fold in the CHO-DG44, CHO-IgG and CHO-TNFR, respectively (Fig. 4.16).

The recombinant protein concentrations measured by ELISA were the same independently of the working volume in the CHO-IgG and CHO-TNFR cultures (data not shown). The average specific productivity increased with the working volume from 12 $\text{pg cell}^{-1} \text{ day}^{-1}$ to 17 $\text{pg cell}^{-1} \text{ day}^{-1}$ in the CHO-IgG cultures and from 9 to 11 $\text{pg cell}^{-1} \text{ day}^{-1}$ in the CHO-TNFR cultures.

For working volumes larger than the thresholds, lower pH values were measured in the CHO cell cultures (Fig. 4.17). The lowest pH values were measured in the 600-mL cultures reaching 6.4 in the CHO-DG44 cultures and 6.5 in the CHO-IgG and CHO-TNFR cultures (Fig. 4.17). For working volumes lower than the threshold, the pH was similar in the cultures and decreased to 6.6 in the CHO-DG44 cultures and to 6.65 in the CHO-IgG and CHO-TNFR cultures (Fig. 4.17).

Lower DO values were measured as the working volume of the cultures increased (Fig. 4.18). The lowest DO values were measured in the 500- and 600-mL cultures where it reached 20% air sat with the CHO-DG44 and CHO-TNFR cell lines and 0% air sat with the CHO-IgG cell line (Fig. 4.18). For each CHO cell line, similar glucose, lactate, glutamine and ammonium profiles were observed with all the working volumes (data not shown).

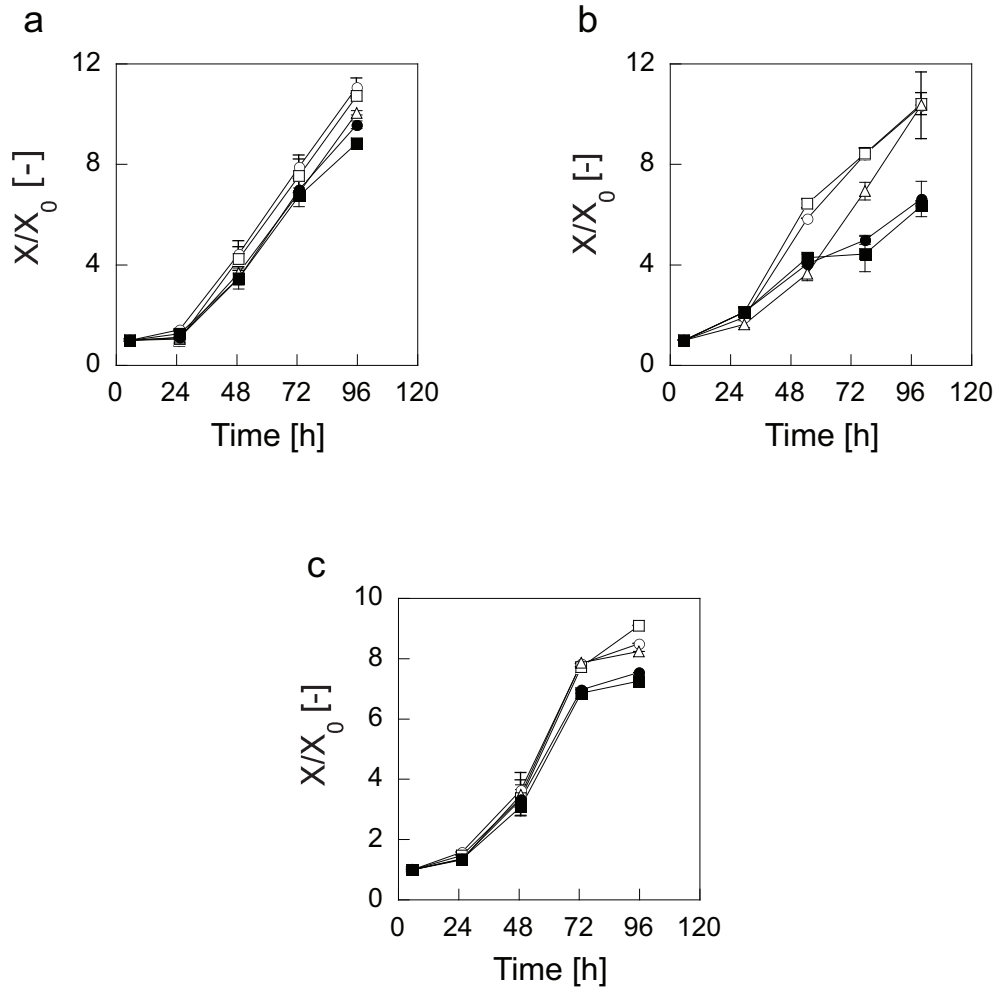


Fig. 4.15: CHO cell growth in 1-L OSRs with working volumes of 200 (○), 300 (□), 400 (△), 500 (●) and 600 mL (■). The CHO-DG44 (a), CHO-IgG (b), and CHO-TNFR (c) cells were incubated at 37°C at 110 rpm. The ratio of the cell density to its initial value was measured at the times indicated.

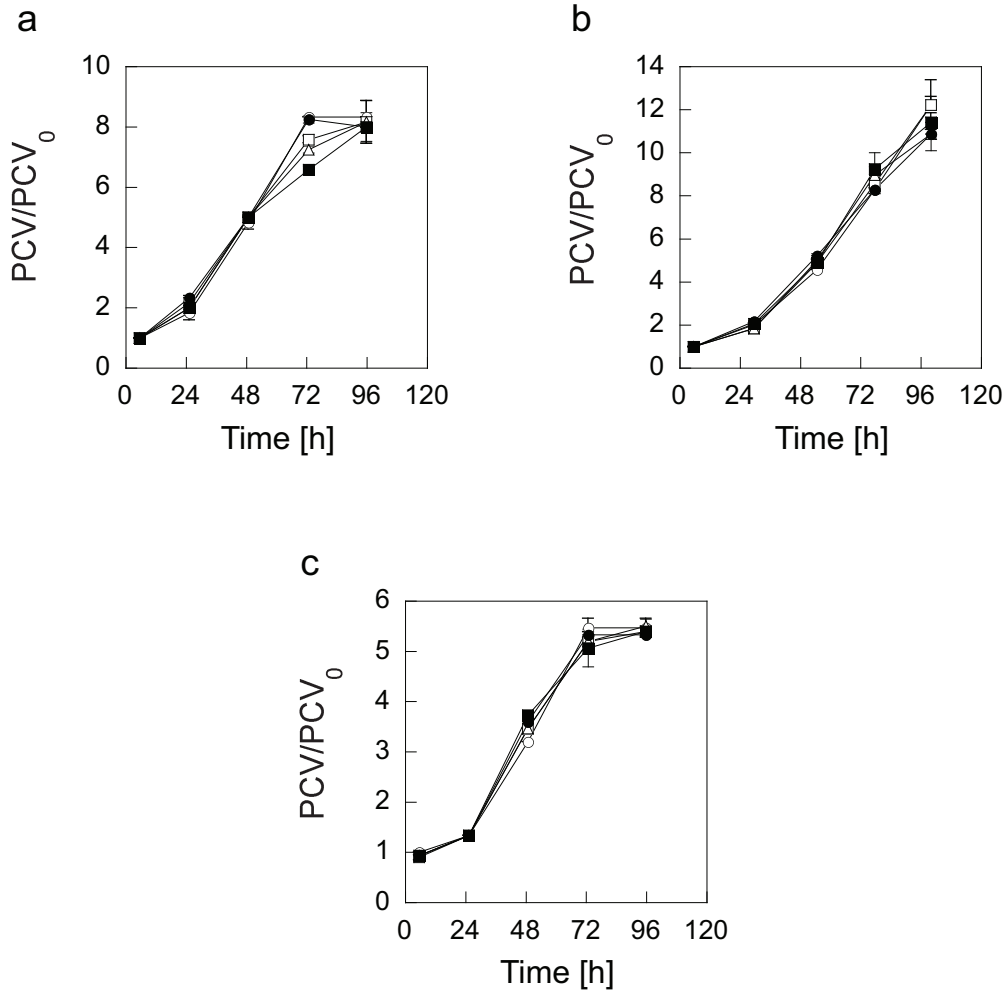


Fig. 4.16: Biomass accumulation during CHO cell growth in 1-L OSRs with working volumes of 200 (○), 300 (□), 400 (△), 500 (●) and 600 mL (■). The CHO-DG44 (a), CHO-IgG (b), and CHO-TNFR (c) cells were incubated at 37°C at 110 rpm. The ratio of the biomass volume to its initial values was measured at the times indicated.

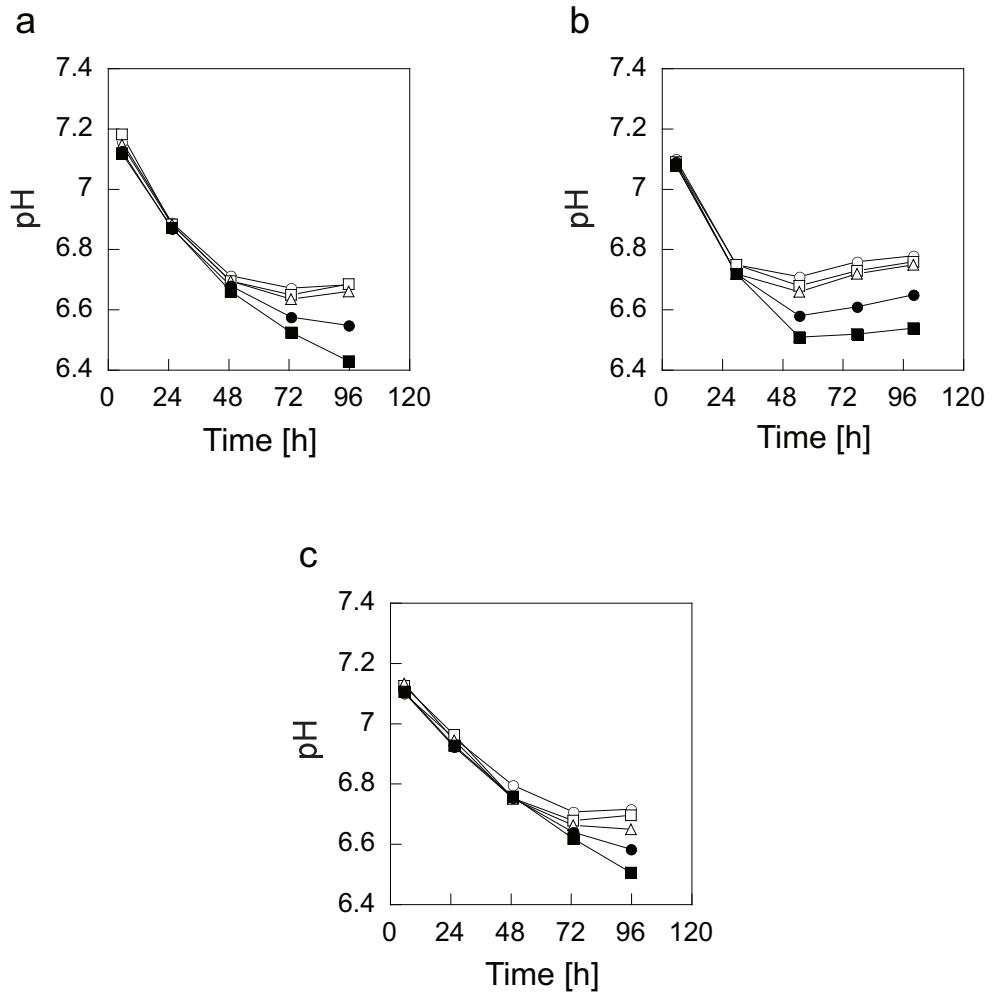


Fig. 4.17: The pH profiles during CHO cell growth and protein recombinant production in 1-L OSRs with working volumes of 200 (○), 300 (□), 400 (△), 500 (●) and 600 mL (■). The CHO-DG44 (a), CHO-IgG (b), and CHO-TNFR (c) cells were incubated at 37°C at 110 rpm. The pH was measured at the times indicated.

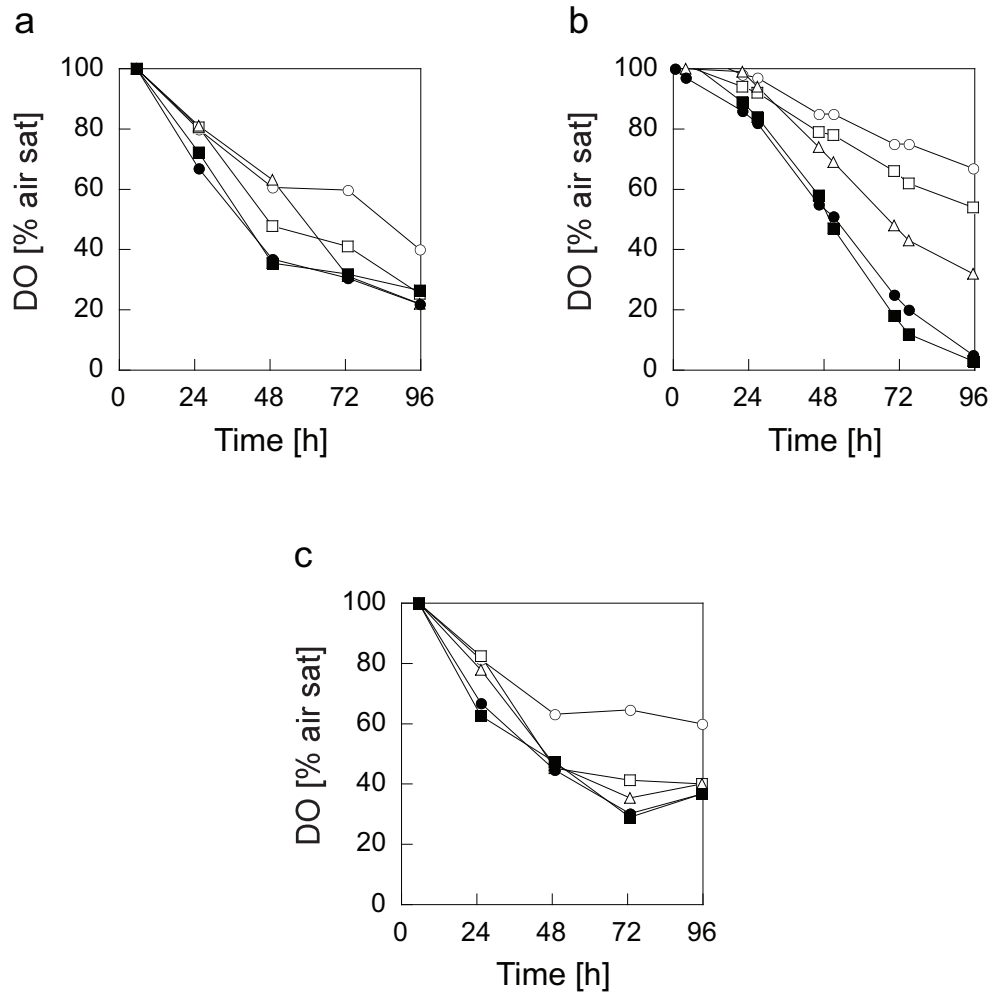


Fig. 4.18: Dissolved oxygen concentrations during CHO cell growth and protein recombinant production in 1-L OSRs with working volumes of 200 (○), 300 (□), 400 (△), 500 (●) and 600 mL (■). The CHO-DG44 (a), CHO-IgG (b), and CHO-TNFR (c) cells were incubated at 37°C at 110 rpm. The DO was measured at the times indicated.

k_La as a scale-up factor for probe-independent bioprocesses

To test if the thresholds of k_La values previously observed in the 1-L OSRs (9 h^{-1} for the CHO-DG44 and 7 h^{-1} for the CHO-IgG and CHO-TNFR cells) were the same independently of the scale, the three CHO cell lines were cultivated in 250-, 500-mL and 1-L OSRs with working volumes from 20 to 60% of the nominal volumes. The cells were incubated for 5 days at 110 rpm and at 37°C . For cultures with the same k_La value, the same ratio of maximal to initial cell density (X_{max}/X_0) was observed independently of the scale (Fig. 4.19). As the k_La increased, the X_{max}/X_0 ratio increased until reaching a plateau at 11 for CHO-DG44 and CHO-IgG cells and 8 for CHO-TNFR cells (Fig. 4.19). The maximal values of X_{max}/X_0 were observed in cultures with k_La values equal to or higher than 10 h^{-1} for CHO-DG44 cells and 7 h^{-1} for CHO-IgG and CHO-TNFR cells (Fig. 4.19).

The ratio of the maximal to initial biomass volume (PCV_{max}/PCV_0) remained within the same range independently of the k_La for CHO-DG44 and CHO-TNFR cells (Fig. 4.20a,c). For CHO-IgG cells, PCV_{max}/PCV_0 increased from 10 to 15 (Fig. 4.20b). The same specific productivity was observed for the same k_La value. The average specific productivity decreased from $18 \text{ pg cell}^{-1} \text{ day}^{-1}$ in CHO-IgG cultures and from $20 \text{ to } 17 \text{ pg cell}^{-1} \text{ day}^{-1}$ in CHO-TNFR cultures as the k_La increased from 4 to 18 h^{-1} (data not shown).

For all the three cell lines, the lowest values of pH measured during the experiments were the same for cultures having the same k_La (Fig. 4.21). The pH values increased with the k_La until they reached a plateau at the same k_La values as previously observed for the cell density (Fig. 4.21). The pH reached a plateau at 6.65 in CHO-DG44 and CHO-TNFR cell cultures (Fig. 4.21a and c) and at 6.70 in CHO-IgG cell cultures (Fig. 4.21b).

The cultures with the same k_La showed the same lowest DO values (Fig. 4.22). The DO values increased with the k_La for all cell lines (Fig. 4.22). As the k_La increased from 4 to 19 h^{-1} , the DO values increased from 30 to 50% air sat, from 0 to 80% air sat and from 20 to 60% air sat for the CHO-DG44, CHO-IgG and CHO-TNFR cell cultures, respectively (Fig. 4.22).

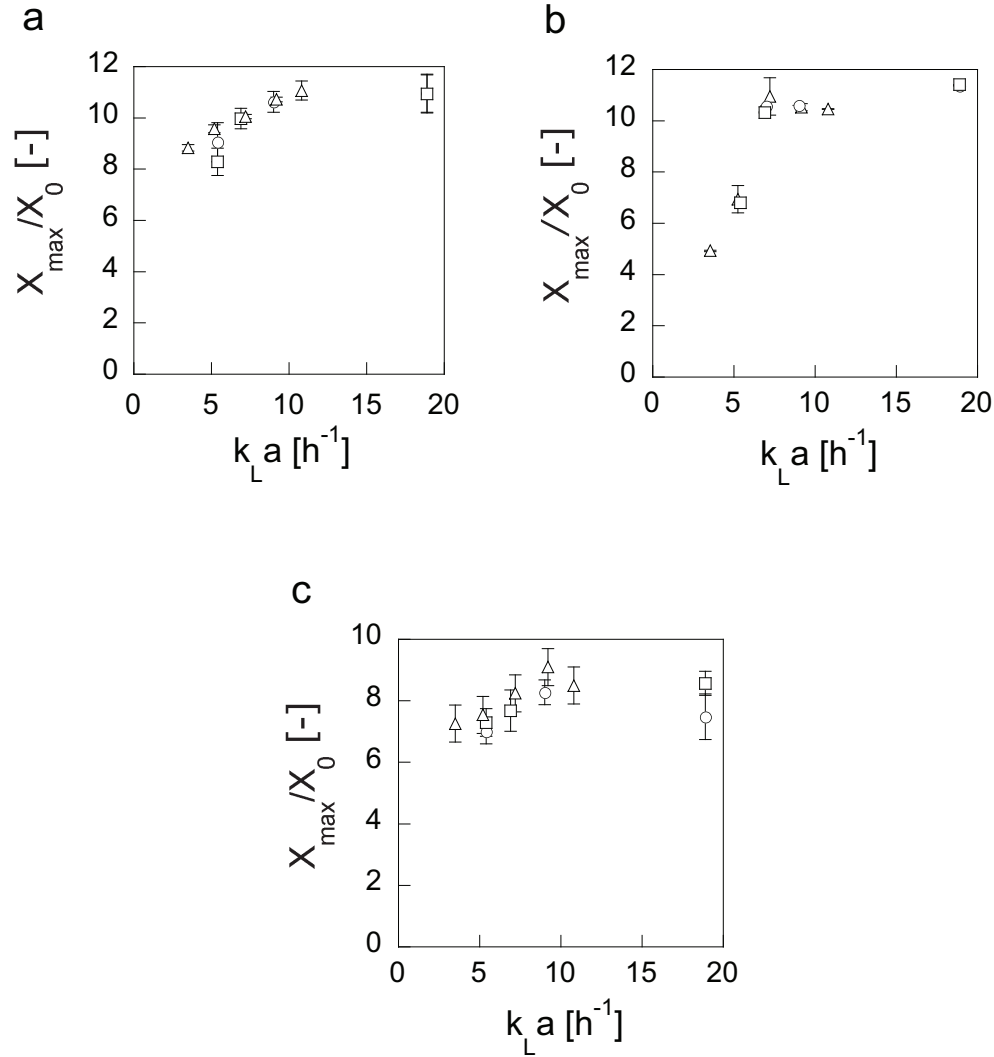


Fig. 4.19: Increase of CHO cell density after 5-days cultures in 250- (\circ), 500-mL (\square) and 1-L (\triangle) OSRs with different $k_L a$ values. CHO-DG44 (**a**), CHO-IgG (**b**), and CHO-TNFR (**c**) cells were incubated at 37°C at 110 rpm. The ratio of the maximal cell density to its initial value is reported as a function of the $k_L a$ of the culture.

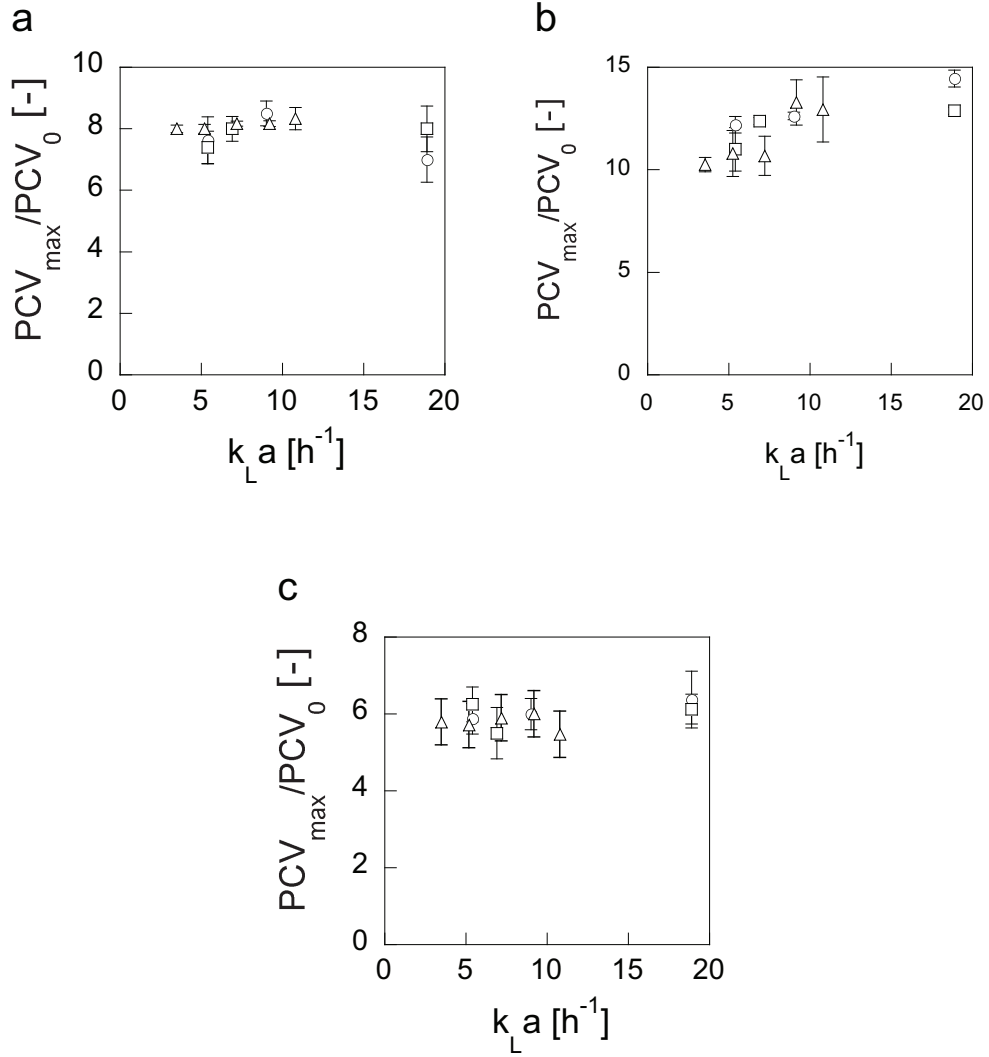


Fig. 4.20: Increase of CHO biomass volume after 5-days cultures in 250- (\circ), 500-mL (\square) and 1-L (\triangle) OSRs with different $k_L a$ values. CHO-DG44 (a), CHO-IgG (b), and CHO-TNFR (c) cells were incubated at 37°C at 110 rpm. The ratio of the maximal biomass volume to its initial value is reported as a function of the $k_L a$ of the culture.

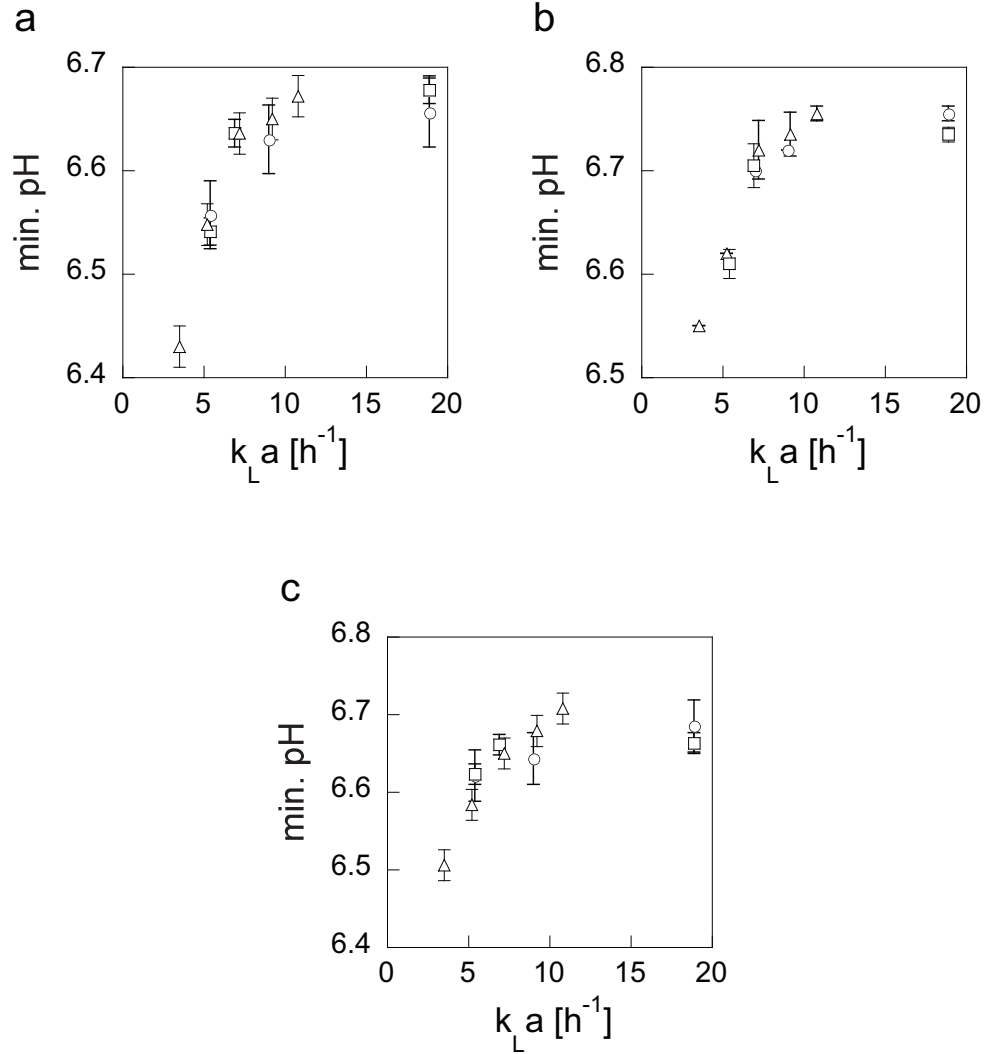


Fig. 4.21: Culture conditions of CHO cell cultures in 250- (\circ), 500-mL (\square) and 1-L (\triangle) OSRs with different k_La values. CHO-DG44 (a), CHO-IgG (b), and CHO-TNFR (c) cells were incubated during 5 days at 37°C at 110 rpm. The lowest pH values measured during the cultures are reported as a function of the k_La of the culture.

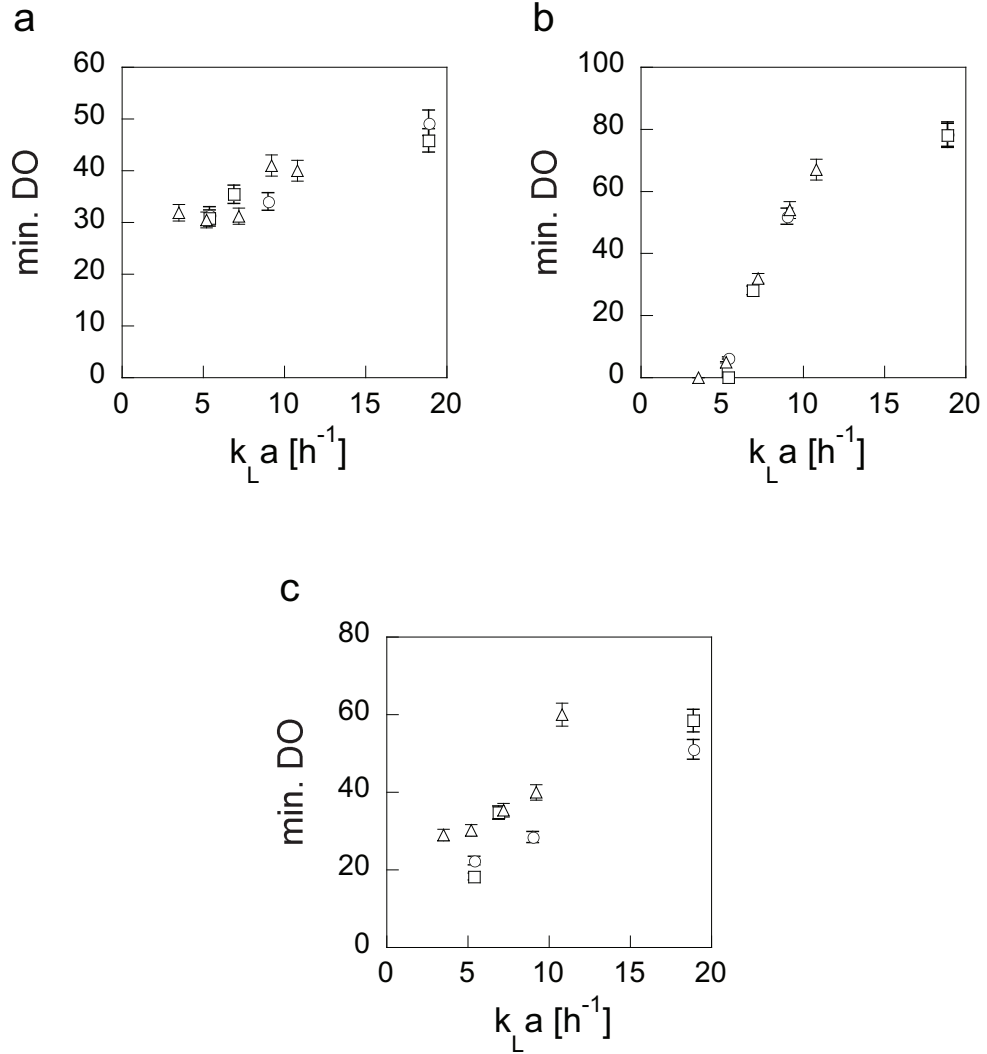


Fig. 4.22: Culture conditions of CHO cell cultures in 250- (○), 500-mL (□) and 1-L (△) OSRs with different $k_L a$ values. CHO-DG44 (a), CHO-IgG (b), and CHO-TNFR (c) cells were incubated during 5 days at 37°C at 110 rpm. The lowest DO values measured during the cultures are reported as a function of the $k_L a$ of the culture.

Probe-independent bioprocesses in large-scale bioreactors

To test the k_La as a scale-up factor for probe-independent bioprocesses, CHO-IgG were inoculated at 0.3 million cells/mL in a 200-L OSR with a working volume of 100 L. After overnight incubation, samples of the 100-L culture were dispatched into satellite cultures in 1- and 5-L OSRs. All the cultures were operated at a k_La of 7 h^{-1} . The cell densities were similar in

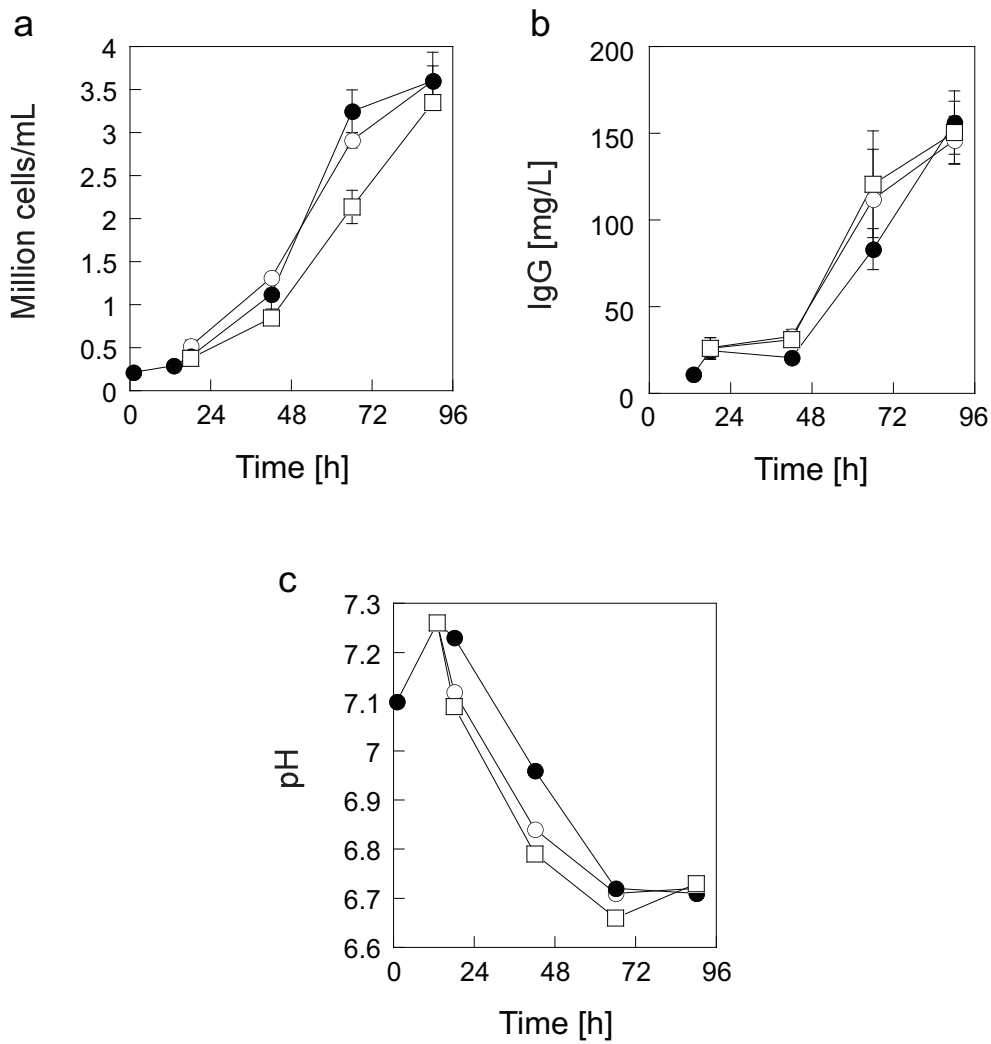


Fig. 4.23: CHO-IgG cell cultures in a 1-L OSR (○), a 5-L OSR (□) and a 200-L bioreactor (●). The viable cell density (a), recombinant IgG concentration (b), and pH (c) were measured at the times indicated.

the three OSRs and reached 3.5 million cells/mL after 90 h (Fig. 4.23a). The recombinant IgG concentrations in the crude supernatants were identical and increased to 150 mg/L (Fig. 4.23b). The pH decreased from 7.25 to 6.7 in the three OSRs (Fig. 4.23c). The glucose, glutamine, lactate and glutamate profiles were similar in all the cultures (data not shown).

4.4 Discussion

Our results show that the k_La is a good parameter to predict suitable conditions for probe-independent cell cultures in OSRs. Furthermore, our study demonstrates that the cultures having the same k_La had also the same cell growth, recombinant protein production and culture conditions (pH and DO) independently of the scale.

CHO-IgG cells cultivated in 1-L OSRs equipped with screw caps reached lower densities than those with vented caps. The lower pH values measured in cultures with screw caps were due to CO₂ accumulation in the medium and in the gas phase of the OSRs. Furthermore, the oxygen concentration in the gas phase of the OSRs with screw caps was lower than in those equipped with vented caps confirming the gas transfer limitations due to this type of closures.

CHO-DG44, CHO-IgG and CHO-TNFR cells were cultivated in 1-L OSRs with various working volumes. As the working volume increased, the k_La decreased and pH and DO limitations occurred in the cultures. The minimal k_La required to avoid these limitations was cell-line dependent and was 10 h⁻¹ for the CHO-DG44 cells and 7 h⁻¹ for the CHO-PIT and CHO-TNFR cells. Our results suggest that the pH was rapidly becoming critical as gas transfer limitations occurred. For example, pH values around or lower than 6.6 were observed in cultures showing lower cell densities, while DO values of about 30% air sat were still measured. As previously reported, a DO of 30% air sat should not be limiting, however a pH of 6.6 is clearly limiting (Trummer et al., 2006). While cultures with a sufficient k_La kept a dissolved CO₂ concentration of about 5%, concentrations up to 10% were observed in the cultures with an insufficient k_La explaining the lower pH values observed in these cultures.

The cell density of cultures experiencing limitations were smaller than that of cultures with a sufficient k_La . However, the volume of biomass was similar in all the cultures independently of the k_La . This suggests that the cell size increased in average in the cultures experiencing pH or DO limitations. Interestingly, cell cycle analysis showed that in cultures experiencing limitations the fraction of cells in G0/G1 phase was 10-20%

higher and the fraction of cells in G2 phase was 10-20% lower than in culture not experiencing these limitations. These results correlate with previous reports showing that cells in G0/G1 phase are generally bigger than cells in the G2 phase (Jorgensen and Tyers, 2004; Kim et al., 2007). While the relationship between a cell cycle phase and a specific productivity is not direct, the cell specific productivity has been reported to increase with the cell size (Lloyd et al., 2000). This could explain why similar recombinant protein titers were obtained in cultures experiencing limitations where the cell density was lower, but the average cell size bigger.

When the CHO-DG44, CHO-IgG and CHO-TNFR cells were cultivated in 250-, 500-mL and 1-L OSRs, similar values and trends in terms of cell density, DO, pH, biomass volume and specific productivity were observed in cultures having the same k_La . These results show that the k_La is a crucial parameter for the scale-up of mammalian cell cultures in probe-independent bioprocesses by ensuring that the pH and DO remain within a suitable range during the cell culture. As the gas transfer occurs through the free surface, different shapes of free surface such as the ones shown in Fig. 3.11 (p. 26) may lead to different gas transfer efficiencies. We have seen in Chapter 3 that the mixing regimes are correlated with the free-surface shape. As a consequence, further work is required to determine if the optimum in terms of free-surface shape is similar for mixing and gas transfer.

CHO-IgG cells cultivated in parallel in a 1-, 5- and 200-L OSRs with the same k_La reached similar cell densities, recombinant protein titers and pH values. Our results suggest that large-scale bioprocesses can be operated without probes and controllers as long as a sufficient k_La is maintained through appropriate cultivation conditions (e.g. working volume, agitation rate, geometry of the vessel). Furthermore, our study shows that for cultures having the same k_La , the same trends and values can be expected for cell density, pH and recombinant protein concentrations independently of the scale. These observations are of the greatest interest for facilitating the scale-up of bioprocesses in OSR with CHO cells. These probe-independent bioprocesses may be very interesting for the research and development in the industry as they are more cost-effective and simpler by avoiding the need for a controller and the use of pure oxygen or bases to keep suitable conditions in the bioreactors. Robustness of such bioprocesses is also higher as they are independent of probe and controller failures. The risks of contamination are also reduced since no equipment or solutions are added to the culture.

Hydrodynamic stress

5.1 Introduction

Since the 1980's, the scale of operation for mammalian cell bioprocesses increased rapidly to scales up to 10'000 L (Ma et al., 2002). As mammalian cells do not possess a cellular wall, the main concern for scale-up focused on their sensitivity to shear stress. As a consequence, stirred-tank bioreactors (STRs) for mammalian cell cultivation in suspension have been equipped with impellers designed to induce low shear stress (Ma et al., 2002). However, these impellers do not provide a sufficient mixing leading to dead zones deprived of oxygen or with an unsuitable pH (Ozturk, 1996). Interestingly, it became more and more evident that the mammalian cells can withstand higher agitation rates than expected and that the main source of hydrodynamic stress came from the small bursting bubbles sparged into the STRs (Kunas and Papoutsakis, 2009; Ma et al., 2002; Nienow, 2006).

The volumetric power consumption (P_V) which represents the energy required to maintain the fluid in motion in a given period of time is commonly used as a scale-up parameter and associated with the hydrodynamic stress in a bioreactor (Godoy-Silva et al., 2009; Marques et al., 2010). As the P_V influences mixing and the gas transfer, it is necessary to maintain it at a sufficient value to obtain homogeneity and avoid oxygen or pH limitations. CHO cells have been reported to withstand P_V values of 10^4 - 10^5 kW/m³ (Godoy-Silva et al., 2009). As a comparison, this values are typically within the range of power generated by the rupture of a bubble with a diameter of 1.7 mm (Garcia-Briones et al., 1994). As gases are sparged into the cultures in STRs, the bubbles generated may be harmful for the cells and induce limitations (Nienow, 2006).

While several correlations for the P_V have been established in orbitally shaken bioreactors (OSRs) (Büchs et al., 2000a,b; Kato et al., 2004; Peter et al., 2006a,b; Raval et al., 2007), the hydrodynamics of these bioreactors is still poorly understood. The free surface of OSRs complicates the relationship between the P_V and the level of hydrodynamic stress in OSRs. We have seen in Chapter 3 that the free surface shape depends upon the geometric ratios (d_s/d , d/h) and operating conditions (Fr). The different wave patterns may influence differently the level of shear stress in the OSRs.

To evaluate the cell damage in OSRs, CHO cells were cultivated in vessels from 1 to 200 L. The shear stress was simulated by computational fluid dynamics (CFD). The P_V was tested as a scale-up factor in a 200-L OSR and thresholds for CHO cell resistance were defined in a 1-L OSR.

5.2 Material and Methods

Shear stress and hydrodynamic simulation

The shear stress and the hydrodynamic of 1-L OSRs were simulated by computational fluid dynamics. These experiments were performed by Samuel Quinodoz (Modeling and Scientific Computing Chair, EPFL, Switzerland). The Navier-Stokes equation was approximated with the finite element method using stabilized finite elements (no turbulence model was therefore used). The interface was tracked using the level set method (Osher and Fedkiw, 2002) and a special correction scheme was used to better approximate the pressure near the interface (Discacciati et al., 2011). The simulations were all based on a mesh containing 50'000 tetrahedra and 10'000 vertices. The area of a finite element was 9.8 cm². Because of the chosen discretization, each time step required the resolution of a linear system composed of 190'000 unknowns. To fasten the computations, parallel computers were used.

Cell culture

Three CHO cell lines, CHO-DG44, CHO-IgG and CHO-TNFR, were cultivated in ProCHO5 medium (Lonza) as described in Section 4.2 (p. 39). To test the resistance of the cells to shear stress, the cells were diluted 10 times into fresh Ex-Cell 302 medium (Sigma-Aldrich, St. Louis, MO, USA) and agitated during 24 h (Kühner AG). The cell growth rate was calculated from Eq. 5.1:

$$\frac{dX}{dt} = \mu X \quad (5.1)$$

where X is the cell density [million cells/mL], t the time [h] and μ the cell growth rate [h^{-1}].

To test the effects of the cell culture age, CHO-IgG cells were cultivated in ProCHO5 medium during 4, 5, 6 or 7 days. The cells were then diluted 10 times into fresh Ex-Cell 302 medium and split into two 1-L OSRs agitated at 110 (control) or 200 rpm for 24 h.

Volumetric power consumption measurement

The volumetric power consumption (P_V) was measured by a thermodynamic method based on the fact that the friction due to the agitation produces heat (Raval et al., 2007). Deionized water was heated to about 40°C and transferred into 5-L OSRs. The OSRs were insulated with polystyrene and agitated at different agitation rates at room temperature. The temperature of water was measured with a temperature sensor (KCG 50, KIMO Instrument, Montpon, France) and recorded every 5 min for 6 h. In the 200- and 2000-L OSRs, deionized water was heated to about 40°C under agitation. The water was kept at this temperature and the bioreactor under agitation for 12 h to ensure homogeneity. The heating element was then switched off and the temperature of the water and of the surroundings were recorded every hour for 24 h (Fig. 5.1).

The volumetric power consumption was calculated from the following heat balance (Eq. 5.2):

$$-C_p \frac{dT}{dt} = \frac{UA}{V}(T - T_{out}) - \frac{P}{V} \quad (5.2)$$

where C_p is the heat capacity [$\text{J m}^{-3} \text{K}^{-1}$], T the temperature of the water [K], U the over-all heat transfer coefficient [$\text{J m}^{-2} \text{K}^{-1}$], A the heat transfer area [$\text{m}^2 \text{m}^{-3}$], T_{out} the temperature of the surroundings [K], and P/V the volumetric power consumption [J m^{-3}].

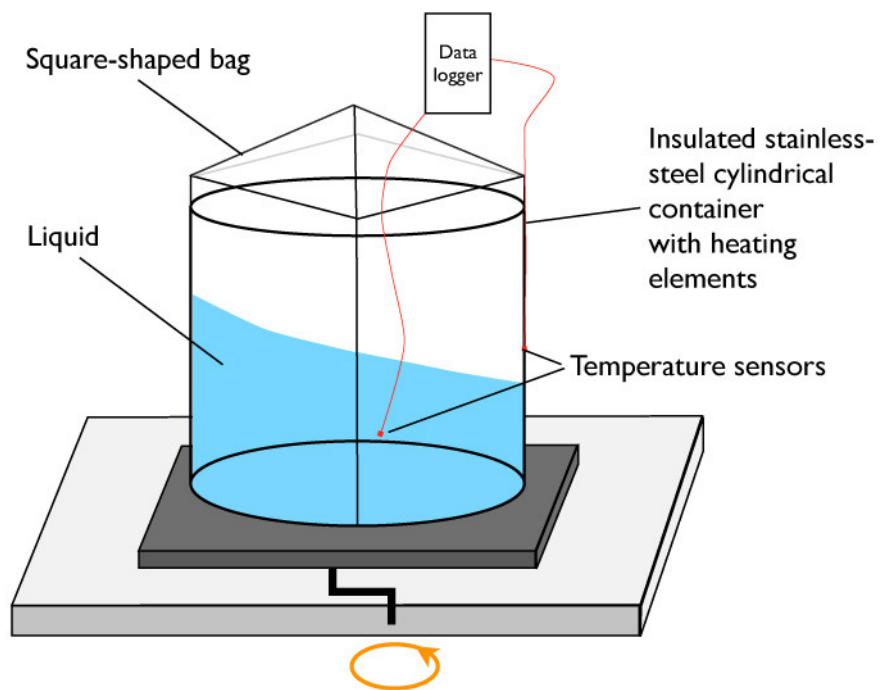


Fig. 5.1: Set-up for thermodynamic measurements of the P_V in large-scale OSRs.

Detection of cell damages

The cell damage was assessed by different methods: the viable cell density and biomass volume measurements and the lactate dehydrogenase detection. The viable cell density was assessed by flow cytometry with a Guava EasyCyte System (Millipore, Billerica, MA). The GFP-fluorescence of CHO-IgG and CHO-TNFR cells was directly measured by the flowcytometer. The CHO-DG44 were treated with the Guava ViaCount Reagent according to manufacturer's protocol prior the analysis. The volume of biomass was measured by PCV as described in Section 4.2 (p. 39). The lactate dehydrogenase was detected with a Cytotoxicity Detection Kit Plus (Roche Diagnostics AG, Rotkreuz, Switzerland). The 0% of cell damage was set at the value obtained for the supernatant of the 4-days old cell culture freshly diluted into Ex-Cell 302. This value was used as the 0% for the experiments with the 5-, 6- and 7-days old cultures as well. To determine the 100% of cell damage, samples of the cultures at the beginning of the experiment were completely lyzed according to the manufacturer's protocol. The resulting value was considered as 100% of cell damage. This value was measured for each cell age.

5.3 Results

Hydrodynamic stress under usual cultivation conditions

The shear stress level under usual cultivation conditions for mammalian cells was simulated by CFD. CHO-DG44, CHO-IgG and CHO-TNFR cells were cultivated in a 1-L OSR at 110 rpm and a shaking diameter of 5 cm as described in Section 4.2 (p. 39). The working volume was 300 mL. The CHO-DG44 cells grew to 5 million cells/mL, while the CHO-IgG and CHO-TNFR reached densities of 4 million cells/mL (Fig. 5.2a). According to the CFD simulations, the maximal shear stress value was situated at the tip of the wave and was about 0.075 Pa (Fig. 5.2b). The shear stress was higher at the walls than in the center of the liquid (Fig. 5.2c). Most of the zones in the liquid phase had a shear stress value equal to or lower than 0.02 Pa (Fig. 5.2d).

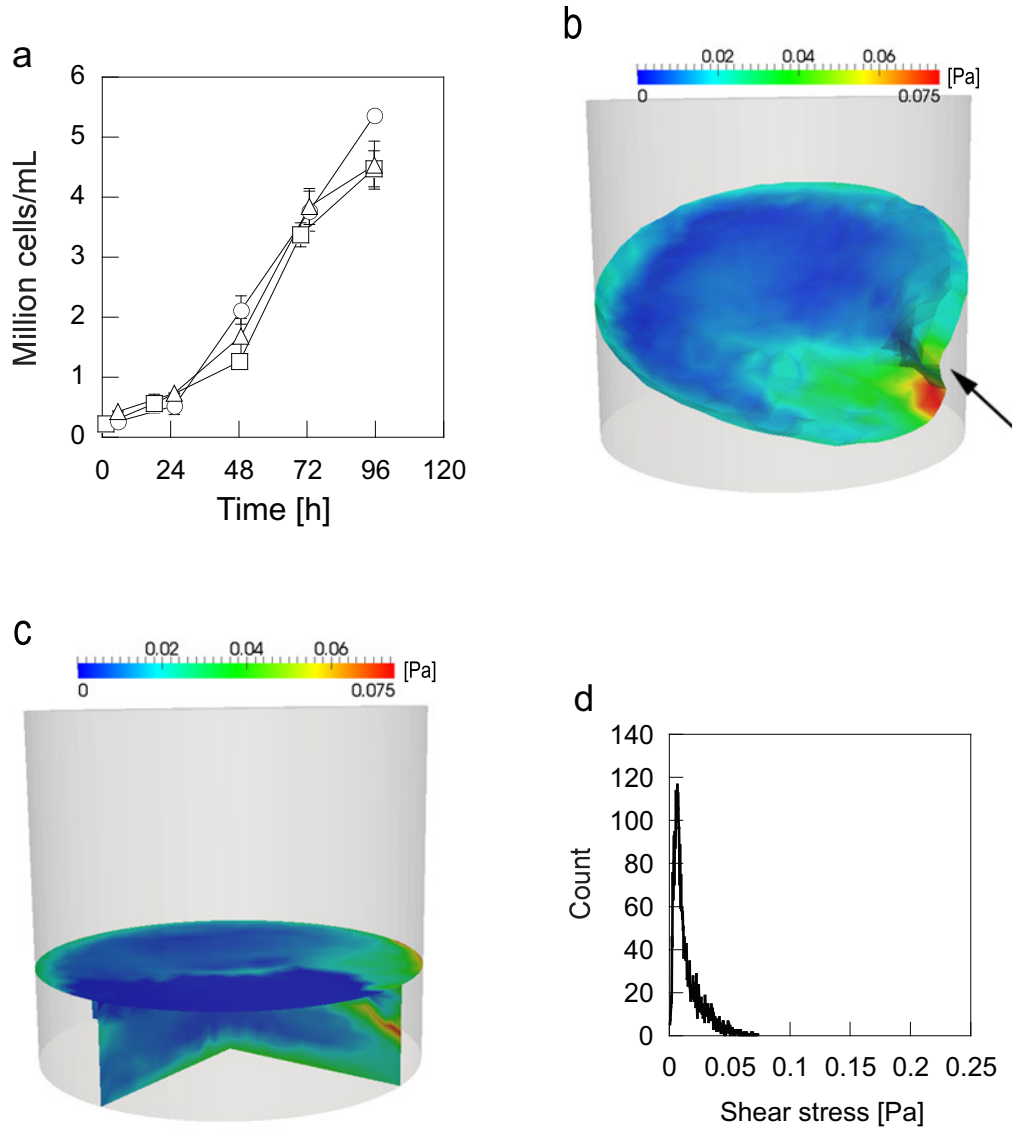


Fig. 5.2: CHO cell cultivation under standard conditions in a 1-L OSR at 110 rpm. The viable cell density **(a)** of CHO-DG44 (○), CHO-IgG (□) and CHO-TNFR (△) cells was measured at 37°C. The shear stress was simulated by CFD at the free surface **(b)** and in the liquid phase (cut view) **(c)**. Histogram of the shear stress values in the liquid phase **(d)**. The shaking diameter was 5 cm and the working volume 300 mL. The arrow indicates the tip of the wave.

The P_V as a scale-up factor for shear stress level

We tested the P_V as a scale-up factor to predict adapted shear stress levels for mammalian cell cultivation in OSRs. We measured the P_V values in 5-, 200- and 2000-L OSRs. While the P_V values in the two large-scale OSRs increased from 0.05 to 0.35 kW/m³, the P_V values in the 5-L OSR increased from 0.1 to 0.9 kW/m³ (Fig. 5.3a). We cultivated CHO-IgG cells in a 5-L

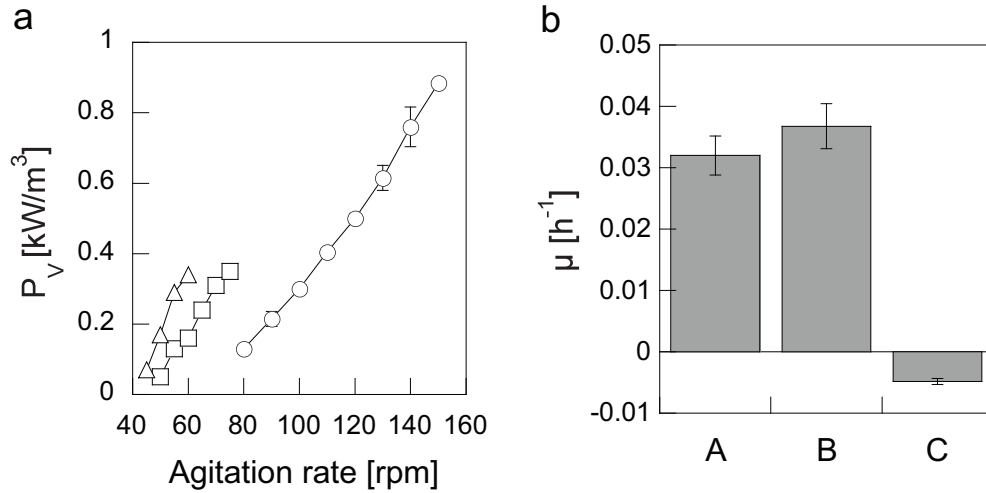


Fig. 5.3: The P_V as a scale-up factor for mammalian cell culture. **(a)** The volumetric power consumption in 5- (○), 200-(□) and 2000-L (△) OSRs was measured by a thermodynamic method. **(b)** The cell growth rate of cultures in a 5-L OSR at 110 rpm (A), a 5-L OSR at 200 rpm (B), and a 200-L OSR at 75 rpm (C) was measured at 37°C over a cultivation period of 24 h.

OSR at 110 rpm and in a 200-L OSR at 75 rpm. Under these cultivation conditions, the P_V values were about 0.4 kW/m³ in the two OSRs. Another culture was operated in a 5-L OSR at 150 rpm corresponding to a P_V value of 0.9 kW/m³. While CHO-IgG cells cultivated in a 5-L OSR at 150 rpm showed similar growth rate than the cells cultivated in the same OSR at 110 rpm, the cells cultivated in a 200-L OSR at 75 rpm showed a decrease in their density (Fig. 5.3b).

Effects of cell culture age

The effects of cell age were tested on CHO-IgG cell cultures in 1-L OSRs with 100 mL of working volume at 37°C. Cell cultures between 4- and 7-days old were diluted into fresh medium and agitated at 110 rpm (control)

or 200 rpm for 24 h. We tested the three following methods in parallel to detect cell damage: cell counting, biomass volume measurement and LDH detection.

Cell counting method

The viable cell density was measured by flow cytometry. The resulting histograms of the 5-day cultures are shown as an example (Fig. 5.4). The peak corresponding to the viable cell size was situated at a forward scatter value of about 5×10^2 (Fig. 5.4a). In the culture at 200 rpm, the peak corresponding to viable cell size was significantly smaller after 24 h and particles of lower sizes were accumulating (Fig. 5.4b).

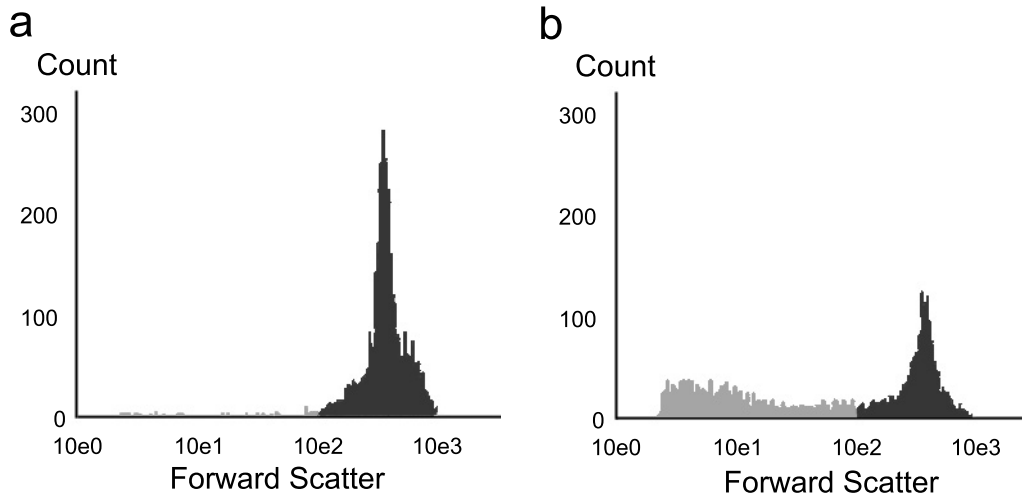


Fig. 5.4: Histograms of forward scatter measurements by flow cytometry of 5-days old CHO-IgG cultures after 24 h at 110 rpm (a) or at 200 rpm (b). The cells were cultivated in 1-L OSR with a working volume of 100 mL at 37°C.

The cell growth rate of the 4-day old cultures was similar at 110 and 200 rpm and was about 0.04 h^{-1} (Fig. 5.5). The cultures older than 4 days and agitated at 110 rpm showed a decrease in the cell growth rate (0.02 h^{-1}) (Fig. 5.5). On the other hand, when these cultures were agitated at 200 rpm, the viable cell density decreased dramatically (Fig. 5.5).



Fig. 5.5: Cell growth rate of CHO-IgG cells assessed by the cell counting method at 37°C in 1-L OSRs at 110 (○) and 200 rpm (□). The cells were cultivated in 100 mL for 24 h.

Biomass volume measurement method

The PCV was used to measure the biomass volume. We evaluated its ability to detect cell damage. As a first step, we investigated the range of particle size measured by PCV using flow cytometry. The dot plots of the 5-day cultures after 24 h at 110 or 200 rpm are shown as an example (Fig. 5.6). Most of the particles measured before centrifugation in the culture agitated at 110 rpm were viable cells (Fig. 5.6a). The dot plot after centrifugation showed that most of the viable cells were centrifuged and thus taken into account in the biomass volume measurement (Fig. 5.6b). In the culture agitated at 200 rpm, the amount of viable cells was significantly lower than at 110 rpm and cellular debris with almost the same values of forward scatter as viable cells were observable (Fig. 5.6c). However, these particles were still detected by the flowcytometer after centrifugation showing that they were not taken into account in the biomass volume measured by PCV (Fig. 5.6d).

The cell growth rates resulting from the PCV measurements showed similar trends as those resulting from the viable cell density measurements (Fig. 5.7). No significant effects of shear stress were detected in the 4-days old cell culture, although the volume of biomass decreased significantly as the cultures became older (Fig. 5.7).

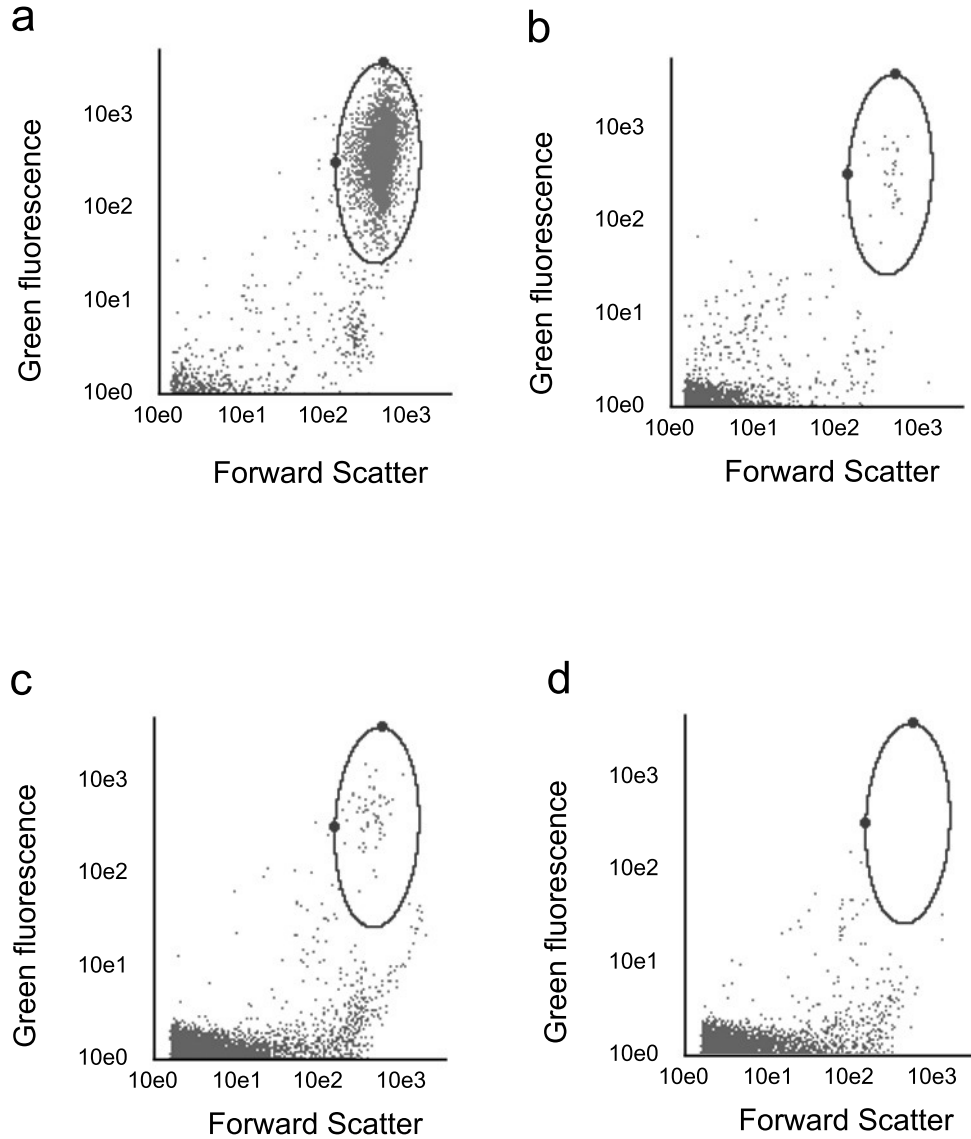


Fig. 5.6: Flow cytometry measurements of 5-days old CHO-IgG cultures agitated at 110 (a,b) or 200 rpm (c,d) in 1-L OSRs with a working volume of 100 mL after 24 h. The analysis were performed on the PCV samples before centrifugation (a,c) and on the supernatants after centrifugation (b,d). The population corresponding to viable cells is encircled.

LDH detection method

We used the LDH detection method to measure the cell damage in the cultures. The 0% cell damage was set at the value obtained for the supernatant

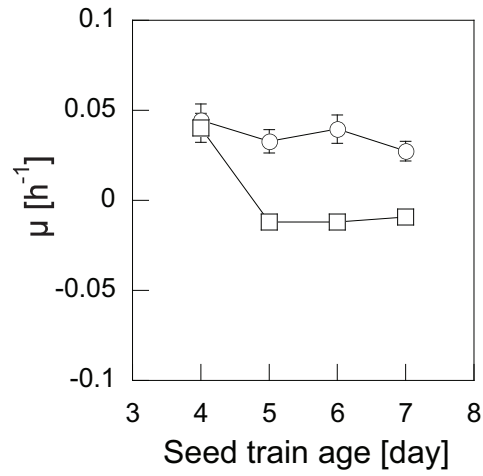


Fig. 5.7: Cell growth rate of CHO-IgG cells assessed by the biomass volume measurement method at 37°C in 1-L OSRs at 110 (○) and 200 rpm (□). The cells were cultivated in 100 mL for 24 h.

of the 4-days old culture freshly diluted at the beginning of the experiment. In the 4-days old culture at 200 rpm no cell damage was detected (Fig. 5.8). The percentage of damaged cells increased with the age of the cultures from 0 to 20% at 110 rpm and from 0 to 70% at 200 rpm (Fig. 5.8).

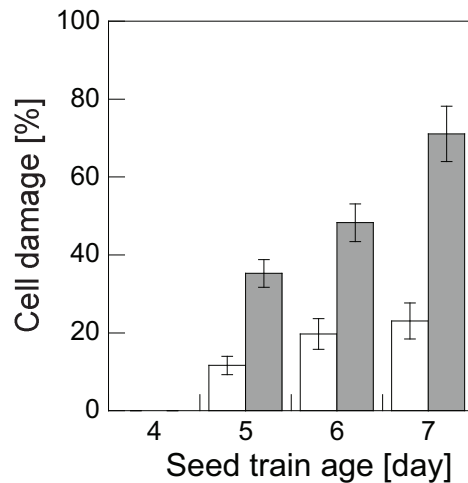


Fig. 5.8: Cell damage of CHO-IgG cells assessed by the LDH detection method at 37°C in 1-L OSRs at 110 (white bars) and 200 rpm (gray bars). The cells were cultivated in 100 mL for 24 h.

Kinetics of cell death induced by shear stress

To evaluate the time necessary to detect cell death induced by shear stress, CHO-IgG cells were cultivated in 1-L OSRs at 110 and 200 rpm during 24 h. Cell counting was performed on samples taken at 0, 5, 7 and 24 h. Significant differences between the two agitation rates were observed after 7 h (Fig. 5.9a). At this time, the viable cell density decreased from 0.2 to 0.1 million cells/mL in the culture agitated at 200 rpm (Fig. 5.9a).

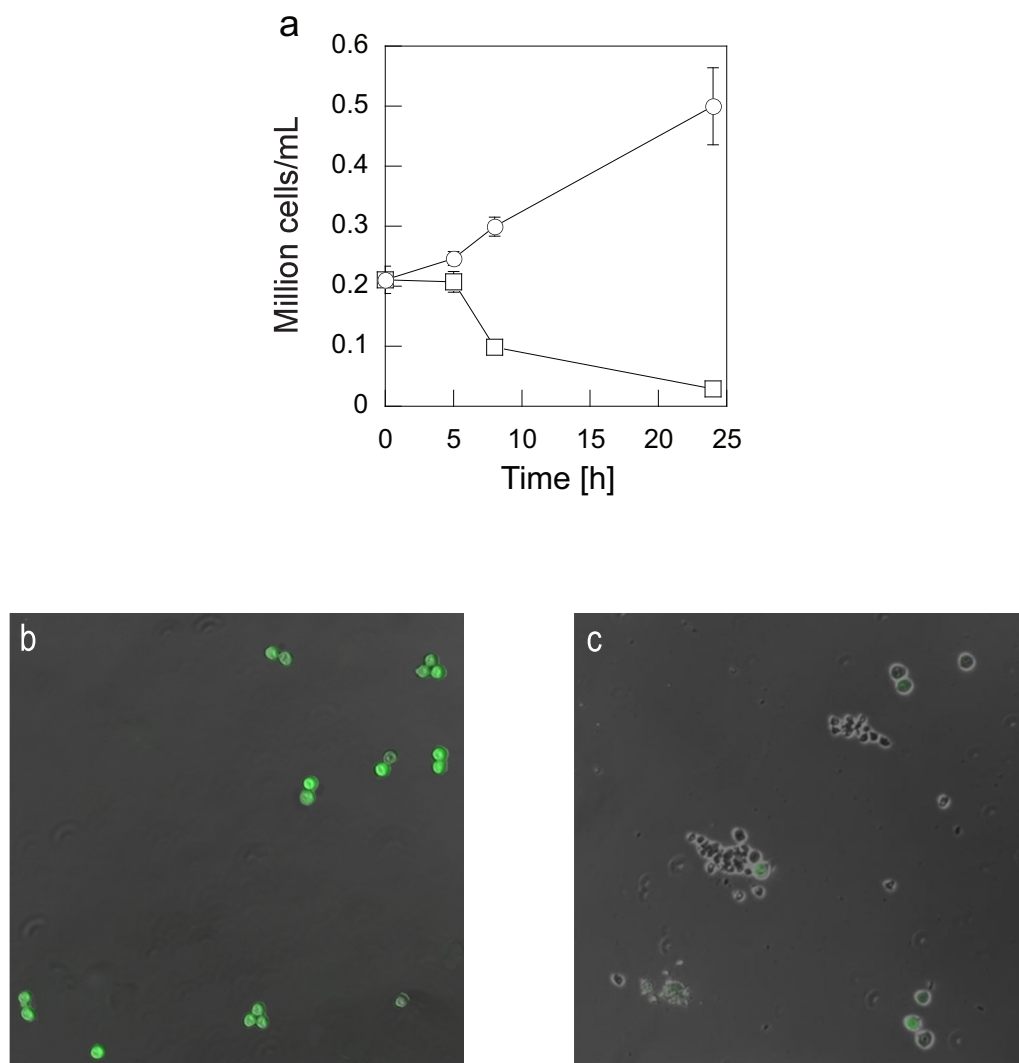


Fig. 5.9: Kinetics of cell death induced by shear stress. Viable cell density of CHO-IgG cells in 1-L OSRs at 110 (○) and 200 rpm (□) (a), pictures of the cells after 7 h at 110 (b) and 200 rpm (c). The cells were cultivated in 100 mL at 37°C.

After 24 h, almost no viable cells were observed at 200 rpm, although a density of 0.5 million cells/mL was measured at 110 rpm (Fig. 5.9a). The cells in the culture agitated at 110 rpm were fluorescent and no debris was observed after 7 h (Fig. 5.9b). Only a few green cells and many cellular debris were observed after 7 h in the culture at 200 rpm (Fig. 5.9c).

Shear stress thresholds in 1-L OSRs

CHO-DG44, CHO-IgG and CHO-TNFR cells were cultivated in 1-L OSRs at agitation rates from 150 to 200 rpm during 24 h to determine conditions under which the shear stress was harmful for the cells. For each cell line and agitation rate a control culture agitated at 110 rpm was run in parallel. The shear stress was calculated from CFD simulations. No significant difference was observed between the control culture and the cultures agitated at 150 or 160 rpm for the three cell lines (Fig. 5.10). The growth rate of the CHO-DG44 culture at 170 rpm was twice lower than that at 110 rpm (control) (Fig. 5.10). The relative growth rate of the CHO-IgG and CHO-TNFR cultures were negative at 170 rpm, indicating that the cell density decreased (Fig. 5.10).

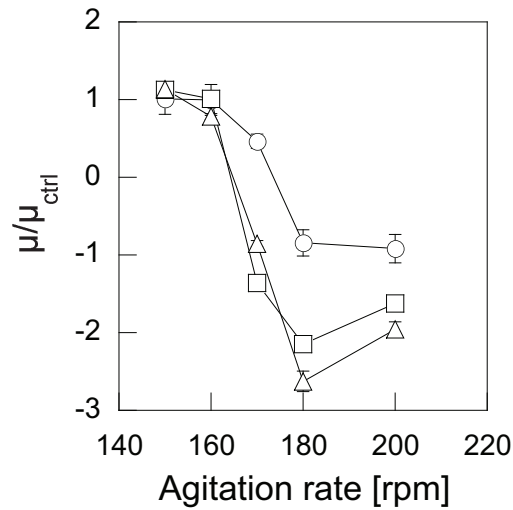


Fig. 5.10: Relative cell growth rate of CHO-DG44 (○), CHO-IgG (□) and CHO-TNFR (△) cells in 1-L OSRs at various agitation rates. The cells were agitated at 37°C for 24 h in a working volume of 100 mL. The cell growth rate was normalized with the cell growth rate of a culture agitated at 110 rpm in parallel (control) for each cell line and experiment.

According to CFD simulations, the maximal value of shear stress was equal to or lower than 0.17 Pa from 150 to 160 rpm (Fig. 5.11a,b). When cell damage was observed at 170 rpm, the maximal shear stress values were about 0.19 Pa (Fig. 5.11c). The maximal values of shear stress were always situated at the tip of the wave independently of the agitation rate (Fig. 5.11).

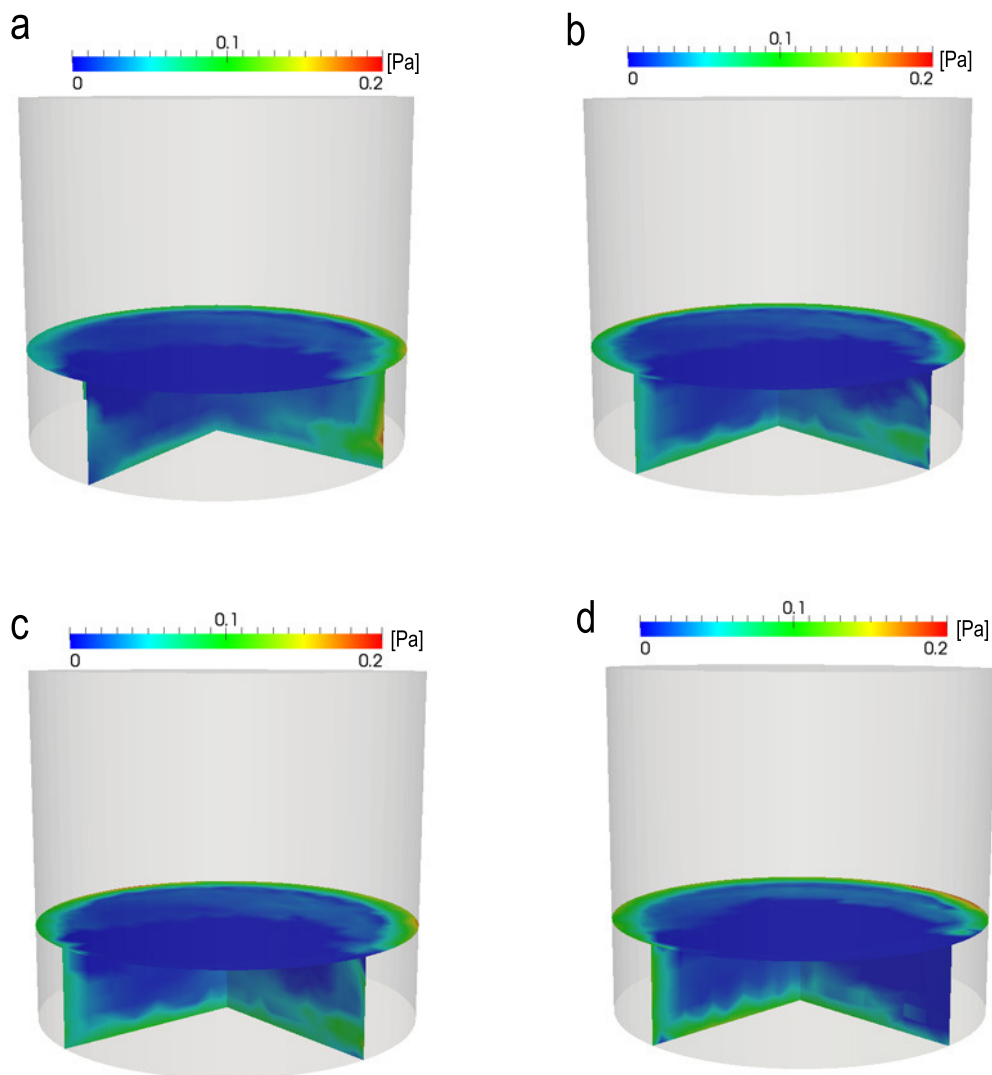


Fig. 5.11: Shear stress in 1-L OSRs at 150 (a), 160 (b), 170 (c) and 180 rpm (d). The working volume was 100 mL and the shaking diameter 5 cm.

At agitation rates from 150 to 180 rpm, most of the zones of the OSRs had shear stress values equal to or lower than 0.05 Pa (Fig. 5.12). The peak

observed at a shear stress value of about 0.01 Pa at 150 rpm shifted to 0.025 at 180 rpm (Fig. 5.12). The value of the maximal shear stress increased with the agitation rate (Fig. 5.12). However, only a small amount of zones had these maximal values (Fig. 5.12).

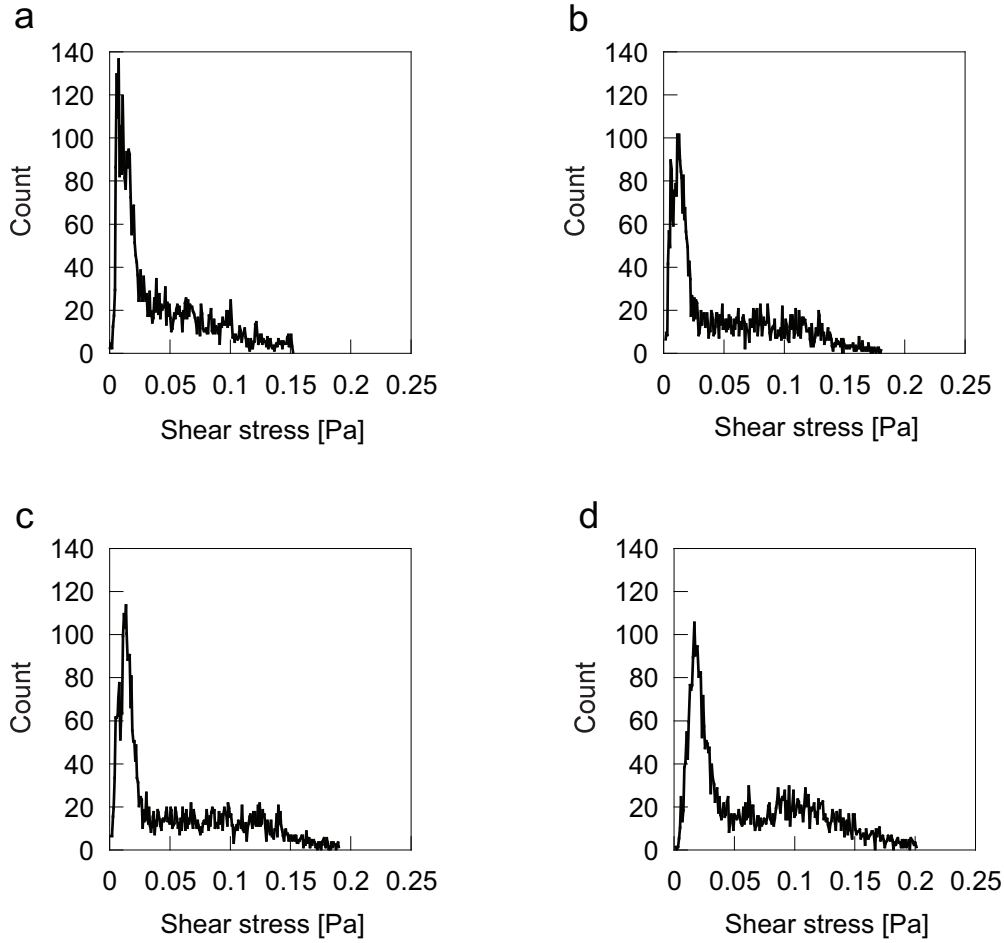


Fig. 5.12: Histograms of the shear stress simulated by CFD in 1-L OSRs at 150 (a), 160 (b), 170 (c) and 180 rpm (d). The working volume was 100 mL and the shaking diameter 5 cm.

5.4 Discussion

We tested the hydrodynamic stress in OSRs for mammalian cell culture using CFD simulations. According to those simulations, the maximal shear stress values were about 0.075 Pa in a 1-L OSR agitated at 110 rpm with a working volume of 300 mL. This value is one to two orders of magnitude lower than the ones reported to be harmful for CHO and HEK cells (Tanzeglock et al., 2009) showing that standard cultivation conditions in OSRs are safe for mammalian cells.

We showed that the cell resistance to shear stress decreased for cell cultures older than 4 days. Under our conditions of cultivation, the transition between the exponential cell growth and the stationary phase occurs after 4 days. These results are in good agreement with previous observations reporting a lower shear stress resistance of hybridoma cells when entering the stationary phase (Petersen et al., 1988). These results are of great importance for example to determine the optimal time for inoculation of a culture into a bioreactor.

We compared the cell counting by flow cytometry, the biomass volume measurement by PCV method and the LDH detection to assess cell damage in the cultures. The three methods gave similar results and thresholds in terms of cell damage due to shear stress exposure. These results validate the use of the PCV method to assess the effects of hydrodynamic stress in cell cultures. This method does not require expensive equipments and can be therefore an interesting alternative to the standard method based on LDH detection. It is also faster and more accurate than cell counting as the measurement is performed on a larger volume of sample (Stettler et al., 2006).

CHO cells showed limited cell growth or a decrease in the cell density at 170 rpm in 1-L OSRs with working volumes of 100 mL. According to CFD simulations, the maximal shear stress level was about 0.19 Pa at this agitation rate. This value was a bit lower than that reported to damage the CHO and HEK cells (Tanzeglock et al., 2009). However, the CFD simulations are still under optimization and the first results showed here may be biased because of too big mesh sizes preventing accurate calculation in the zones close to the tip of the wave. As a consequence, the shear stress values presented here must be taken with care. Nevertheless, the thresholds obtained in the 1-L OSR in terms of agitation rate can be useful for the optimization of the large-scale OSRs together with an improved CFD simulation.

The volumetric power consumption (P_V) was evaluated as a scale-up factor for shear stress level in the OSRs. The 200- and 2000-L OSRs ex-

hibited very low P_V values compared to the 5-L OSR. However, when the CHO-IgG cells were cultivated at the same P_V values in the 200-L OSR as in the 5-L OSR, the cell density decreased in the 200-L OSR and the viability dropped to 60% in one night of culture. These results suggest that P_V may not be suitable to evaluate the level of shear stress in an OSR. Contrary to stirred-tank bioreactors (STRs), the OSRs have a free surface whose shape and behavior is dependent on the geometric factors (inner diameter, shaking diameter and liquid height) (see Chapter 3). Despite the same P_V values, the shape of the wave was different in the two OSRs. While a double wave was observed in the 5-L OSR, a single-peak wave was observed in the 200-L OSR. These results suggest that the different wave patterns as presented in Chapter 3 may lead to different maximal shear stress values. Nevertheless, further analysis of correlation between the shape of the wave and the maximal shear stress level is required to determine a scale-up factor for the hydrodynamic stress in OSRs. Further analysis of CFD simulations showed that the maximal shear stress was located at the tip of the wave of the free surface. Interestingly, these zones represented less than 1% of the liquid phase. However, as the wave of the free surface rotates with time, many zones of the liquid will be touched by this amount of shear stress at a certain time point. This is why even if this amount of shear stress is located in a very small fraction of the liquid at a defined time point, its potential to harm the cells can not be neglected in the OSRs.

Variability of probe-independent bioprocesses

6.1 Introduction

STRs are currently considered the standard in the biotechnology industry for recombinant protein production by mammalian cells (Chu and Robinson, 2001). In general, recombinant protein production in STRs is monitored and strictly controlled to maintain the pH and dissolved oxygen concentration (DO) within suitable ranges during the bioprocess (Marks, 2003; Nienow, 2006). Consequently, it is still a widely held view that high recombinant protein yields can only be achieved under strict pH and DO control throughout the entire bioprocess (Merten, 2006). However, in the biotechnology industry more than 50% of all batch losses are due to material or equipment failure (Langer, 2008). Therefore, reducing the needs for probes and controllers is expected to decrease these losses. We showed in the previous chapters that mammalian cell cultivation in OSRs could be operated without probes and controllers if sufficient mixing times and k_La values were obtained at suitable hydrodynamic conditions.

Before comparing bioprocesses in STRs and OSRs, the two types of bioreactors were characterized for mixing, gas transfer and hydrodynamic stress. Mixing aims to minimize concentration gradients leading to zones with reduced oxygen or an inappropriate pH (Lara et al., 2006) and is typically evaluated by measuring the mixing time, defined as the time needed to achieve a specified degree of homogeneity in the liquid (Zlokarnik, 2003). We showed in Chapter 4 that the mixing times in OSRs are in the range of 10-30 s at nominal volumes of 5 mL to 1500 L, ensuring homogeneity for mammalian cell cultures for these scales of operation. In STRs, the mix-

ing time increases with the scale and is typically more than 1 minute for large-scale bioreactors suggesting the existence of significant concentration gradients with respect to nutrients, dissolved oxygen and ions (pH) (Xing et al., 2009).

Efficient gas-liquid transfer is required to ensure the oxygen supply to the cells and CO₂ removal from the medium (Bonvillani et al., 2006; Garcia-Ochoa and Gomez, 2009). The gas transfer study in Chapter 4 demonstrated that a sufficient k_La (typically about 7 h⁻¹) is required to keep a suitable cell culture environment without needing probes and controllers. In various OSRs including TubeSpins®, 1- and 5-L glass bottles, and 2000-L bioreactors, k_La values in the range of 4-30 h⁻¹ have been measured at agitation rates suitable for mammalian cell cultivation (Zhang et al., 2009a).

It is also important that the conditions to reach sufficient mixing and gas transfer for cell growth do not damage the cells through hydrodynamic stress (Marks, 2003). The intensity of mixing can be evaluated by determining the volumetric power consumption (P_V), defined as the amount of energy required to maintain fluid motion within a vessel in a given period of time (Marques et al., 2010). The P_V is a commonly used criterion for bioreactor scale-up, and it directly influences both mass transfer and hydrodynamics in the bioreactor (Marques et al., 2010).

In this chapter, we address the following questions: Are probe-independent bioprocesses in OSRs as efficient than fully controlled bioprocesses in STRs ? How much do probe-independent bioprocesses vary ? The mixing time, k_La and P_V were evaluated in both bioreactor types.

6.2 Materials and Methods

Cell cultivation systems

A 3-L glass STR (Applikon Biotechnology, Schiedam, Netherlands) was equipped with a pitch blade impeller (diameter: 45 mm) and three baffles (Fig. 6.1a). A 5-L cylindrical glass bottle (Pyrex laboratory glassware, SciLabware Ltd, Stone, United Kingdom) was used as an OSR and agitated in an ISF-4W incubator (Kühner AG, Birsfelden, Switzerland) with a shaking diameter of 5 cm (Fig. 6.1b). To reduce the mass transfer resistance from the surroundings to the headspace, the OSR was sealed with a vented cap (polyether sulfones membrane, diameter: 1.5 cm) (Fig. 6.1b).

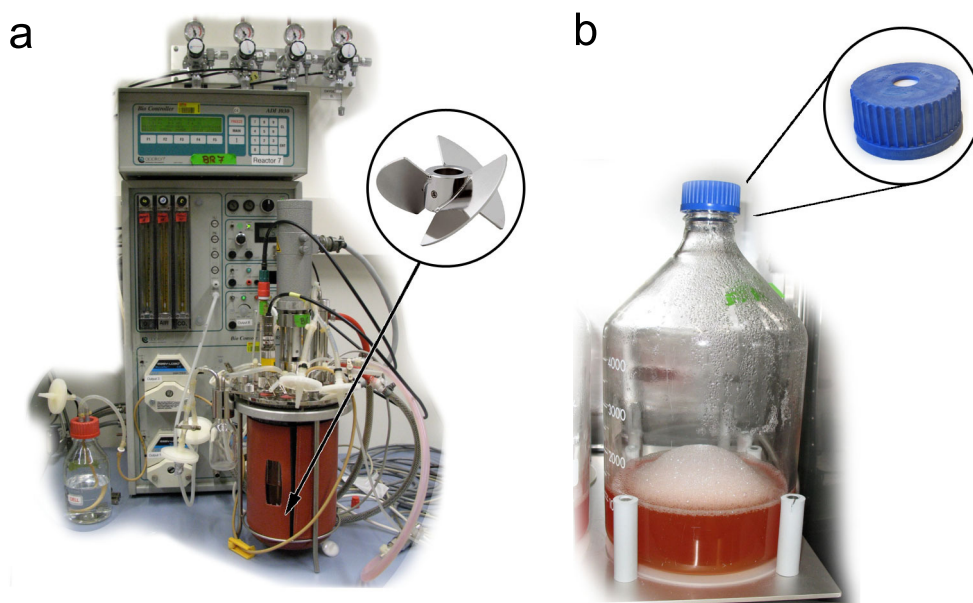


Fig. 6.1: Cell cultivation systems used in the comparison between stirring and orbital shaking. (a) A 3-L STR with a Bio Controller ADI 1030 and a pitched blade impeller. (b) A 5-L OSR with a vented cap.

Mixing time measurements and mixing maps

The mixing time was measured in 1.5 L of deionized water at room temperature with the Dual Indicator System for Mixing Time (DISMT) using two pH indicators as described in Chapter 3 (Melton et al., 2002; Tissot et al., 2010). The solution was acidified with addition of 10 μL of 5 M HCl, and the mixing time was determined after rapid addition of a stoichiometric amount of 5 M NaOH from a constant position near the vessel wall. Each measurement was repeated three times. The mixing experiments performed at 120 rpm in the OSR and at 150 rpm in the STR were filmed with a video camera to generate mixing maps as described in Chapter 3 (Tissot et al., 2010).

Volumetric mass transfer coefficient of oxygen

The k_La [h^{-1}] was measured in 1.5 L of deionized water at 37°C with a dynamic method using a non-invasive O_2 sensor (PreSens, Regensburg, Germany) as described in Chapter 4 (Gupta and Rao, 2003). N_2 was sparged into the water until the DO was close to 0 mg/L. The OSR and STR were then agitated at various rates. Air was flushed into the gas phase of the

OSR and air was continuously sparged into the liquid phase of the STR at a flow rate of 0.3 L/min. The $k_L a$ [h^{-1}] was calculated from the following mass balance equation (Eq. 6.1):

$$\frac{dc_L}{dt} = k_L a (c^* - c_L) \quad (6.1)$$

where c_L is the dissolved concentration of oxygen in the liquid phase [M], c^* is the dissolved oxygen concentration at saturation [M], and t is the time [h]. Each experiment was performed twice.

Volumetric power consumption measurement

The P_V was measured by the thermodynamic method described in Chapter 5 (Büchs et al., 2000a; Kato et al., 2004; Sumino et al., 1972). Deionized water was heated to about 40°C and transferred into the OSR or STR to a final volume of 1.5 L. The bioreactors were insulated with polystyrene and agitated at different agitation rates at room temperature. The temperature of water was measured with a temperature sensor (KCG 50, KIMO Instrument, Montpon, France) and recorded every 5 min for 6 h. The P_V was calculated from the following heat balance equation (Eq. 6.2):

$$-C_p \frac{dT}{dt} = \frac{UA}{V} (T - T_{out}) - P_V \quad (6.2)$$

where C_p is the heat capacity [$\text{J m}^{-3} \text{K}^{-1}$], T is the temperature of the water [K], t is the time [s], U is the over-all heat transfer coefficient [$\text{W m}^{-2} \text{K}^{-1}$], A is the heat transfer area [$\text{m}^2 \text{m}^{-3}$], V is the working volume [m^3], T_{out} is the temperature of the surroundings [K], and P_V is the volumetric power consumption [W m^{-3}]. Each experiment was repeated twice.

Mammalian cell culture

Two recombinant CHO cell lines derived from CHO-DG44 were tested in this study: one expressing the tumor necrosis factor receptor 2 fused with the Fc portion of a human IgG (TNFR:Fc) (CHO-TNFR) (Oberbek et al., 2011) and another expressing a human anti-RhesusD IgG monoclonal antibody (CHO-IgG) (Matasci et al., 2011). Both cell lines were routinely cultivated in ProCHO5 medium (Lonza, Verviers, Belgium) at 37°C in orbitally shaken glass bottles of various sizes at 120 rpm in an ISF4-W incubator with 5% CO_2 (Kühner AG, Birsfelden, Switzerland) as described (Muller et al., 2005). The cultures in the 3-L STR and the 5-L OSR were

inoculated at 0.3 million cells/mL in 1.5 L of ProCHO5 medium. The STRs were stirred at 150 rpm, and the pH and DO were measured on-line with a Bio Controller ADI 1030 (Applikon Biotechnology, Schiedam, The Netherlands). In the controlled STR, the pH was maintained at 7.0 ± 0.1 by sparging with air containing CO₂ and by addition of 1 M NaOH, and the DO was maintained at 50% air saturation (air sat) by sparging with air or pure oxygen. The non-controlled STR was sparged with air containing 5% CO₂ at a rate of 0.3 L/min (0.2 vvm), and the OSR was agitated at 120 rpm in an incubator with 5% CO₂. In the two latter cultures, the pH and DO were not maintained at specific settings. In the OSR, the DO was measured on-line with an optical sensor (PreSens, Regensburg, Germany) and the pH was measured off-line with a 340 pH meter (Mettler-Toledo, Greifensee, Switzerland).

The CHO-TNFR and CHO-IgG cell lines were used to test the variability of probe-independent bioprocesses in OSRs. For each cell line, six 5-L glass bottles were inoculated at 0.3 million cells/mL in 1.5 L of ProCHO5 medium. The cultures were grown for 5 days at 37°C in an incubator shaker containing 5% CO₂. Agitation was set at 120 rpm and there was no pH or DO control.

For all cultures, the cell density and viability were determined manually by the Trypan blue exclusion method. The biomass was determined by the packed cell volume (PCV) method using VoluPAC tubes (Sartorius AG, Goettingen, Germany) as described (Stettler et al., 2006). The DO and pH were measured as described above. Glucose, lactate, glutamine and glutamate concentrations were determined off-line with a BioProfile 200 Analyzer (Nova Biomedical, Waltham, MA).

Protein quantification and analysis

Recombinant TNFR:Fc and anti-RhD IgG were quantified by sandwich ELISA. As coating, a goat anti-human Fc γ antibody (Jackson ImmunoResearch Laboratories, Inc., West Grove, PA, USA) and a goat anti-human κ light chain antibody (ADB Serotec, Düsseldorf, Germany) was used for TNFR:Fc and anti-RhD IgG, respectively. For both recombinant proteins, an alkaline phosphatase (AP)-conjugated goat anti-human gamma chain antibody (Invitrogen Corp., Basel, Switzerland) was used for detection (Meissner et al., 2001). As standards, affinity-purified recombinant human TNFR:Fc fusion protein (Enbrel®; Amgen, Zug, Switzerland) and ChromPure human IgG (Jackson ImmunoResearch Laboratories, Inc., West Grove, PA) were used for TNFR:FC and anti-RhD IgG quantification, respectively. TNFR:Fc and anti-RhD IgG were purified with Streamline®

rProtein A (GE Healthcare, Uppsala, Sweden) according to the manufacturer's protocol and analyzed by 10% SDS-PAGE using Coomassie staining.

6.3 Results

Mixing times and mixing maps

The time needed to achieve mixing to homogeneity was determined with the DISMT method in 1.5 L of water in both the OSR and the STR at agitation rates from 80 to 150 rpm. Between 80 and 100 rpm, the mixing times in the OSR were greater than those in the STR (Fig. 6.2a). At agitation rates ≥ 110 rpm, the mixing times tended to be about 7 s in the OSR and about 11 s in the STR (Fig. 6.2a). Thus at the agitation rates used for cell culture in this study (120 rpm in the OSR and 150 rpm in the STR) the mixing times in the two reactors were similar. From mixing maps generated at these agitation rates, it was observed that the mixing zones were distributed differently in the two bioreactors. In the OSR the most rapidly mixed zone was close to the vessel wall and the last zone to achieve mixing was in the center of the liquid (Fig. 6.2b). In the STR the rapidly mixed zones were found at the bottom of the bioreactor and around the impeller, while the most slowly mixed zone extended in a V-shape along the impeller to the top of the liquid (Fig. 6.2c).

Oxygen transfer

The k_La was measured in the two bioreactors containing 1.5 L of deionized water at 37°C. Air was sparged at 0.3 L/min into the STR but sparging was not used for the OSR. In the latter, the k_La increased from 5 to 15 h⁻¹ as the agitation rate increased from 80 to 150 rpm (Fig. 6.3a). In the STR, the k_La remained constant at about 4 h⁻¹ at agitation rates from 80 to 150 rpm (Fig. 6.3a). At agitation rates used for CHO cell culture (120 rpm in the OSR and 150 rpm in the STR) k_La values of about 9 h⁻¹ and 4 h⁻¹ were measured, respectively (Fig. 6.3a).

At low agitation rates the free surface in the OSR was a flat and smooth inclined plane, rotating at the shaking frequency. The complexity of the free surface increased with the shaking frequency and at 120 rpm a breaking wave was observed (Fig. 6.3b). In the STR the free surface remained flat, and the gas transfer depended on the ability of the impeller to split and

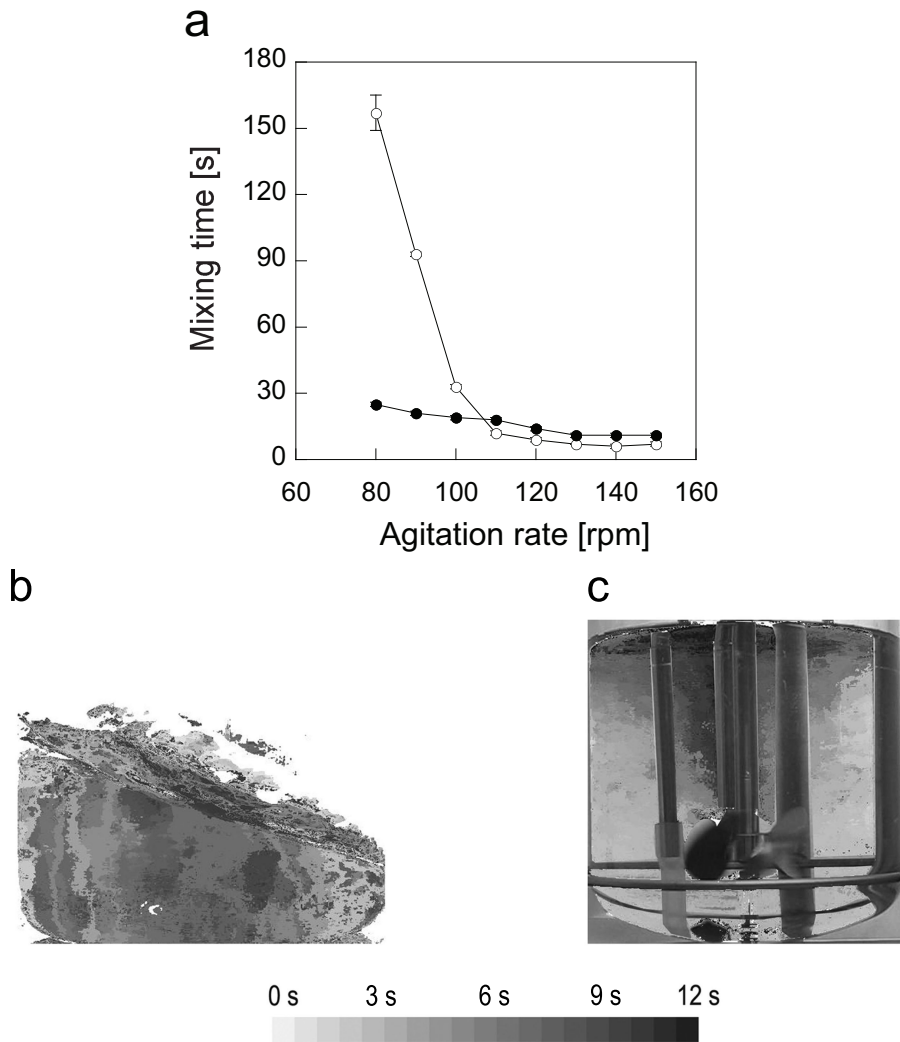


Fig. 6.2: (a) Mixing times measured with DISMT in an OSR (○) and in an STR (●). (b) The mixing map of an OSR at 120 rpm. (c) The mixing map of an STR at 150 rpm. The bar below the mixing maps indicates the color associated with the mixing times. The working volume was 1.5 L for all experiments.

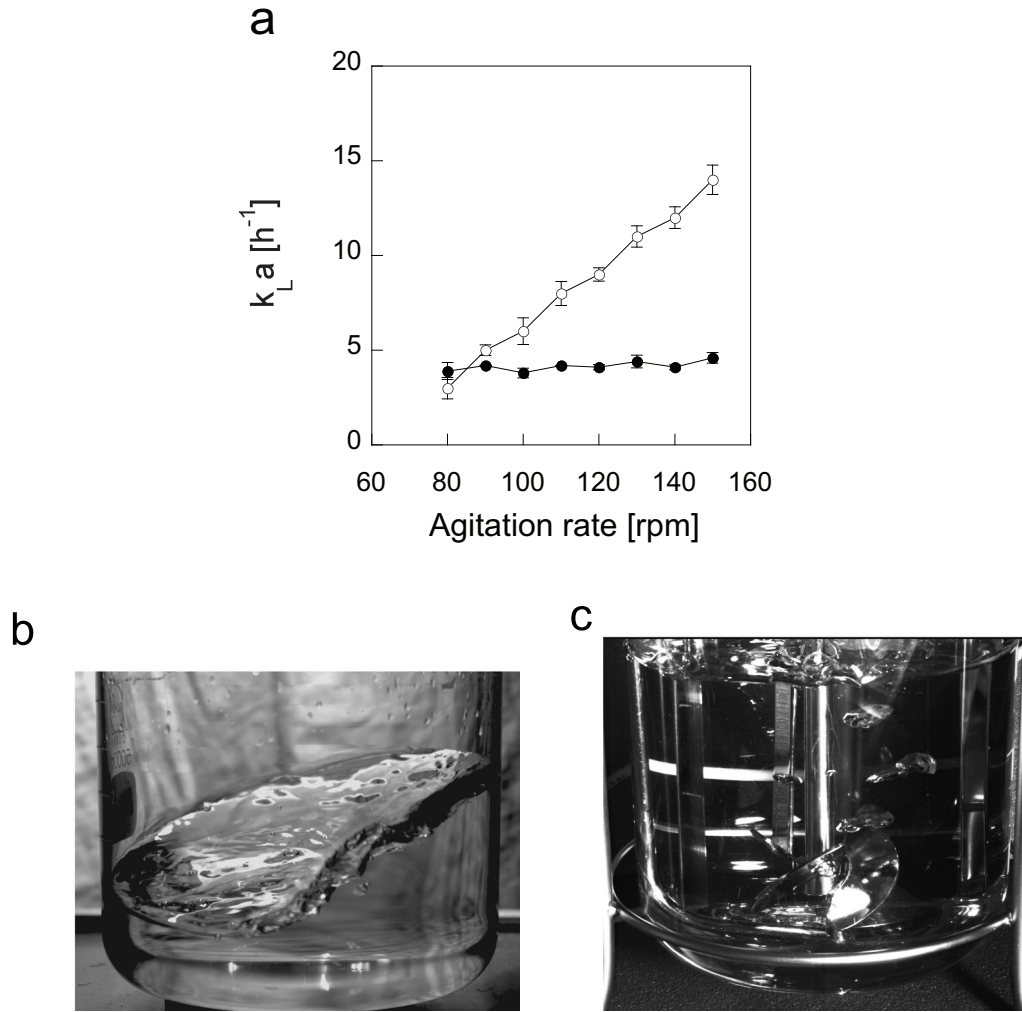


Fig. 6.3: (a) $k_L a$ measured with a dynamic method in the OSR (○) and the STR (●). The working volume was 1.5 L and the temperature was 37°C. (b) Free surface of the OSR at 120 rpm. (c) Bubble dispersion in the STR at 150 rpm.

disperse the bubbles from the sparger. However, the bubble size did not decrease significantly as the agitation rate increased (Fig. 6.3c).

Volumetric power consumption

The P_V was measured with a thermodynamic method in the two bioreactors at agitation rates ranging from 80 to 150 rpm in 1.5 L of deionized water. The experimental values of P_V were compared with previously published correlations. For the STR, the P_V was calculated from the definition of the Newton number (Ne) (Eq. 6.3) (Zlokarnik, 2003):

$$P_V = \frac{Ne\rho n^3 d_i^5}{V} \quad (6.3)$$

where the value of Ne is 3 according to the bioreactor manufacturer, ρ represents the fluid density [kg/m^3], n is the rotation rate of the impeller [s^{-1}], d_i is the impeller diameter [m], and V is the working volume [m^3]. For the OSR, the following correlation was used (Eq. 6.4) (Kato et al., 2004):

$$Ne = \frac{P}{\rho n^3 d^4 V^{1/3}} = 200 Re^{-0.5} \left(Re = \frac{nD^2}{\nu} \right) \quad (6.4)$$

where Re is the Reynolds number [-], D is the inner diameter of the container [m], ν is the kinematic viscosity [m^2/s], and P is the power consumption [W].

In both bioreactors, the P_V increased as the agitation rate increased (Fig. 6.4). The P_V was higher in the STR than in the OSR at all agitation rates tested, and the difference in the P_V increased with the agitation rate (Fig. 6.4). At agitation rates used for cell cultivation in this study, P_V s of 0.5 and 1.5 kW/m^3 were measured in the OSR (120 rpm) and the STR (150 rpm), respectively (Fig. 6.4). In both cultivation systems experimental values fitted well with previously published correlations (Fig. 6.4) (Kato et al., 2004; Zlokarnik, 2003).

Comparison between bioprocesses in STR and OSR

To evaluate the need for pH and DO control in bioprocesses, CHO-TNFR cells were grown in three different cultivation systems: a non-controlled 5-L OSR and a 3-L STR in both controlled and non-controlled modes. In the OSR and the controlled STR, maximal cell densities of 8 and 5 million cells/ mL , respectively, were achieved at 96 h post-inoculation (Fig. 6.5a).

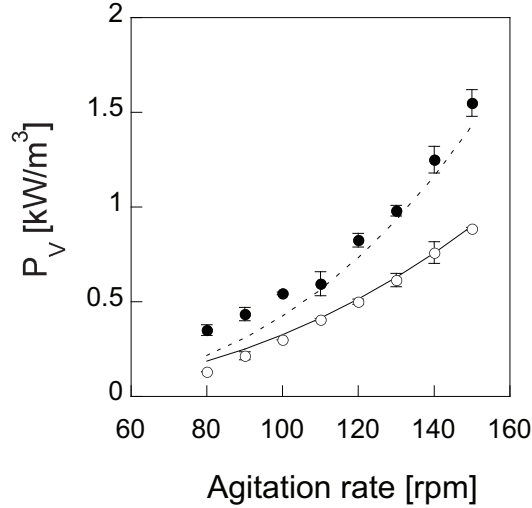


Fig. 6.4: Volumetric power consumption (P_V) measured with a thermodynamic method in the OSR (\circ) and the STR (\bullet). The dashed line represents the correlation for STR (Eq. 6.3) (Zlokarnik, 2003) and the black line the correlation for OSR (Eq. 6.4) (Kato et al., 2004). The working volume was 1.5 L.

In contrast, cells in the non-controlled STR only reached a density of 1 million cells/mL and then began to die (Fig. 6.5a,b). Similar levels of cell viability were observed in the OSR and in the controlled STR, whereas in the non-controlled STR no viable cells remained at 96 h post-inoculation (Fig. 6.5b). The level of biomass accumulation correlated with the cell density in all three cultures (Fig. 6.5c).

In the OSR, the pH decreased from 7.0 to 6.7 by 48 h post-inoculation and remained near this value until the end of the culture (Fig. 6.6a). In the controlled STR, the pH was maintained between 6.9 and 7.1, and in the non-controlled STR the pH decreased to less than 6.6 by 48 h post-inoculation (Fig. 6.6a). Interestingly, even if the pH was not maintained at 7 in the OSR, the culture reached a higher cell density than in the STR with pH control (Fig. 6.6a). No oxygen limitation was observed in the OSR without DO control or active aeration. The lowest DO value was 75% air sat after 72 h of culture (Fig. 6.6b). In the controlled STR, on the other hand, pulses of pure oxygen were required when the culture reached a density of about 1 million cells/mL at 24 h post-inoculation. Then as the cell density reached 2 million cells/mL, pure oxygen was sparged into the STR at rates up to 5 L/min to keep the DO at 50% air sat. The DO in the non-controlled

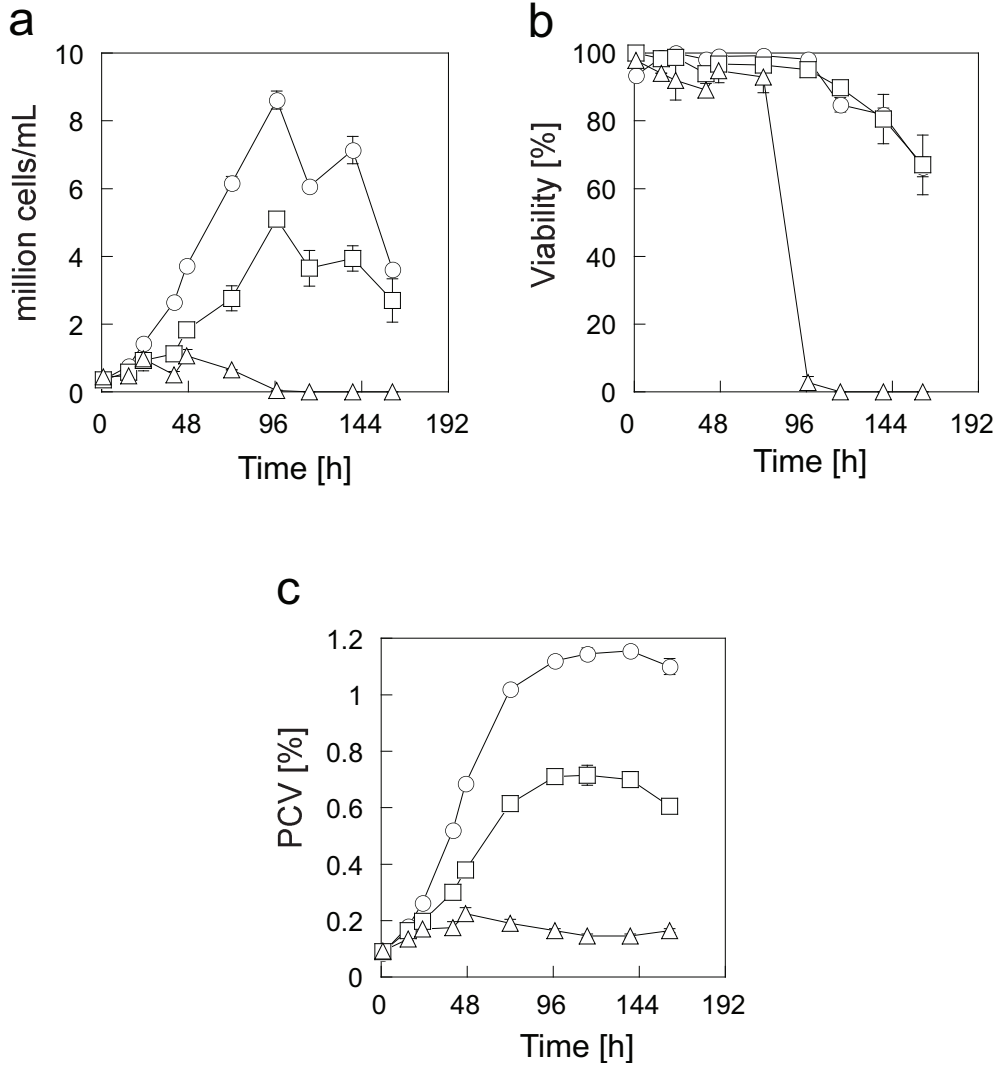


Fig. 6.5: Cell growth of CHO-TNFR cells in a non-controlled OSR (○), a controlled STR (□) and a non-controlled STR (Δ). The cells were cultivated at 37°C and the agitation rate was set at 120 rpm for the OSR and 150 rpm for the two STRs. The working volume was 1.5 L. The viable cell density (**a**), cell viability (**b**), and biomass (**c**) were determined at the times indicated.

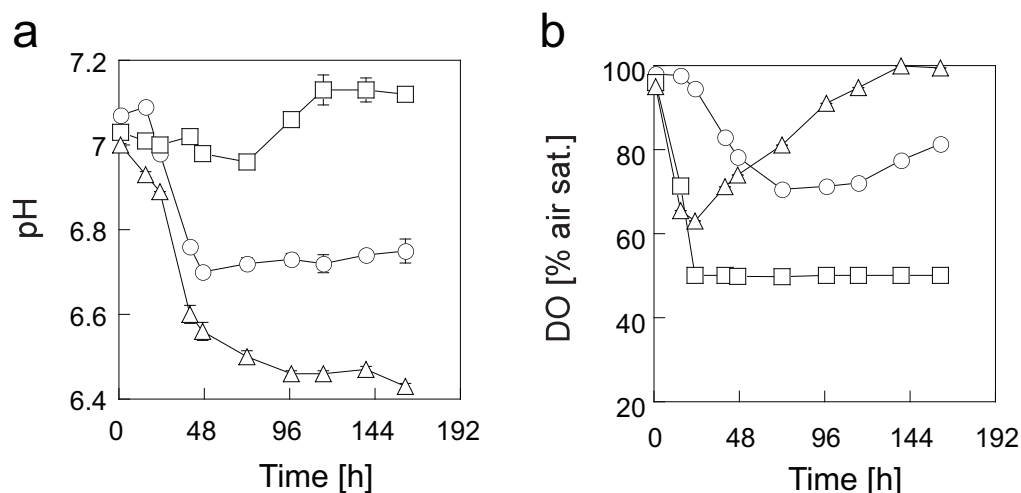


Fig. 6.6: Culture conditions of CHO-TNFR cells in an OSR (○), a controlled STR (□) and a non-controlled STR (△). The cells were cultivated at 37°C and the agitation rate was set at 120 rpm for the OSR and 150 rpm for the two STRs. The working volume was 1.5 L. The pH (a) and DO (b) were determined at the times indicated.

STR dropped to 60% air sat after 24 h and then increased as the cells died (Fig. 6.6b).

The glucose concentration decreased more slowly in the OSR than in the controlled STR. After 96 h of culture, more than 2 g/L of glucose were present in the OSR, whereas no glucose was detected in the controlled STR (Fig. 6.7a). The glucose concentration decreased to 5.5 g/L during the first two days of culture in the non-controlled STR and remained constant once the viable cell density decreased (Fig. 6.7a). The maximum lactate concentrations in the OSR and the controlled STR, were 2 and 4 g/L, respectively (Fig. 6.7b). The lactate concentration in the non-controlled STR remained about 2 g/L once most of the cells died (Fig. 6.7b). The glutamine was completely consumed after 72 h in the OSR and after 110 h in the controlled STR (Fig. 6.7c). In the non-controlled STR, the glutamine concentration decreased to about 2 mM (Fig. 6.7c). The glutamate profiles were similar in the three vessels reaching about 1.5 mM after 161 h of culture (Fig. 6.7d).

The recombinant TNFR:Fc concentrations measured by ELISA reached about 400 mg/L in the OSR, 330 mg/L in the controlled STR, and 50 mg/L in the non-controlled STR (Fig. 6.8a). However, the specific productivity was similar in the three vessels (about 20 pg cell⁻¹ day⁻¹). Recombinant

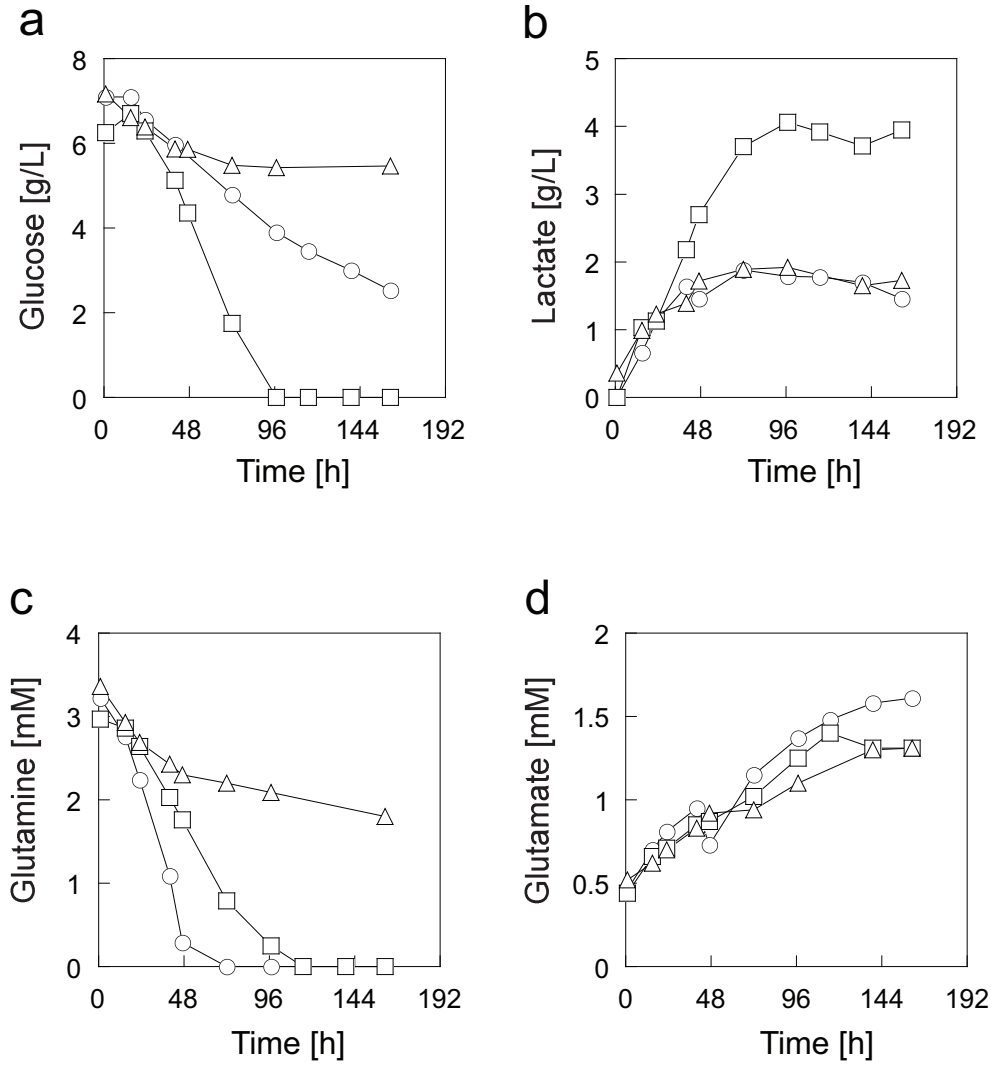


Fig. 6.7: Metabolite consumption and production in CHO-TNFR cell cultures in an OSR (○), a controlled STR (□) and a non-controlled STR (△). The cells were cultivated at 37°C and the agitation rate was set at 120 rpm for the OSR and 150 rpm for the two STRs. The working volume was 1.5 L. The glucose (a), lactate (b), glutamine (c), and glutamate (d) concentrations were determined at the times indicated.

TNFR:Fc was purified from each culture and analyzed by SDS-PAGE. No difference in the protein size or aggregation level was observed (Fig. 6.8b). When the samples were analyzed under reducing conditions, a major band

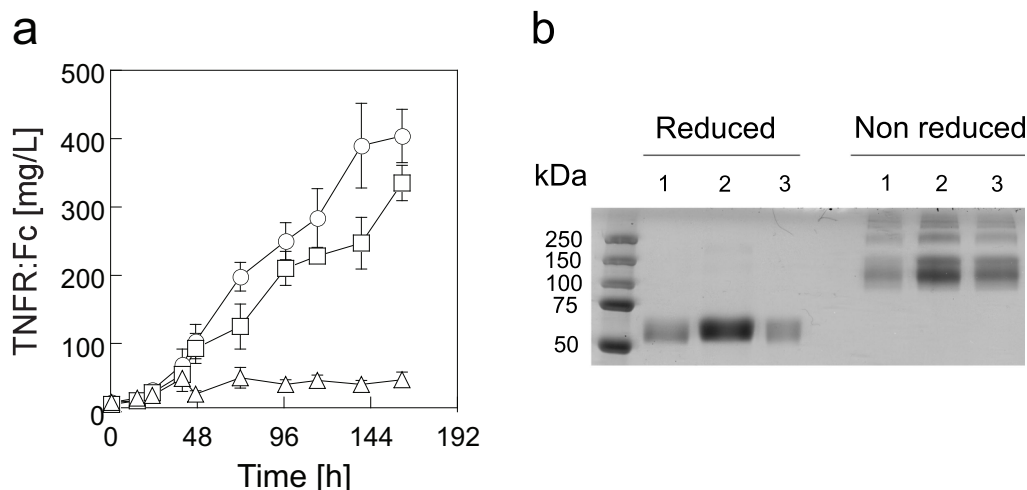


Fig. 6.8: Recombinant protein production in CHO-TNFR cell cultures. The cells were cultivated at 37°C and the agitation rate was set at 120 rpm for the OSR and 150 rpm for the two STRs. The working volume was 1.5 L. **(a)** TNFR:Fc concentration was measured during CHO cell culture in an OSR (○), a controlled STR (□) and a non-controlled STR (△) at the times indicated. **(b)** SDS-PAGE analysis of purified recombinant TNFR:Fc from the OSR (lanes 1), the controlled STR (lanes 2) and the non-controlled STR (lanes 3). The proteins were purified at 161 h post-inoculation with affinity chromatography with protein A.

with an apparent molecular weight (MW) of about 55 kD, corresponding to monomeric TNFR:Fc, was observed (Fig. 6.8b). Under non-reducing conditions, the dimeric form of TNFR:Fc (apparent MW of 110 kD) was observed along with some higher MW species that may have been TNFR:Fc aggregates (Fig. 6.8b). No TNFR:Fc monomers were observed under non-reducing conditions (Fig. 6.8b).

To confirm these data, a second CHO cell line (CHO-IgG) was cultivated in parallel in a non-controlled 5-L OSR and a 3-L STR in both controlled and non-controlled modes. Maximal cell densities of about 6, 4, and 3 million cells/mL were reached in the OSR, the controlled STR, and the non-controlled STR, respectively (Fig. 6.9a). Similar cell viability profiles were observed in the OSR and the controlled STR with cell viabilities equal to or higher than 90% over the course of the experiment (Fig. 6.9b). In the

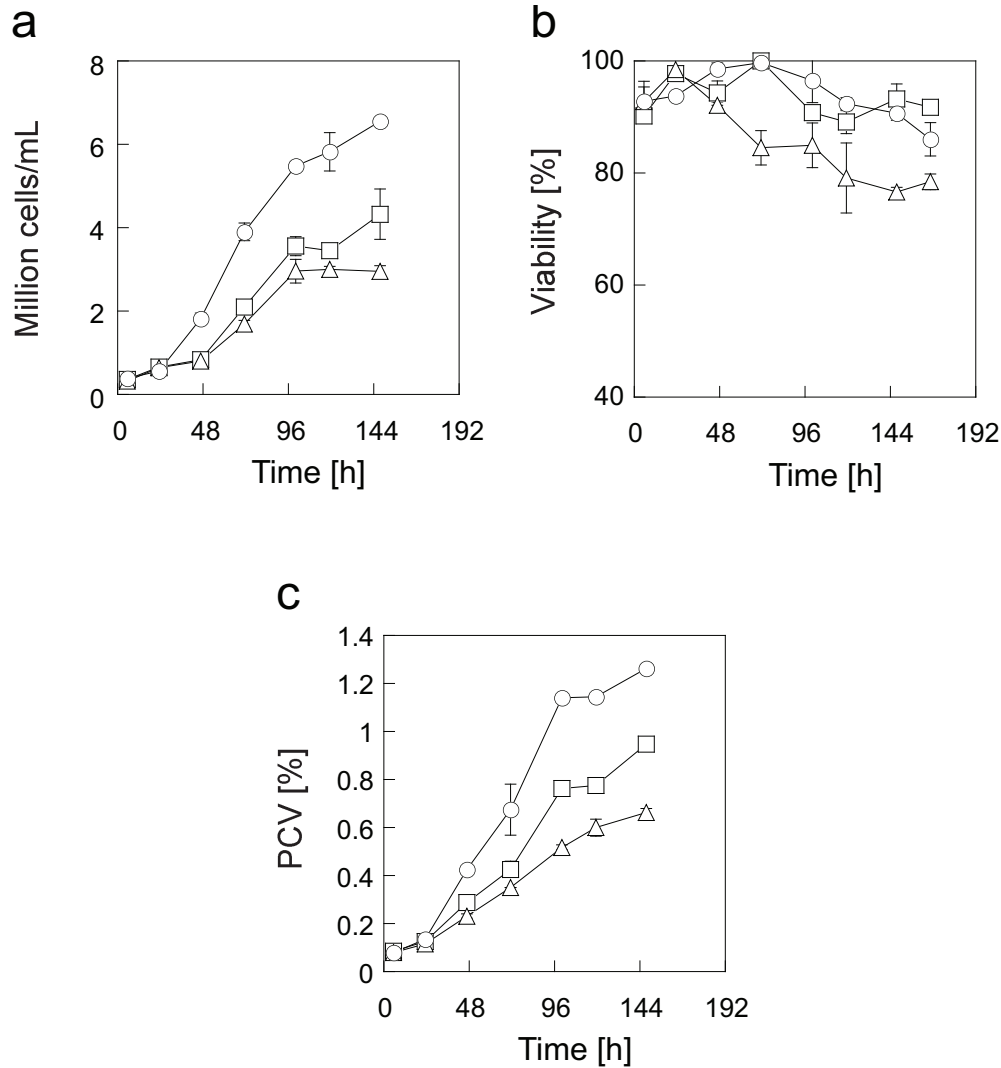


Fig. 6.9: Cell growth of CHO-IgG cells in an OSR (○), a controlled STR (□) and a non-controlled STR (△). The cells were cultivated at 37°C and the agitation rate was set at 120 rpm for the OSR and 150 rpm for the two STRs. The working volume was 1.5 L. The viable cell density (a), cell viability (b), and biomass (c) were determined at the times indicated.

non-controlled STR, the viability decreased after 48 h and reached 76% by the end of the culture. The biomass levels corresponded to the cell density of each culture (Fig. 6.9c).

In the controlled STR the pH was maintained between 6.9 and 7.1 using NaOH, while in the OSR the pH decreased from 7.1 to 6.65 by 72 h post-

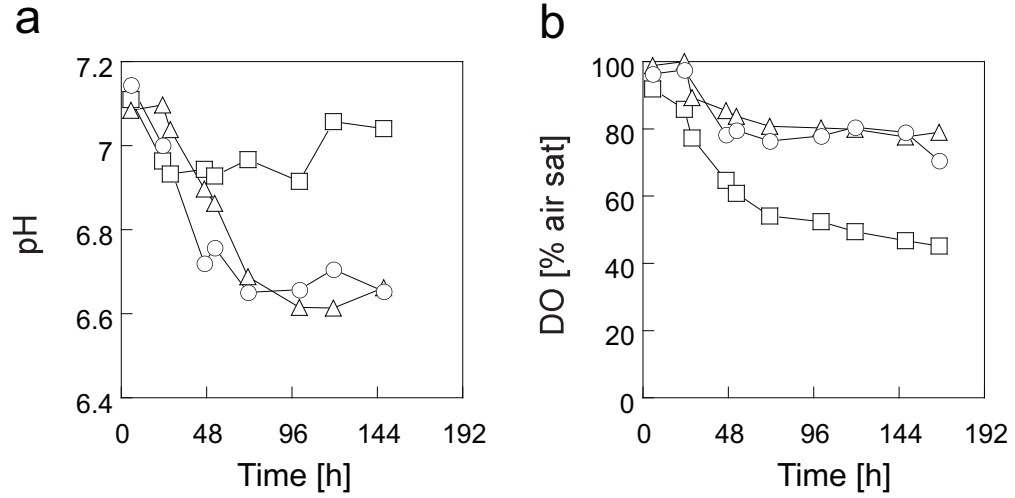


Fig. 6.10: Culture conditions of CHO-IgG cells in an OSR (○), a controlled STR (□) and a non-controlled STR (△). The cells were cultivated at 37°C and the agitation rate was set at 120 rpm for the OSR and 150 rpm for the two STRs. The working volume was 1.5 L. The pH (a) and DO (b) were determined at the times indicated.

inoculation and then remained around this value (Fig. 6.10a). The pH in the non-controlled STR followed the same trend as in the OSR (Fig. 6.10a). In the controlled STR the DO was maintained at 50% air sat by using pure oxygen (Fig. 6.10b). In the OSR and the non-controlled STR the DO profiles were similar with the lowest value at about 80% air sat using air as the oxygen source (Fig. 6.10b).

The glucose was completely consumed after 120 h in the controlled STR, although its concentration was still around 2 g/L in the OSR and the non-controlled STR (Fig. 6.11a). The lactate concentration reached a plateau at 6 g/L in the controlled STR and 2 g/L in the OSR and the non-controlled STR 96 h post-inoculation (Fig. 6.11b). The glutamine profiles were similar in the three vessels and reached almost 0 mM at 120 h post-inoculation (Fig. 6.11c). The glutamate concentration increased similarly in the three vessels and reached about 1.5 mM after 161 h (Fig. 6.11d).

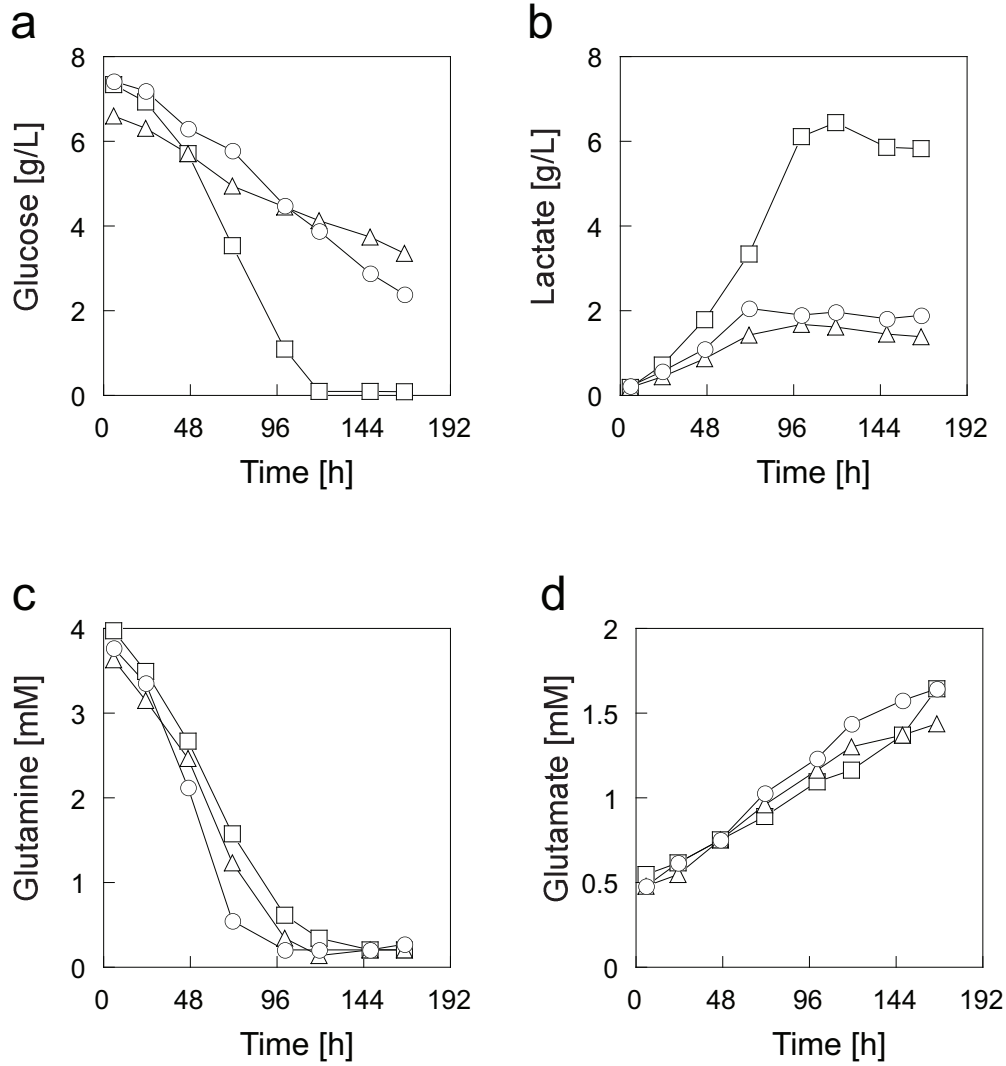


Fig. 6.11: Metabolite consumption and production in CHO-IgG cell cultures in an OSR (○), a controlled STR (□) and a non-controlled STR (△). The cells were cultivated at 37°C and the agitation rate was set at 120 rpm for the OSR and 150 rpm for the two STRs. The working volume was 1.5 L. The glucose (a), lactate (b), glutamine (c), and glutamate (d) concentrations were determined at the times indicated.

The anti-RhD IgG concentration measured by ELISA reached about 200 mg/L in the OSR and 160 mg/L in both STRs (Fig. 6.12a). Nevertheless, as previously observed for CHO-TNFR, the specific productivity of CHO-IgG (around 10 pg cell⁻¹ day⁻¹) was similar for all the cultures. Recombinant anti-RhD IgG was purified from each culture and analyzed by SDS-PAGE. When the samples were analyzed under non-reducing conditions, no difference in the protein size or aggregation level was observed (Fig. 6.12b). Under reducing conditions, two bands with an apparent molecular weight (MW) of about 50 kD and 25 kD were observed in all samples, corresponding to the IgG heavy and light chains, respectively (Fig. 6.12b).

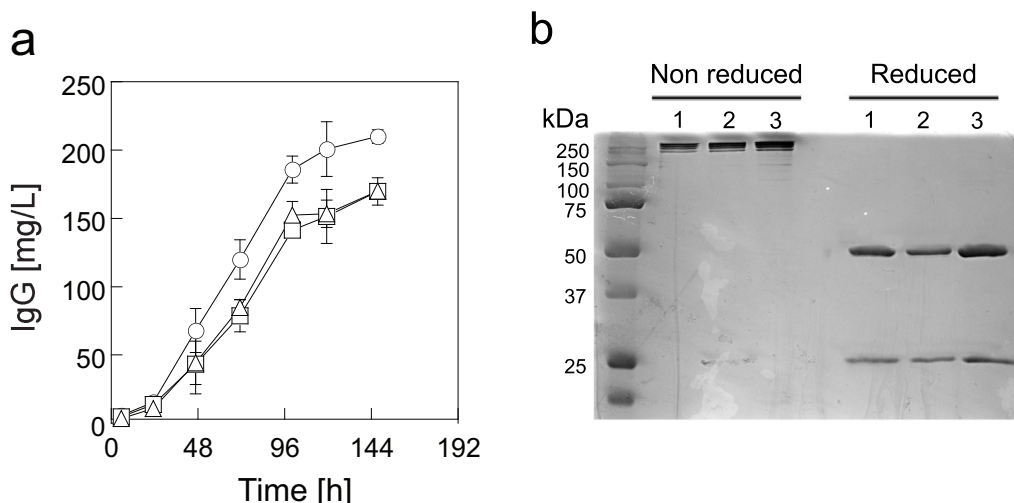


Fig. 6.12: Recombinant protein production in CHO-IgG cell cultures. The cells were cultivated at 37°C and the agitation rate was set at 120 rpm for the OSR and 150 rpm for the two STRs. The working volume was 1.5 L. **(a)** Anti-RhD IgG concentration was measured during CHO cell culture in an OSR (○), a controlled STR (□) and a non-controlled STR (△) at the times indicated. **(b)** SDS-PAGE analysis of purified recombinant anti-RhD IgG from the OSR (lanes 1), the controlled STR (lanes 2) and the non-controlled STR (lanes 3). The proteins were purified at 166 h post-inoculation with affinity chromatography with protein A.

Variability of non-controlled bioprocesses in OSR

To evaluate the variability of non-controlled bioprocesses in OSRs, CHO-TNFR and CHO-IgG cells were each cultivated for 5 days at 37°C in six 5-L OSRs in parallel.

CHO-TNFR cultures

The CHO-TNFR cells reached a maximum cell density of about 5 million cells/mL and showed a viability higher than 95% during the whole culture (Fig. 6.13a). The biomass accumulation assessed by PCV was similar in the six cultures and reached 1% (Fig. 6.13b).

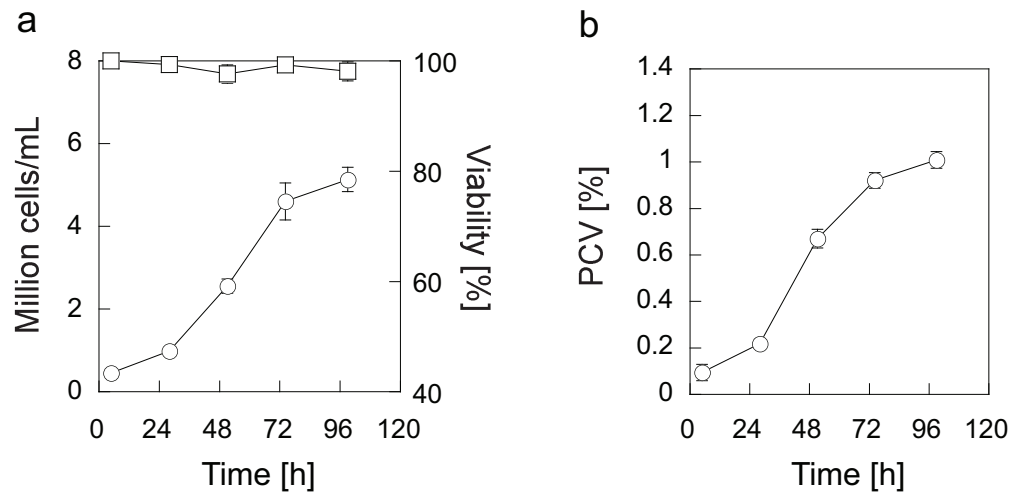


Fig. 6.13: Variability of CHO-TNFR cell growth in non-controlled bioprocesses in six 5-L OSRs. The cells were cultivated at 37°C at 120 rpm. The working volume was 1.5 L. The viable cell density (○) and viability (□) (a), and the PCV (b) were measured at the times indicated. The error bars represent the standard deviation of the six OSRs.

The recombinant TNFR:Fc concentrations were the same in the six cultures and reached about 240 mg/L after 100 h (Fig. 6.14a). Analysis of the purified TNFR-Fc by non-reducing SDS-PAGE did not reveal any differences in protein size or aggregation level (Fig. 6.14b).

No controller was used to keep the pH and DO within a defined range, the pH and DO profiles for the six cultures of CHO-TNFR cells were nonetheless nearly the same (Fig. 6.15a,b). The pH decreased from 7 to

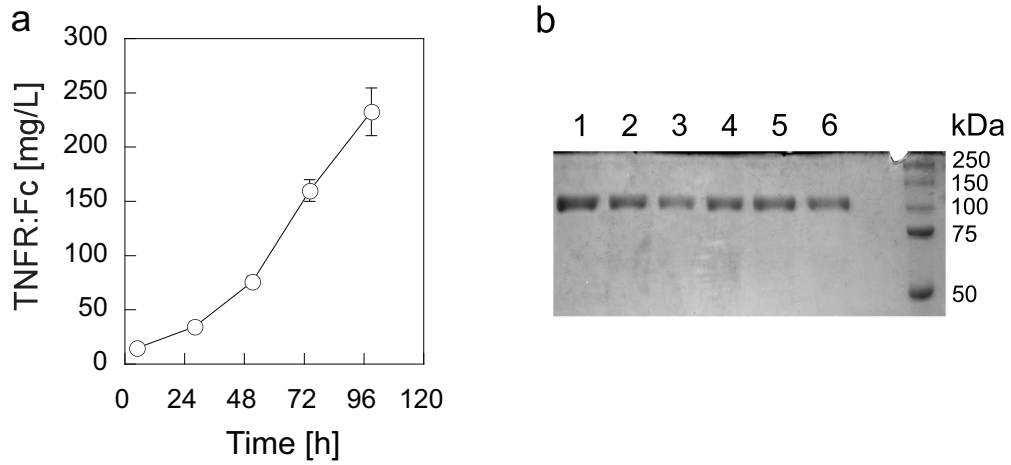


Fig. 6.14: Variability of recombinant protein production in non-controlled bioprocesses with CHO-TNFR cells in six 5-L OSRs. The cells were cultivated at 37°C and the agitation rate was set at 120 rpm. The working volume was 1.5 L. The TNFR-Fc concentrations (**a**) were measured by ELISA at the times indicated. The error bars represent the standard deviation of six OSRs. SDS-PAGE analysis (**b**) of purified recombinant TNFR:Fc from six OSRs (lanes 1-6). The proteins were purified at 100 h post-inoculation with affinity chromatography with protein A.

6.6 in 48 h and remained within this range (Fig. 6.15a). The DO gradually decreased during the culture and reached 70% air sat after 100 h (Fig. 6.15b).

The metabolite profiles were identical in all the CHO-TNFR cell cultures (Fig. 6.16). The final concentrations of glucose and lactate were about 4 g/L and 2 g/L, respectively (Fig. 6.16a). The glutamine was completely consumed after 72 h and the glutamate concentration reached about 1.5 mM after 100 h (Fig. 6.16b).

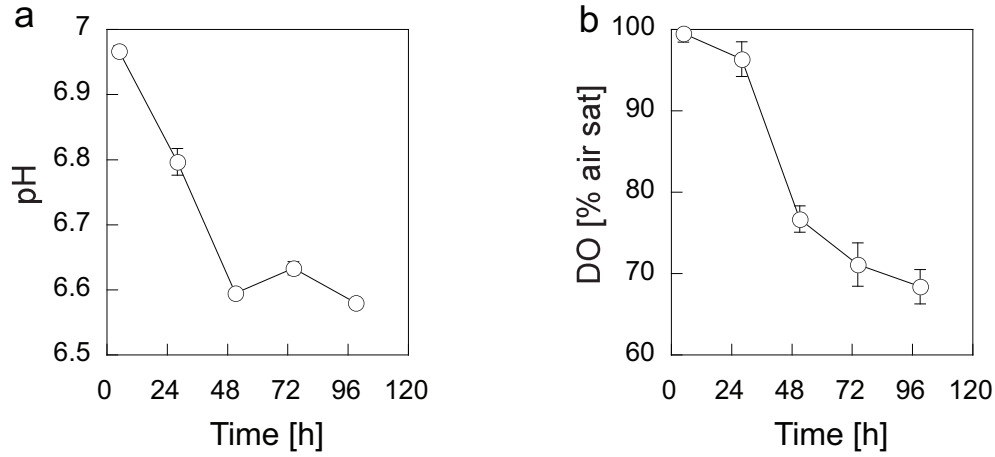


Fig. 6.15: Variability of culture conditions in non-controlled bioprocesses with CHO-TNFR cells in six 5-L OSRs. The cells were cultivated at 37°C and the agitation rate was set at 120 rpm. The working volume was 1.5 L. The pH (a) and DO (b) were measured at the times indicated. The error bars represent the standard deviation of six OSRs.

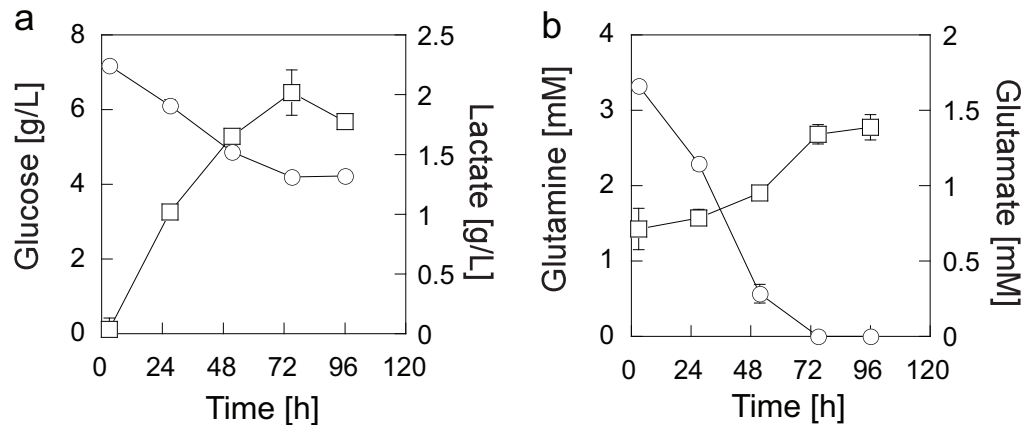


Fig. 6.16: Variability of metabolite consumption/production in non-controlled bioprocesses with CHO-TNFR cells in six 5-L OSRs. The cells were cultivated at 37°C and the agitation rate was set at 120 rpm. The working volume was 1.5 L. The glucose (○) and lactate (□) concentrations (a), and the glutamine (○) and glutamate (□) concentrations (b) were measured at the times indicated. The error bars represent the standard deviation of six OSRs.

CHO-IgG cultures

The CHO-IgG cells reached a cell density of 7 million cells/mL with a viability equal to or higher than 98% (Fig. 6.17a). The biomass accumulation assessed by PCV was similar in the six cultures and reached 1.2% (Fig. 6.17b).

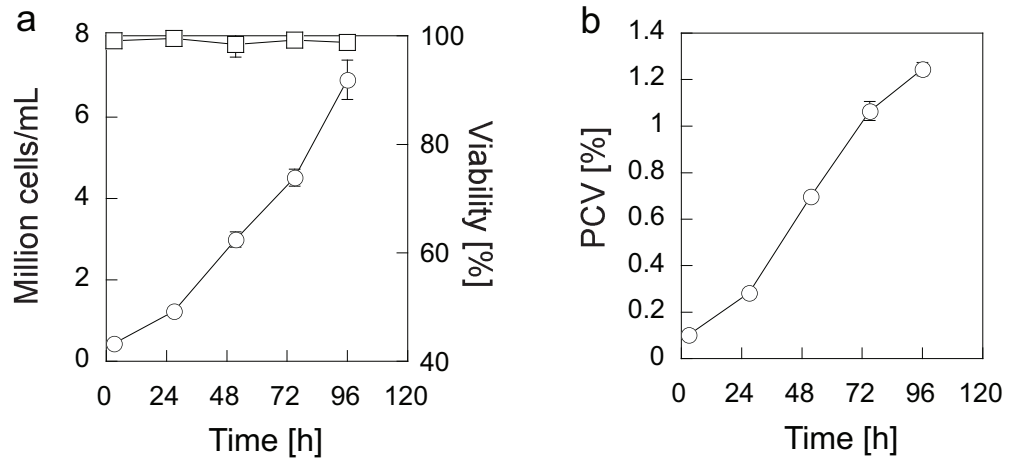


Fig. 6.17: Variability of CHO-IgG cell growth in non-controlled bioprocesses in six 5-L OSRs. The cells were cultivated at 37°C at 120 rpm. The working volume was 1.5 L. The viable cell density (○) and viability (□) (a), and the PCV (b) were measured at the times indicated. The error bars represent the standard deviation of the six OSRs.

The recombinant protein concentrations were the same in the six CHO-IgG cell cultures and reached 180 mg/L after 100 h (Fig. 6.18a). Analysis of the purified recombinant IgG by non-reducing SDS-PAGE did not reveal any differences in protein size or aggregation level (Fig. 6.18b).

The pH and DO profiles for the six CHO-IgG cultures were similar (Fig. 6.19). The pH decreased from 7.3 to 6.8 in 48 h and remained in that range (Fig. 6.19a). The DO decreased to 50% air sat (Fig. 6.19b).

The metabolite profiles were identical in the six CHO-IgG cultures (Fig. 6.20). The final concentrations of glucose and lactate were about 4 and 2 g/L, respectively (Fig. 6.20a). The glutamine concentration decreased to nearly 0.2 mM after 72 h in CHO-IgG cultures while the glutamate reached about 1.2 mM after 100 h (Fig. 6.20b).

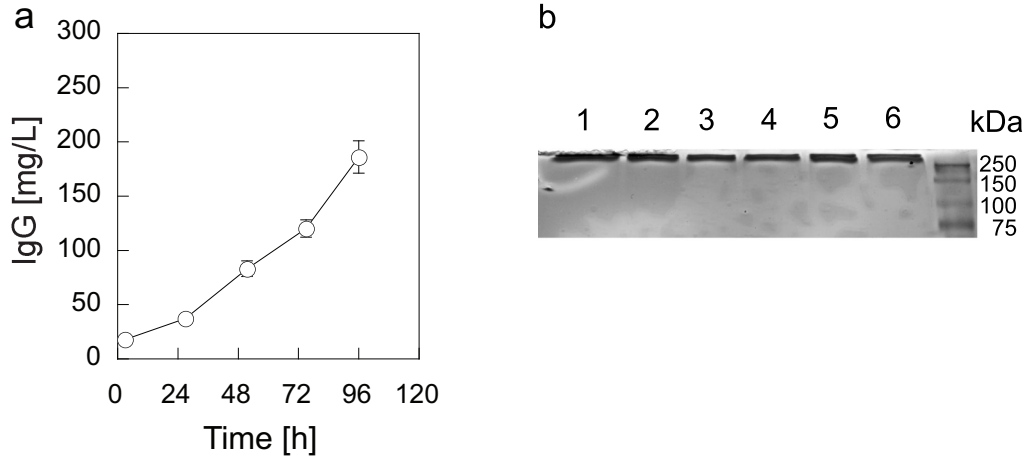


Fig. 6.18: Variability of recombinant protein production in non-controlled bioprocesses with CHO-IgG cells in six 5-L OSRs. The cells were cultivated at 37°C and the agitation rate was set at 120 rpm. The working volume was 1.5 L. The IgG concentrations (a) were measured by ELISA at the times indicated. The error bars represent the standard deviation of six OSRs. SDS-PAGE analysis (b) of purified recombinant IgG from six OSRs (lanes 1-6). The proteins were purified at 100 h post-inoculation with affinity chromatography with protein A.

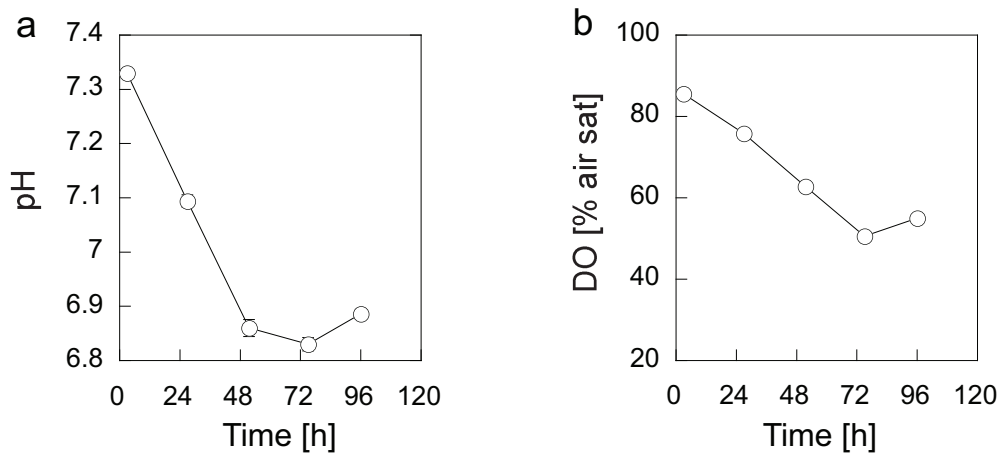


Fig. 6.19: Variability of culture conditions in non-controlled bioprocesses with CHO-IgG cells in six 5-L OSRs. The cells were cultivated at 37°C and the agitation rate was set at 120 rpm. The working volume was 1.5 L. The pH (a) and DO (b) were measured at the times indicated. The error bars represent the standard deviation of six OSRs.

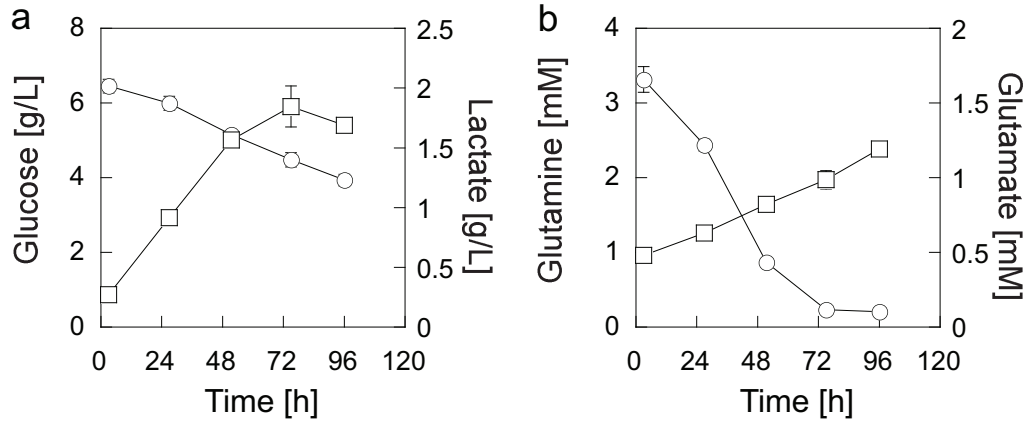


Fig. 6.20: Variability of metabolite consumption/production in non-controlled bioprocesses with CHO-IgG cells in six 5-L OSRs. The cells were cultivated at 37°C and the agitation rate was set at 120 rpm. The working volume was 1.5 L. The glucose (○) and lactate (□) concentrations (**a**), and the glutamine (○) and glutamate (□) concentrations (**b**) were measured at the times indicated. The error bars represent the standard deviation of six OSRs.

The standard deviations of the parameters measured among the six OSRs was within the range of the standard deviation of measurements on a single OSR for both cell lines and lower than 20% (Table 6.1). One-way

Table 6.1: Maximal relative standard deviations (%) between the 6 OSRs during variability experiments.

Parameter	CHO-TNFR	CHO-IgG
Cell density	10	10
Viability	2	2
PCV	9	6
Recombinant protein concentration ^a	13	9
pH	0.2	0.2
DO	3	3
Glucose	3	4
Lactate	9	9
Glutamine	17	16
Glutamate	7	6

^a Measured by ELISA on crude supernatants.

analysis of variance (ANOVA) for each set of experiments demonstrated that there was no significant difference between the six OSRs (p-values higher than 0.9) for cell growth, viability, recombinant protein concentration, pH, DO and metabolite concentrations.

6.4 Discussion

CHO cell lines stably expressing recombinant TNFR:Fc or monoclonal IgG antibody were cultivated in an OSR and an STR to determine if pH and DO controls are required for efficient bioprocesses with low variability. CHO-TNFR and CHO-IgG cells were cultivated in a non-controlled OSR and in an STR in both controlled and non-controlled modes. The culture in the OSR had a slightly higher cell density and recombinant protein titer as compared to the controlled STR. Interestingly, CHO-TNFR cells died after 4 days in the non-controlled STR but CHO-IgG cells reached almost the same cell density in the non-controlled and controlled STRs. These results may be explained if the two cell lines have different sensitivities to environmental conditions such as pH (Trummer et al., 2006). Nevertheless, for both cell lines the viability profiles in the non-controlled STR were lower than those in the controlled STR and the OSR. Yield and biomass differences observed between the OSR and the controlled STR could possibly be reduced by further optimization of the two processes.

The cultures in the STR and OSR were performed under conditions in which the mixing times were approximately the same. Since the mixing times were significantly lower than 100 s, the characteristic time reported for complete oxygen uptake in mammalian cell culture (Lara et al., 2006), problems related to concentration gradients were not expected in either bioreactor. Our results also demonstrated that the cell cultures described in this study were performed at significantly lower P_V values than those reported to be harmful for mammalian cells in suspension (10^4 - 10^5 kW/m³) (Ma et al., 2002; Mollet et al., 2004).

Under conditions used for cell cultivation, the k_La was higher in the OSR (9 h^{-1} at 120 rpm) than in the sparged STR (4 h^{-1} at 150 rpm). In the OSR the gas transfer is ensured through surface aeration, and a highly dynamic gas-liquid interface is a primary requirement to maintain a DO concentration sufficient for cell culture. The deformation of the free surface increased with the agitation rate, resulting in an increased interfacial area per unit volume and therefore a larger k_La (Garcia-Ochoa and Gomez, 2009). At 120 rpm, a breaking wave, contributing to the enhancement of gas transfer due to small bubble entrainment and a local increase of mixing

quality, was observed (Melville, 1996). This effect was difficult to quantify given the lack of theoretical insights into wave breaking and two-phase flow at free surfaces. In the STR, even with agitation at 150 rpm the dispersion of gas bubbles released from the sparger was not efficient. The bubble size did not decrease significantly as the agitation rate increased. This may explain why the k_La of the STR did not increase within the range of agitation rates tested in this study.

The k_La in the OSR (9 h^{-1} at 120 rpm) was sufficient to keep the DO higher than 50% air sat using air only as the source of oxygen. In contrast, the culture in the STR required sparging with pure oxygen to increase the oxygen transfer rate (OTR) as the k_La (4 h^{-1} at 150 rpm) was not sufficient to maintain suitable conditions for high-density cell culture. The pH dropped in the non-controlled STR leading to CHO-TNFR cell death within 3 days and NaOH was required in the controlled STR to keep the pH around 7. These results suggest CO_2 accumulation in the medium as the k_La and hence the gas transfer efficiency were significantly lower in the STR than in the OSR. These results confirmed that the k_La is the key parameter to determine the ability of a system to keep the environmental conditions (pH and DO) within a suitable range and hence to operate without a controller.

The renewal of the gas phase in OSRs is critical since a decrease of partial pressure of oxygen in the headspace will lead to a decrease of c^* and thus to a decrease in the oxygen transfer rate according to Eq. 6.1. Thus the 5-L OSRs were equipped with a vented cap to ensure a sufficient mass transfer into and out of the bottle.

A low variability is crucial for commercial bioprocesses. Batch-to-batch variation in volumetric protein yield up to 20% is considered acceptable (Dobhoff-Dier and Bliem, 1999). CHO-TNFR and CHO-IgG cells each cultivated in six OSRs in parallel showed a low variability with standard deviations about 10% for cell density, recombinant protein concentration and pH and DO profiles. The variability between the bottles were typically within the range of the experimental error (standard deviation of a measurement performed on the same OSR).

We conclude that bioprocesses performed with mammalian cells in OSRs without pH and DO controllers have a very low variability. This study confirms our previous observations in Chapter 4 that if the gas-liquid transfer of a cultivation system is sufficient, the pH and the DO will remain within a suitable operating range for cell culture without the need for a controller. There are many advantages to a non-controlled bioprocess. The cost of a bioprocess will be reduced by eliminating the controller. Moreover, the risk of contamination will be reduced since less interventions will be required in the bioreactor. Finally, the robustness of the bioprocess will be increased

by making it simple and independent of pH and DO probes, avoiding batch losses caused by their failure.

Conclusion

Biopharmaceuticals produced by animal cells are expensive (ten thousand to one billion dollar/kg) and the demands are usually small (1 kg/year for EPO in the USA in 1998). However, during the past decade the demand for recombinant monoclonal antibodies (mAbs) and vaccines have increased significantly (Kretzmer, 2002). These biopharmaceuticals are needed in large amounts (100-1000 kg/year) (Kretzmer, 2002) and therefore require the development of more cost-effective bioprocesses with higher yields to meet the worldwide demand at an affordable price (Kelley, 2009). Stainless-steel stirred-tank bioreactors (STRs) are most commonly used for large-scale bioprocesses (Kretzmer, 2002). However, gas transfer and homogeneity issues are often reported in these bioreactors as well as sterility issues due to the presence of invasive and moving components (stirrer, sparger) (Ozturk, 1996; Rodrigues et al., 2010). Orbitally shaken bioreactors (OSRs) are disposable bioreactors based on the same agitation system as the shaken flasks. No invasive components are used in these bioreactors (no impellers, spargers or baffles). OSRs are increasingly used for mammalian cell cultivation as an alternative to STRs, and optimizations of the working conditions are becoming important issues (Muller et al., 2005; Stettler et al., 2007; Zhang et al., 2009b). For this reason, this thesis aimed to improve our understanding of the engineering principles of OSRs focusing on mixing, gas transfer and hydrodynamic studies. Based on these results, we provided a proof-of-concept of the possibility to operate OSRs without using pH or DO controllers at scales up to 200 L.

In the past, pharmaceutical industries have been oriented towards higher-yielding bioprocesses. However, nowadays, the majority of pharmaceutical companies are establishing more standardized bioprocesses to facilitate and shorten the validation by regulatory agencies. In this thesis, we showed

that bioprocesses developed at a few mL scale could be linearly scaled-up to a 100-L scale using OSRs. This may help to reduce the costs and shorten the time for bioprocess development.

Probe-independent bioprocesses, such as the ones in OSRs described in this thesis, did not require pH or DO controllers. Without controllers, the basic investments for a facility equipped with OSRs would be significantly reduced in comparison with a facility equipped with STRs. The OSRs do not have impellers, spargers or baffles and thus require less maintenance than most of the bioreactors available on the market. The operating costs may be further reduced as no pure oxygen or bases are required to run bioprocesses in OSRs. This technology could therefore be of interest for small pharmaceutical companies or companies located in emerging countries.

These bioreactors are based on the disposable technology at all scales of operation and thereby are highly flexible. During the last decade, pharmaceutical companies have started using disposables because they eliminate cleaning requirements and decrease campaign turn-around times, thus increasing facility's total annual capacity. As the risk of cross-contamination is significantly decreased with disposables, the OSRs can be used to produce various recombinant proteins for clinical trials. Consequently, the OSRs may be particularly interesting at an early stage of research and development for new drugs.

This study, in addressing its specific aims, has produced several conclusions as follows:

1. At all scales tested, the fastest mixed zones were situated close to the wall and a poorly mixed zone was observed in the center of the bioreactor. Mixing times ≤ 30 s were measured at scales from 10 mL to 1000 L. Mixing and free-surface behavior were scalable by keeping constant the inner to shaking diameter ratio, the inner diameter to liquid height ratio and the Froude number. These results showed that OSRs ensure homogeneity of mammalian cell cultures at scales up to 1000 L.
2. The k_La was a reliable predictor of suitable conditions for probe-independent mammalian cell cultivation. The cultures with the same k_La had similar cell growth, recombinant protein production and culture conditions (pH and DO) at all scales. This was further demonstrated with a probe-independent bioprocess run in a 200 L OSR which showed the same culture characteristics (growth, recombinant protein production, pH) as those run in 1- and 5-L OSRs. This confirmed that probe-independent bioprocesses are scalable in OSRs because of their sufficiently high k_La values.

3. The shear stress calculated by CFD simulations for standard cultivation conditions in OSRs was one to two orders of magnitude lower than the value considered harmful for the cells. The maximal shear stress values were situated at the tip of the wave and close to bioreactor walls, suggesting that the free surface influences the level of shear stress in OSRs.
4. Cell growth and recombinant protein production were as good in probe-independent OSRs as in controlled STRs. Furthermore, the variability of cell growth, recombinant protein concentration, pH and DO profiles was approximately 10% for probe-independent bioprocesses in 5-L OSRs. This work showed that bioprocesses do not necessarily require pH and DO controllers to obtain high yields at a low variability.

These studies showed that the free surface is the key phenomenon in OSRs as it influences mixing, gas transfer and hydrodynamic stress. Nevertheless, further studies on these correlations are required to optimize the geometry of the OSRs and the operating parameters. Thus, we should answer the following questions: How to get a sufficient gas transfer at suitable conditions (mixing, hydrodynamic stress) for mammalian cell culture? Is there a free-surface shape that is more beneficial for all these parameters?

The cell distribution in OSRs is also an important question to address. Are there any gradients of cell concentration in the bioreactors? To know where the cells are located in the bioreactor may help to determine the impact of hydrodynamic stress on the cells.

In this work, recombinant proteins were produced by mammalian cells without extensively controlling the pH or DO. We showed that such bioprocesses were as efficient as those performed in fully controlled STRs and with a variability of 10%. However, to validate a bioprocess in a pharmaceutical company, further product quality characterization (protein glycosylation, isoforms) would be required.

Optimization of CFD simulations and cell growth models are ongoing and may help answer several of these questions. The combination of fluid dynamic and cell growth models will be a powerful tool to simulate bioprocesses at larger scales (200-3500 L) and further optimize the OSRs as well as the culture conditions.

Bibliography

- ACTIP, 2010. Animal Cell Technology Industrial Platform (visited 05.2011).
URL <http://www.actip.org/>
- Beek, J. J., Miller, R., 1959. Turbulent transport in chemical reactors. Chem. Eng. Prog. Symp. Ser. 25, 23–28.
- Bonvillani, P., Ferrari, M. P., Ducrós, E. M., Orejas, J. A., 2006. Theoretical and experimental study of the effects of scale-up on mixing time for a stirred-tank bioreactor. Braz. J. Chem. Eng. 23 (1), 1–7.
- Büchs, J., Maier, U., Milbradt, C., Zoels, B., 2000a. Power consumption in shaking flasks on rotary shaking machines: I. Power consumption measurement in unbaffled flasks at low liquid viscosity. Biotechnol. Bioeng. 68 (6), 589–593.
- Büchs, J., Maier, U., Milbradt, C., Zoels, B., 2000b. Power consumption in shaking flasks on rotary shaking machines: II. nondimensional description of specific power consumption and flow regimes in unbaffled flasks at elevated liquid viscosity. Biotechnol. Bioeng. 68 (6), 594–601.
- Cabaret, F., Bonnot, S., Fradette, L., Tanguy, P. A., 2007. Mixing time analysis using colorimetric methods and image processing. Ind. Eng. Chem. Res. 46 (14), 5032–5042.
- Chu, L., Robinson, D. K., 2001. Industrial choices for protein production by large-scale cell culture. Curr. Opin. Biotechnol. 12 (2), 180–187.
- De Jesus, M. J., Girard, P., Bourgeois, M., Baumgartner, G., Jacko, B., Amstutz, H., Wurm, F. M., 2004. Tubespin satellites: A fast track ap-

- proach for process development with animal cells using shaking technology. *Biochem. Eng. J.* 17 (3), 217–223.
- Deo, Y., Mahadevan, M., Fuchs, R., 1996. Practical considerations in operation and scale-up of spin-filter based bioreactors for monoclonal antibody production. *Biotechnol. Prog.* 12 (1), 57–64.
- Discacciati, M., Hacker, D., Quarteroni, A., Quinodoz, S., Tissot, S., Wurm, F. M., 2011. Numerical simulation of orbitally shaken viscous fluids with free surface. *Internat. J. Numer. Methods Fluids* (submitted).
- Doblhoff-Dier, O., Bliem, R., 1999. Quality control and assurance from the development to the production of biopharmaceuticals. *Trends Biotechnol.* 17 (7), 266–270.
- Duchene, M., Peetermans, J., D’Hondt, E., Harford, N., Fabry, L., Stephenne, J., 1990. Production of poliovirus vaccines: Past, present, and future. *Viral Immunol.* 3 (4), 243–272.
- Eagle, H., 1955. Nutrition needs of mammalian cells in tissue culture. *Science* 122 (3168), 501–504.
- Eibl, R., Kaiser, S., Lombriser, R., Eibl, D., 2010a. Disposable bioreactors: the current state-of-the-art and recommended applications in biotechnology. *Appl. Microbiol. Biotechnol.* 86 (1), 41–49.
- Eibl, R., Werner, S., Eibl, D., 2010b. Bag bioreactor based on wave-induced motion: Characteristics and applications. In: Eibl, R., Eibl, D. (Eds.), *Disposable Bioreactors*. Vol. 115 of *Advances in Biochemical Engineering/Biotechnology*. Springer Berlin / Heidelberg, pp. 55–87.
- Everett, J., Kerr, D., 1994. Changing from porcine to human insulin. *Drugs* 47 (2), 286–296.
- Garcia-Briones, M. A., Brodkey, R. S., Chalmers, J. J., 1994. Computer simulations of the rupture of a gas bubble at a gas–liquid interface and its implications in animal cell damage. *Chem. Eng. Sci.* 49 (14), 2301 – 2320.
- Garcia-Ochoa, F., Gomez, E., 2009. Bioreactor scale-up and oxygen transfer rate in microbial processes: an overview. *Biotechnol. Adv.* 27 (2), 153–176.

- Godoy-Silva, R., Mollet, M., Chalmers, J. J., 2009. Evaluation of the effect of chronic hydrodynamical stresses on cultures of suspended CHO-6E6 cells. *Biotechnol. Bioeng.* 102 (4), 1119–1130.
- Gupta, A., Rao, G., 2003. A study of oxygen transfer in shake flasks using a non-invasive oxygen sensor. *Biotechnol. Bioeng.* 84 (3), 351–358.
- Hacker, D. L., Chenuet, S., Wurm, F. M., 2010. Chinese hamster ovary cells, recombinant protein production. In: Flickinger, M. C. (Ed.), *Encyclopedia of Industrial Biotechnology: Bioprocess, Bioseparation, and Cell Technology*. John Wiley & Sons, Inc.
- Harrison, R. G., Greenman, M. J., Mall, F. P., Jackson, C. M., 1907. Observations of the living developing nerve fiber. *The Anatomical Record* 1 (5), 116–128.
- Hiby, J. W., 1981. Definition and measurement of the degree of mixing in liquid mixtures. *Int. Chem. Eng.* 21 (2), 197–204.
- Jorgensen, P., Tyers, M., 2004. How cells coordinate growth and division. *Curr. Biol.* 14 (23), 1014–1027.
- Ju, L.-K., Chase, G., 1992. Improved scale-up strategies of bioreactors. *Bioprocess. Eng.* 8, 49–53.
- Junker, B. H., 2004. Scale-up methodologies for *Escherichia coli* and yeast fermentation processes. *J. Biosci. Bioeng.* 97 (6), 347–364.
- Kaoppel, M., 1979. Development and application of a method for measuring the mixture quality of miscible liquids - 1. State of research and theoretical principles. *Int. Chem. Eng.* 19 (2), 196–215.
- Kasat, G. R., Pandit, A. B., 2004. Mixing time studies in multiple impeller agitated reactors. *Can. J. Chem. Eng.* 82 (5), 892–904.
- Kato, Y., Peter, C. P., Akgün, A., Büchs, J., 2004. Power consumption and heat transfer resistance in large rotary shaking vessels. *Biochem. Eng. J.* 21, 83–91.
- Kelley, B., 2009. Industrialization of mab production technology the bioprocessing industry at a crossroads. *mAbs* 1 (5), 443–452.
- Kim, U., Shu, C.-W., Dane, K. Y., Daugherty, P. S., Wang, J. Y. J., Soh, H. T., 2007. Selection of mammalian cells based on their cell-cycle phase using dielectrophoresis. *Proc. Natl. Acad. Sci. USA* 104 (52), 20708–20712.

- Köhler, G., Milstein, C., 1975. Continuous cultures of fused cells secreting antibody of predefined specificity. *Nature* 256 (5517), 495–497.
- Koynov, A., Tryggvason, G., Khinast, J. G., 2007. Characterization of the localized hydrodynamic shear forces and dissolved oxygen distribution in sparged bioreactors. *Biotechnol. Bioeng.* 97 (2), 317–331.
- Kretzmer, G., 2002. Industrial processes with animal cells. *Appl. Microbiol. Biotechnol.* 59 (2-3), 135–142.
- Kunas, K. T., Papoutsakis, E. T., 2009. Damage mechanisms of suspended animal cells in agitated bioreactors with and without bubble entrainment. *Biotechnol. Bioeng.* 102 (4), 980–987.
- Langer, E., 2008. Fifth Annual Report and Survey of Biopharmaceutical Manufacturing Capacity and Production. BioPlan Associates, Rockville, MD.
- Langer, E. S., 2009. Trends in capacity utilization for therapeutic monoclonal antibody production. *mAbs* 1 (2), 151–156.
- Langheinrich, C., Nienow, A. W., 1999. Control of pH in large-scale, free suspension animal cell bioreactors: Alkali addition and pH excursions. *Biotechnol. Bioeng.* 66 (3), 171–179.
- Lara, A. R., Galindo, E., Ramírez, O. T., Palomares, L. A., 2006. Living with heterogeneities in bioreactors: Understanding the effects of environmental gradients on cells. *Mol. Biotechnol.* 34 (3), 355–381.
- Li, F., Zhou, J. X., Yang, X., Tressel, T., Lee, B., 2005. Current therapeutic antibody production and process optimization. *Bioprocess. J.* 4 (5), 1–8.
- Lloyd, D. R., Holmes, P., Jackson, L. P., Emery, A. N., Al-Rubeai, M., 2000. Relationship between cell size, cell cycle and specific recombinant protein productivity. *Cytotechnology* 34, 59–70.
- Ma, N., Koelling, K. W., Chalmers, J. J., 2002. Fabrication and use of a transient contractional flow device to quantify the sensitivity of mammalian and insect cells to hydrodynamic forces. *Biotechnol. Bioeng.* 80 (4), 428–437.
- Marks, D. M., 2003. Equipment design considerations for large scale cell culture. *Cytotechnology* 42 (1), 21–33.

- Marques, M. P. C., Cabral, J. M. S., Fernandes, P., 2010. Bioprocess scale-up: quest for the parameters to be used as criterion to move from microreactors to lab-scale. *J. Chem. Technol. Biotechnol.* 85, 1184–1198.
- Matasci, M., Baldi, L., Hacker, D. L., Wurm, F. M., 2011. The piggybac transposon enhances the frequency of CHO stable cell line generation and yields recombinant lines with superior productivity and stability. *Biotechnol. Bioeng.* DOI: 10.1002/bit.23167.
- Meissner, P., Pick, H., Kulangara, A., Chatellard, P., Friedrich, K., Wurm, F. M., 2001. Transient Gene Expression: Recombinant Protein Production with Suspension-Adapted HEK293-EBNA Cells. *Biotechnol. Bioeng.* 75 (2), 197–203.
- Melton, L. A., Lipp, C. W., Spradling, R. W., Paulson, K. A., 2002. DISMT - Determination of mixing time through color changes. *Chem. Eng. Commun.* 189 (3), 322–338.
- Melville, W. K., 1996. The role of surface-wave breaking in air-sea interaction. *Annu. Rev. Fluid Mech.* 28, 279–321.
- Merten, O.-W., 2006. Introduction to animal cell culture technology-past, present and future. *Cytotechnology* 50 (1-3), 1–7.
- Micheletti, M., Barrett, T., Doig, S. D., Baganz, F., Levy, M. S., Woodley, J. M., Lye, G. J., 2006. Fluid mixing in shaken bioreactors: Implications for scale-up predictions from microlitre-scale microbial and mammalian cell cultures. *Chem. Eng. Sci.* 61 (9), 2939–2949.
- Mithani, R., Shenoi, S., Fan, L. T., Walawender, W. P., 1990. Ranking dimensionless groups in fluidized-bed reactor scale-up. *Int. J. Approx. Reason.* 4 (1), 69–85.
- Mollet, M., Ma, N., Zhao, Y., Brodkey, R., Taticek, R., Chalmers, J. J., 2004. Bioprocess equipment: Characterization of energy dissipation rate and its potential to damage cells. *Biotechnol. Prog.* 20 (5), 1437–1448.
- Muller, N., Girard, P., Hacker, D. L., Jordan, M., Wurm, F. M., 2005. Orbital shaker technology for the cultivation of mammalian cells in suspension. *Biotechnol. Bioeng.* 89 (4), 400–406.
- Nienow, A. W., 2006. Reactor engineering in large scale animal cell culture. *Cytotechnology* 50 (1-3), 9–33.

- Nikakhtari, H., Hill, G. A., 2006. Closure effects on oxygen transfer and aerobic growth in shake flasks. *Biotechnol. Bioeng.* 95 (1), 15–21.
- Oberbek, A., Matasci, M., Hacker, D. L., Wurm, F. M., 2011. Generation of stable, high-producing CHO cell lines by lentiviral vector-mediated gene transfer in serum-free suspension culture. *Biotechnol. Bioeng.* 108 (3), 600–610.
- Osher, S., Fedkiw, R., 2002. *Level Set Methods and Dynamic Implicit Surfaces*. Springer.
- Ozturk, S., Hu, W., 2006. *Cell culture technology for pharmaceutical and cell-based therapies*. Vol. 30. CRC.
- Ozturk, S. S., 1996. Engineering challenges in high density cell culture systems. *Cytotechnology* 22, 3–16.
- Peter, C. P., Suzuki, Y., Büchs, J., 2006a. Hydromechanical stress in shake flasks: Correlation for the maximum local energy dissipation rate. *Biotechnol. Bioeng.* 93 (6), 1164–1176.
- Peter, C. P., Suzuki, Y., Rachinskiy, K., Lotter, S., Büchs, J., 2006b. Volumetric power consumption in baffled shake flasks. *Chem. Eng. Sci.* 61 (11), 3771–3779.
- Petersen, J. F., McIntire, L. V., Papoutsakis, E., 1988. Shear sensitivity of cultured hybridoma cells (crl-8018) depends on mode of growth, culture age and metabolite concentration. *J. Biotechnol.* 7 (3), 229 – 246.
- Pierce, L., Shabram, P., 2004. Scalability of a disposable bioreactor from 25L-500L run in perfusion mode with a CHO-based cell line: A tech review. *Bioprocess. J.* 3 (4), 51–56.
- Puck, T. T., Cieciura, S. J., Robinson, A., 1958. Genetics of somatic mammalian cells III. Long-term cultivation of euploid cells from human and animal subjects. *J. Exp. Med.* 108 (6), 945–956.
- Raval, K., Kato, Y., Büchs, J., 2007. Comparison of torque method and temperature method for determination of power consumption in disposable shaken bioreactors. *Biochem. Eng. J.* 34 (3), 224–227.
- Rodrigues, M. E., Costa, A. R., Henriques, M., Azeredo, J., Oliveira, R., 2010. Technological progresses in monoclonal antibody production systems. *Biotechnol. Prog.* 26 (2), 332–351.

- Rushton, J., 1952. Applications of fluid mechanics and similitude to scale-up problems. Part 1. *Chem. Eng. Prog.* 48, 33–38.
- Salk, J. E., Bazeley, P. L., Bennett, B. L., Krech, U., Lewis, L. J., Ward, E. N., Youngner, J. S., 1954. Ii. a practical means for inducing and maintaining antibody formation. *Am. J. Public Health Nations Health* 44 (8), 994–1009.
- Shukla, A. A., Thömmes, J., 2010. Recent advances in large-scale production of monoclonal antibodies and related proteins. *Trends Biotechnol.* 28 (5), 253–261.
- Singh, V., 1999. Disposable bioreactor for cell culture using wave-induced agitation. *Cytotechnology* 30, 149–158.
- Stettler, M., 2007. Bioreactor processes based on disposable materials for the production of recombinant proteins from mammalian cells. Ph.D. thesis, EPFL.
- Stettler, M., Jaccard, N., Hacker, D., De Jesus, M., Wurm, F. M., Jordan, M., 2006. New disposable tubes for rapid and precise biomass assessment for suspension cultures of mammalian cells. *Biotechnol. Bioeng.* 95 (6), 1228–1233.
- Stettler, M., Zhang, X., Hacker, D. L., De Jesus, M., Wurm, F. M., 2007. Novel orbital shake bioreactors for transient production of CHO derived IgGs. *Biotechnol. Prog.* 23 (6), 1340–1346.
- Sumino, Y., Akiyama, S., Fukuda, H., 1972. Performance of the shaking flask. I. Power consumption. *J. Ferment. Technol.* 50 (3), 203–208.
- Tanzeglock, T., Soos, M., Stephanopoulos, G., Morbidelli, M., 2009. Induction of mammalian cell death by simple shear and extensional flows. *Biotechnol. Bioeng.* 104 (2), 360–370.
- Tissot, S., Farhat, M., Hacker, D. L., Anderlei, T., Kühner, M., Comninellis, C., Wurm, F., 2010. Determination of a scale-up factor from mixing time studies in orbitally shaken bioreactors. *Biochem. Eng. J.* 52, 181–186.
- Trummer, E., Fauland, K., Seidinger, S., Schriebl, K., Lattenmayer, C., Kunert, R., Vorauer-Uhl, K., Weik, R., Borth, N., Katinger, H., Müller, D., 2006. Process parameter shifting: Part I. Effect of DOT, pH, and temperature on the performance of Epo-Fc expressing CHO cells cultivated in controlled batch bioreactors. *Biotechnol. Bioeng.* 94 (6), 1033–1044.

- Verma, M., Brar, S. K., Sreekrishnan, T. R., Tyagi, R. D., Surampalli, R. Y., 2007. Dimensionless groups as scale-up parameter for wastewater and wastewater sludge treatment in a stirred tank reactor. *J. Residuals Sci. Tech.* 4 (1), 35–43.
- Voisard, D., Meuwly, F., Ruffieux, P. A., Baer, G., Kadouri, A., 2003. Potential of cell retention techniques for large-scale high-density perfusion culture of suspended mammalian cells. *Biotechnol. Bioeng.* 82 (7), 751–765.
- Wurm, F. M., 2004. Production of recombinant protein therapeutics in cultivated mammalian cells. *Nat. Biotechnol.* 22 (11), 1393–1398.
- Xing, Z., Kenty, B. M., Li, Z. J., Lee, S. S., 2009. Scale-up analysis for a CHO cell culture process in large-scale bioreactors. *Biotechnol. Bioeng.* 103 (4), 733–746.
- Yamaguchi, H., 2008. *Engineering Fluid Mechanics*. Springer, Dordrecht, The Netherlands.
- Zhang, X., Burki, C.-A., Stettler, M., De Sanctis, D., Perrone, M., Discacciati, M., Parolini, N., DeJesus, M., Hacker, D. L., Quarteroni, A., Wurm, F. M., 2009a. Efficient oxygen transfer by surface aeration in shaken cylindrical containers for mammalian cell cultivation at volumetric scales up to 1000 L. *Biochem. Eng. J.* 45 (1), 41–47.
- Zhang, X., Stettler, M., Sanctis, D., Perrone, M., Parolini, N., Discacciati, M., De Jesus, M., Hacker, D., Quarteroni, A., Wurm, F., 2009b. Use of orbital shaken disposable bioreactors for mammalian cell cultures from the milliliter-scale to the 1,000-liter scale. *Adv. Biochem. Eng. Biotechnol.* 115, 33–53.
- Zlokarnik, M., 2003. Stirring. In: *Ullmann's Encyclopedia of Industrial Chemistry*, Electronic Release, 7th Edition. Wiley-VCH, Weinheim, Germany, pp. 1–40.

Stéphanie Tissot

Ing. chim. dipl. EPF - PhD

Rue des Fontaines 2
CH-1437 Suscévaz
Switzerland

+41 79 945 22 42

✉ stephanie.tissot@a3.epfl.ch

🌐 <http://ch.linkedin.com/in/stephanietissot>

Education

- 2008–2011 **PhD in Biotechnology and Bioengineering**, *Ecole Polytechnique Fédérale de Lausanne (EPFL)*, Lausanne, Switzerland, Laboratory of Cellular Biotechnology.
Thesis: Engineering characterization and scale-up of orbitally shaken bioreactors for mammalian cells.
- 2005–2007 **Master of Science in Chemical and Biological engineering**, *EPFL*, Lausanne, Switzerland.
Master thesis in the Laboratory of Cellular Biotechnology: Gene expression in CHO cells at low temperatures. This project led to improved recombinant protein production in transiently transfected mammalian cells.
- 2002–2005 **Bachelor of Science in Chemistry and Chemical engineering**, *EPFL*, Lausanne, Switzerland.
Semester project in the Laboratory of Chemical Reaction Engineering: Study on the decomposition of nitrous oxide, a greenhouse gas, catalyzed by Fe-ZSM-5.
- 1999–2002 **Highschool**, *Gymnase de Burier*, La Tour-de-Peilz, Switzerland.
Biology and Chemistry

Experience

- 2008–2011 **PhD student**, *EPFL*, Lausanne, Switzerland.
Project in collaboration with Kühner AG, Sartorius Stedim Biotech SA and ExcellGene SA which aims to deliver large-scale bioreactors for mammalian cell culture and recombinant protein production on the market. Responsible to organize the study and characterization of the bioreactors in collaboration with two other laboratories. Formation and supervision of trainees and master students. Bioprocess development for mammalian cells (Reduction by 50% of batch losses and bioprocess costs). Presentation of this work at international conferences and publication of the results in journals (Biochem. Eng. J., N. Biotech., Chimia).
- 2007 **Research Assistant**, *ExcellGene SA*, Monthey, Switzerland (10 months).
Project management in R&D and production involving recombinant protein production in mammalian cells with high time, quality and cost constraints.
- 2005 **Internship in Microbiology**, *Nestlé Research Center*, Vers-chez-les-Blanc, Switzerland (2 months).
Multidisciplinary R&D projects in an international environment involving interactions with technicians, scientists and project managers.
- 2002 **Internship in Chemical Engineering on Unit and Process maintenance**, *Ciba Specialty Chemicals, CIMO*, Monthey, Switzerland (1 month).
Inventory and control of a process unit using the SAP system. This work was used for the maintenance of the process unit during the annual production break.

Languages

French	Mother tongue.
English	Fluent , <i>used at work since 2006.</i>
German	Good knowledge , <i>B2 in the Common European Framework of Reference.</i>
Italian	Basic knowledge.

Qualifications

Upstream Processing	Mammalian cell cultivation and recombinant protein production in suspension in stirred-tank (STR) and orbitally-shaken bioreactors (OrbShake), large-scale bioprocesses (up to 500 L), bioreactor characterization and scale-up, transient transfection, flow cytometry.
Protein analysis	ELISA, Western Blot, SDS-PAGE, Protein A purification, Cytotoxicity LDH assays.
Microbiology	Plasmid- and Protein- production, Plasmid digestion and purification.
IT	Windows and Mac OS X operating systems, MS-Office Tools, \LaTeX , Python, MatLab, Adobe suites (Photoshop, Illustrator).

Continuing education

2010	Swiss/European BioTechnology Workshop , <i>Ittingen</i> , Switzerland.
2009	Design of experiment , <i>EPFL</i> , Switzerland.
2008	Micro-Bioreactors in R&D for fine chemicals and pharmaceutical production , <i>Lonza Workshop</i> , Visp, Switzerland.
2008	Management of innovation and technology transfer , <i>EPFL</i> , Switzerland.
2008	Cellular Bioprocess technology , <i>Prof. Wei-Shu Hu</i> , Minneapolis, USA.

Awards and honors

ACTIP Fellowship 2010	Award for excellent research carried-out in the field of animal cell technology granted by the Animal Cell Technology Industrial Platform (ACTIP). The ACTIP is an informal forum of European biotechnology companies with significant activities in animal cell technology.
-----------------------	--

Poster and oral presentations

May 2011	22nd ESACT Meeting , <i>Vienna</i> , Austria, Posters.
Dec. 2010	ACTIP Annual Meeting , <i>Penzberg</i> , Germany, Oral presentation.
Sep. 2010	5th European BioTechnology Workshop , <i>Ittingen</i> , Switzerland, Posters.
Sep. 2010	Life Science Symposium , <i>Lausanne</i> , Switzerland, Posters.
Jun. 2009	21st ESACT Meeting , <i>Dublin</i> , Ireland, Oral presentation.

Publications

Tissot, S., Farhat, M., Hacker, D. L., Anderlei, T., Kühner, M., Comninellis, C., and Wurm, F. Determination of a scale-up factor from mixing time studies in orbitally shaken bioreactors. *Biochem. Eng. J.* 52, 2-3 (2010), 181–186.

Tissot, S., Oberbek, A., Reclari, M., Dreyer, M., Hacker, D. L., Baldi, L., Farhat, M., and Wurm, F. M. Efficient and reproducible mammalian cell bioprocesses without probes and controllers? *N. Biotechnol.* 28, 4 (2011), 382–390.

Werner, S., Eibl, R., Lettenbauer, C., Röhl, M., Eibl, D., De Jesus, M., Zhang, X., Stettler, M., Tissot, S., Bürkie, C., Broccard, G., Kühner, M., Tanner, R., Baldi, L., Hacker, D., and Wurm, F. M. Innovative, Non-stirred Bioreactors in Scales from Milliliters up to 1000 Liters for Suspension Cultures of Cells using Disposable Bags and Containers – A Swiss Contribution. *CHIMIA Int. J. for Chem.* 64, 11 (2010), 819–823.

Wulhfard, S., Tissot, S., Bouchet, S., Cevey, J., De Jesus, M., Hacker, D., and Wurm, F. Mild hypothermia improves transient gene expression yields several fold in Chinese hamster ovary cells. *Biotechnol. Prog.* (2008).

Personal

Date of Birth 16th April 1984

Nationality Swiss

Marital
status Single